OXFORD UNIVERSITY PRESS | Brain

Glycation potentiates α-synuclein-associated neurodegeneration in synucleinopathies

Journal:	*Brain*
Manuscript ID	BRAIN-2016-01133.R3
Manuscript Type:	Original Article
Date Submitted by the Author:	n/a
Complete List of Authors:	Vicente Miranda, Hugo; CEDOC, Chronic Diseases Research Centre, NOVA Medical School, Cell and Molecular Neuroscience; Instituto de Medicina Molecular, Faculty Medicine, University of Lisbon Szegö, Éva; Center for Nanoscale Microscopy and Molecular Physiology of the Brain (CNMPB), University Medical Center Göttingen Oliveira, Luis; Centro de Investigação Interdisciplinar Egas Moniz, Instituto Superior de Ciências da Saúde Egas Moniz; Max Planck Institute for Biophysical Chemistry, Laboratory of Cellular Dynamics Breda, Carlo; Department of Genetics, University of Leicester Darendelioglu, Ekrem; Department of Genetics, University of Leicester; Bingol University, Science and Letters Faculty de Oliveira, Rita; CEDOC, Chronic Diseases Research Centre, NOVA Medical School, Cell and Molecular Neuroscience; Instituto de Medicina Molecular, Faculty Medicine, University of Lisbon Ferreira, Diana; Instituto de Medicina Molecular, Faculty Medicine, University of Lisbon, Gomes, Marcos; Instituto de Medicina Molecular, Faculty Medicine, University of Lisbon Rott, Ruth; Rappaport Faculty of Medicine and Research Institute Oliveira, Márcia; Instituto de Medicina Molecular, Faculty Medicine, University of Lisbon Munari, Francesca; Max Planck Institute for Biophysical Chemistry; German Center for Neurodegenerative Diseases (DZNE), Enguita, Francisco; Instituto de Medicina Molecular, Faculty Medicine, University of Lisbon Simões, Tânia; Instituto Nacional de Saúde Dr. Ricardo Jorge Rodrigues, Eva Ferreira; Center for Nanoscale Microscopy and Molecular Physiology of the Brain (CNMPB), University Medical Center Göttingen Heinrich, Michael; University Hospital Erlangen, Department of Molecular Neurology Martins, Ivo; Instituto de Medicina Molecular, Faculty Medicine, University of Lisbon Zamolo, Irina; University of Tuebingen, Institute of Medical Genetics and Applied Genomics Riess, Olaf; University of Tuebingen, Medical Genetics Cordeiro, Carlos; Centro de Quimica e Bioquimica, Faculdade de Ciencias da Universidade de Lisboa Ponces-Freire, Ana; Centro de Quimica e Bioquimica, Faculdade de Ciencias

	da Universidade de Lisboa Lashuel, Hilal; The Swiss Federal Institute of Technology-Lausanne, Santos, Nuno; Instituto de Medicina Molecular, Faculty Medicine, University of Lisbon Lopes, Luísa; Instituto de Medicina Molecular, Faculty of Medicine, University of Lisbon, Xiang, Wei; FAU Erlangen-Nürnberg, Institute of Biochemistry (Emil-Fischer-Center) Jovin, Thomas; Max Planck Institute for Biophysical Chemistry, Laboratory of Cellular Dynamics Penque, Deborah; Instituto Nacional de Saúde Dr. Ricardo Jorge Engelender, Simone; Rappaport Faculty of Medicine and Research Institute Zweckstetter, Markus; Max-Planck-Institut fur biophysikalische Chemie; DFG Research Center for Nanoscale Microscopy and Molecular Physiology of the Brain (CNMPB); German Center for Neurodegenerative Diseases (DZNE) Klucken, Jochen; University Hospital Erlangen, Department of Molecular Neurology Giorgini, Flaviano; Department of Genetics, University of Leicester Quintas, Alexandre; Centro de Investigação Interdisciplinar Egas Moniz, Instituto Superior de Ciências da Saúde Egas Moniz Outeiro, Tiago; Center for Nanoscale Microscopy and Molecular Physiology of the Brain (CNMPB), University Medical Center Göttingen, Department of Neurodegeneration and Restorative Research; CEDOC, Chronic Diseases Research Centre, NOVA Medical School, Cell and Molecular Neuroscience; Max Plank Institute for Experimental Medicine
Subject category:	Neurodegeneration – cellular and molecular
To search keyword list, use whole or part words followed by an *:	Parkinson's disease: cellular mechanisms < NEURODEGENERATION: CELLULAR AND MOLECULAR, alpha-Synuclein < NEURODEGENERATION: CELLULAR AND MOLECULAR, NEURODEGENERATION: CELLULAR AND MOLECULAR, Neuroprotection < NEURODEGENERATION: CELLULAR AND MOLECULAR, Protein aggregation < NEURODEGENERATION: CELLULAR AND MOLECULAR

Glycation potentiates α-synuclein-associated neurodegeneration in synucleinopathies

Hugo Vicente Miranda[1,2], Éva Mónika Szegő[3], Luís Miguel Oliveira[4,5], Carlo Breda[6], Ekrem Darendelioglu[6,7], Rita Machado de Oliveira[1,2], Diana Gabriela Ferreira[2,3], Marcos António Gomes[2], Ruth Rott[8], Márcia Oliveira[2], Francesca Munari[9,10], Francisco Javier Enguita[2], Tânia Simões[11], Eva Ferreira Rodrigues[3], Michael Heinrich[12], Ivo Cristiano Martins[2], Irina Zamolo[13], Olaf Riess[13], Carlos Cordeiro[14], Ana Ponces-Freire[14], Hilal Ahmed Lashuel[15], Nuno Correia Santos[2], Luisa Vaqueiro Lopes[2], Wei Xiang[16], Thomas Michael Jovin[5], Deborah Penque[11], Simone Engelender[8], Markus Zweckstetter[9,10,17], Jochen Klucken[12], Flaviano Giorgini[6], Alexandre Quintas[4], and Tiago Fleming Outeiro[1,3,18]*

[1]CEDOC, Chronic Diseases Research Centre, NOVA Medical School | Faculdade de Ciências Médicas, Universidade NOVA de Lisboa, Campo dos Mártires da Pátria, 130, 1169-056 Lisboa, Portugal

[2]Instituto de Medicina Molecular, Faculdade de Medicina, Universidade de Lisboa, Lisboa, Portugal

[3]Department of Neurodegeneration and Restorative Research, Center for Nanoscale Microscopy and Molecular Physiology of the Brain (CNMPB), University Medical Center Göttingen, Waldweg 33, 37073 Göttingen, Germany

[4]Centro de Investigação Interdisciplinar Egas Moniz, Instituto Superior de Ciências da Saúde Egas Moniz, 2829-511 Monte de Caparica, Caparica, Portugal

[5]Laboratory of Cellular Dynamics, Max Planck Institute for Biophysical Chemistry, 37077 Göttingen, Germany

[6]Department of Genetics, University of Leicester, Leicester LE1 7RH, United Kingdom

[7]Bingol University, Science and Letters Faculty, Molecular Biology and Genetics Department, 12000, Bingol/Turkey

[8]Department of Biochemistry, Rappaport Faculty of Medicine and Research Institute, Technion-Israel Institute of Technology, Haifa 31096, Israel.

[9]Department for NMR-based Structural Biology, Max Planck Institute for Biophysical Chemistry, 37077 Göttingen, Germany

[10]German Center for Neurodegenerative Diseases (DZNE), 37077 Göttingen, Germany.

[11]Laboratório de Proteómica, Departamento de Genética Humana, Instituto Nacional de Saúde Dr. Ricardo Jorge, 1649-016 Lisboa, Portugal

[12]Department of Molecular Neurology, University Hospital Erlangen, Schwabachanlage 6, 91054 Erlangen, Germany

[13]Institute of Medical Genetics and Applied Genomics, University of Tuebingen, 72074 Tuebingen, Germany

[14]Enzymology Group, Departamento de Quimica e Bioquimica, Centro de Quimica e Bioquimica, Faculdade de Ciencias da Universidade de Lisboa, Campo Grande, Edificio C8, 1749-016, Lisboa, Portugal.

[15]Laboratory of Molecular and Chemical Biology of Neurodegeneration, Swiss Federal Institute of Technology Lausanne (EPFL), FSV-BMI AI 2137.1, Station 15, CH-1015 Lausanne, Switzerland.

[16]Institute for Biochemistry, Friedrich-Alexander-University Erlangen-Nürnberg (FAU), Erlangen, Germany.

[17]Center for Nanoscale Microscopy and Molecular Physiology of the Brain, University Medical Center, 37075 Göttingen, Germany.

[18]Max Plank Institute for Experimental Medicine, Goettingen, Germany.

* Correspondence to:

Address: Department of Neurodegeneration and Restorative Research, Center for Nanoscale Microscopy and Molecular Physiology of the Brain (CNMPB), University Medical Center Göttingen, Waldweg 33, 37073 Göttingen, Germany

Email: touteir@gwdg.de

Running Title: Glycation potentiates synucleinopathies

Abstract

α-synuclein (aSyn) misfolding and aggregation is a hallmark in Parkinson's disease (PD) and in several other neurodegenerative diseases known as synucleinopathies. The toxic properties of aSyn are conserved from yeast to man, but the precise underpinnings of the cellular pathologies associated are still elusive, complicating the development of effective therapeutic strategies. Combining molecular genetics with target-based approaches, we established that glycation, an unavoidable age-associated posttranslational modification, enhanced aSyn toxicity in vitro and in vivo, in *Drosophila* and in mice. Glycation affected primarily the N-terminus of aSyn, reducing membrane binding, impaired the clearance of aSyn, and promoted the accumulation of toxic oligomers that impaired neuronal synaptic transmission. Strikingly, using glycation inhibitors, we demonstrated that normal clearance of aSyn was reestablished, aggregation was reduced, and motor phenotypes in *Drosophila* were alleviated. Altogether, our study demonstrates glycation constitutes a novel drug-target that can be explored in synucleinopathies as well as in other neurodegenerative conditions.

Keywords

Glycation, Parkinson's Disease, Neurodegeneration, alpha-synuclein

Introduction

The molecular underpinnings of neurodegenerative diseases (NDs) such as Parkinson's disease (PD) and Alzheimer's disease remain unclear, as genetics explains only a minor fraction of cases. Therefore, the study of non-genetic factors that may contribute to the development of NDs is urgent. NDs are known to be associated with the misfolding and accumulation of various proteins. PD is a common disorder known for typical motor symptoms that result from the loss of nigrostriatal dopaminergic neurons (DA), and for the accumulation of pathognomonic intraneuronal inclusions known as Lewy bodies (LBs) and Lewy neurites. These inclusions are primarily composed of alpha-synuclein (aSyn) (Spillantini *et al.*, 1998; Wales *et al.*, 2013), a protein also associated with other disorders known as synucleinopathies.

We and others have extensively exploited yeast cells expressing ND-associated proteins to recapitulate important cellular pathologies, thereby accelerating our understanding of the molecular basis of these disorders (Outeiro and Lindquist, 2003; Tenreiro and Outeiro, 2010). Recently, we found that DJ-1, the product of the *PARK7* gene, interacts with and protects against aSyn aggregation and toxicity in yeast and in mammalian cell models of PD (Zondler *et al.*, 2014). DJ-1 mutations cause autosomal recessive PD through a loss of function mechanism. Recently, this protein was shown to have both glyoxalase (Lee *et al.*, 2012) and deglycase activities (Richarme *et al.*, 2015), suggesting glycation, an unavoidable age-associated process, might play a role in PD. In a previous unbiased genetic screen in yeast, we identified another component of the glyoxalase system (Glo4) as an enhancer of aSyn toxicity (Willingham *et al.*, 2003). In fact, glucose is readily metabolized generating reducing-sugars that covalently react with

proteins generating advanced glycation end-products (AGEs) that invariably impact on protein function (Vicente Miranda and Outeiro, 2010). Intriguingly, diabetes, a widespread condition of impaired glucose metabolism, has been established as an important risk factor for PD (Hu *et al.*, 2007; Sun *et al.*, 2012; Vicente Miranda *et al.*, 2016a). The levels of AGEs are increased in the brains of patients suffering from synucleinopathy (Dalfo *et al.*, 2005), and AGEs can be detected at the periphery of LBs (Castellani *et al.*, 1996). A similar staining pattern of AGEs was reported in early Lewy bodies in patients with Lewy body disease. This suggested that an excess of carbonyl compounds could play a role in the pathogenesis of PD (Munch *et al.*, 2000). However, it has been unclear whether AGEs are causally related to disease and whether aSyn is glycated. Here, we asked whether manipulation of the major component of the glyoxalase system (Glo1) would affect aSyn aggregation and toxicity. Glo1 constitutes a major line of defense against methylglyoxal (MGO), a dicarbonyl metabolite that is formed unavoidably via multiple catabolic processes (Reichard *et al.*, 1986; Lyles and Chalmers, 1992; Richard, 1993; Thornalley *et al.*, 1999; Baynes and Thorpe, 2000). MGO glycates arginine and lysine residues. With the latter, MGO forms N(epsilon)-(carboxyethyl)lysine (CEL) (Ahmed *et al.*, 1997) and the imidazolium crosslink, methylglyoxal-lysine dimer (MOLD) (Frye *et al.*, 1998). Glo1 activity depends on reduced forms of glutathione (GSH), to which MGO reversibly associates with, forming an MGO-GSH hemithioacetal (substrate of *Glo1*), and NADPH, respectively (Vander Jagt *et al.*, 1992; Gomes *et al.*, 2005). Therefore, the catabolism of MGO leads to a decrease in the levels of these cofactors, which are also crucial for oxidative stress responses. Interestingly, in hyperglycemia conditions and in diabetic patients, MGO is increased leading to higher

MGO-glycation levels (2-4 fold) (Yao and Brownlee, 2010; Bierhaus *et al.*, 2012). Notably, the brain's defenses against glycation, such as GSH and *Glo1*, decrease with aging (Chen *et al.*, 1989; Kuhla *et al.*, 2006), and in the substantia nigra of PD patients (Pearce *et al.*, 1997), suggesting that MGO levels may increase with aging and in PD. Altogether, determining the molecular mechanisms through which glycation alters proteostasis and contributes to synucleinopathies enables an important breakthrough that links aging to neurodegeneration and uncovers novel therapeutic targets for intervention in synucleinopathies.

Materials and Methods

MGO purification

MGO was produced as in (Gomes *et al.*, 2005). Briefly, MGO was prepared by sulfuric acid hydrolysis of 1,1-dimethyl acetal. The resulting MGO was purified by fractional distillation under reduced pressure and nitrogen bleed. MGO was evaporated at ~72ºC and three fractions were obtained. The first fraction was discarded, as it contained MGO mixed with methanol. The second fraction was collected and stored at -80ºC until further use.

aSyn aggregation and toxicity in yeast

Saccharomyces cerevisiae strain BY4741 and mutant strains Δ*glo1* and Δ*tpi* (Euroscarf collection) were used. Cells were grown and transformed as in (Vicente Miranda *et al.*, 2013). Briefly, aSyn and familial variants A30P, E46K and A53T were expressed using the p426GFP after transformation into yeast cells using the lithium

acetate method. Transformants were selected in Yeast Nitrogen Base complete media without uracil (YNB-U). D-glucose treatment was performed challenging cells for 24 h with 4 % D-glucose in media. Fluorescent micrographs were acquired with a Zeiss Axiovert 200M. Toxicity assays were performed as previously (Outeiro and Lindquist, 2003) by spotting serial dilutions of yeast cells onto agar-YNB-U plates. Cell viability was assessed by counting colony-forming units (CFUs) after growth for 2 days at 30º C on YEP-glucose as previously (Tenreiro *et al.*, 2014b).

H4 Cells immunocytochemistry, immunobloting and toxicity

H4 neuroglioma cells were maintained, grown and transfected with aSyn, SynT and Synph 1 as in (Vicente Miranda *et al.*, 2013) by using Fugene 6 (Roche diagnostics, Mannheim, Germany) using standard procedures. 24h after SynT and Synph 1 co-transfection, cells seeded at 20 000 cells cm^2 in 35 mm imaging dishes (Ibidi) or seeded at 30 000 cells cm^2 in 10cm, 6cm, 6-well plates or 12-well plates (TPP) were treated with vehicle (H_2O) or MGO (0.5mM) for 16h. Cells washed with PBS were fixed and permeabilized in 100% ice-cold methanol (-20°C, 10min). Cells were incubated with blocking solution (1.5 % Normal Goat Serum in PBS) for 1h at RT. Cells were incubated with the primary antibody anti-aSyn (Cell Signaling Technology, 2642) 1:75 in blocking solution, overnight at 4 °C alone, or co-stained with anti-ubiquitin antibody (Abcam, P4G7) 1:500 in blocking solution. Cells, washed with PBS, were incubated for 4h at RT with Alexa Fluor® 488 Goat Anti-Rabbit conjugated secondary antibody (Invitrogen, A11008) or Alexa Fluor® 568 Goat Anti-Mouse conjugated secondary antibody (Invitrogen, A11031) using a dilution of 1:1000 in blocking solution. Widefield

fluorescent microscope Zeiss Axiovert 200M (Carl Zeiss MicroImaging) and point scanning confocal microscope Zeiss LSM 710 were used to visualize aSyn inclusions.

Sucrose gradient fractions were applied in a dot-blot system and immunobloting performed according to standard procedures as in (Basso *et al.*, 2013). For immunobloting, we used the following antibodies: anti aSyn (BD Transduction laboratories, S63320, 1:3000); anti V5 (Santa Cruz, SC-83849-R, 1:1000); anti LC3 (Nano Tools, 0260-100/LC3-2G6, 1:2000); anti β-actin (Ambion, AM4302, 1:5000); and anti GAPDH (Ambion, AM4300, 1:5000).

Cytotoxicity was measured using Caspase-3 or LDH kit (Clontech). Total protein lysates were obtained as in (Vicente Miranda *et al.*, 2013).

aSyn immunoprecipitation

H4 neuroglioma cells were transfected with aSyn or cotransfected with SynT and Synph 1. 24h post-transfection, cells were challenged with PBS (Ctrl) or MGO (0,5mM) for 16h. Media was renewed and cells challenged for 6h. Protein was extracted using IP buffer (150mM Tris-HCl, pH 7.4, 1mM EDTA, 1% NP-40, 0.1% SDS and complete protease inhibitors). 500mg of protein extract where pre-cleared in 10 µl of protein G beaded agarose resin (Invitrogen) for 1h under nutation at 4º C. Protein supernatant was incubated with 2.4 µg of anti aSyn antibody (BD Transduction laboratories, S63320) and nutated at 4º C overnight. Beads were collected and washed 4x in IP Buffer. Samples were immunoblotted as previously indicated using anti-aSyn (C-20 Santa Cruz biotechnology, sc-7011-R, 1:1000) and anti-AGEs (Millipore, AB9890, 1:1000).

MGO measurement

MGO was extracted from yeast or H4 cells with $HClO_4$ 3 M at 4 °C for 10 min and stored at -80 °C. After derivatization with 1,2-phenylenediamine 0.92 mM and solid-phase extraction of quinoxalines, MGO levels (as 2-methylquinoxaline) were determined by reverse phase HPLC on a Merck Hitachi system: Pump L-2130; Column Oven L-2300; UV detector L-2400. Samples were separated on LiChroCART LiChrospher® RP-18 endcapped (5 µm, 250-4.6) with methanol/ammonium formate 20 mM pH3.4 (60/40) used as mobile phase (1 $ml.min^{-1}$); 20 µl as injection volume; and detection at 320 nm. Dimethylquinoxaline, added prior to solid-phase extraction was used as internal standard. MGO was normalized to dimethylquinoxaline.

LUHMES cells

Proliferating LUHMES cells (a kind gift of Prof. M. Leist, University of Konstanz, Germany) were cultivated in LUHMES proliferation medium containing advanced DMEM/F12, 1 % N-2 supplement (Invitrogen), 2 mM L-glutamine (Gibco), and 40 ng/ml recombinant basic fibroblast growth factor (R&D Systems) on cell culture T75 and T175 flasks or multi-well plates (Nunc) pre-coated with 50 ng/ml poly-L-ornithine (PLO) and 1 µg/ml fibronectin (Sigma-Aldrich) at 37 °C and 5 % CO2. Differentiated LUHMES cells were generated by replacing proliferation medium by differentiation medium containing advanced DMEM/F12, 1 % N-2 supplement, 2 mM L-glutamine, 1 mM dibutyryl 3′,5′-cyclic AMP, (Sigma-Aldrich), 1 µg/ml tetracycline, and 2 ng/ml recombinant human glial derived neurotrophic factor (R&D Systems). After two days, cells were seeded into PLO/fibronectin pre-coated multi-well plates.

Generation of stable expressing clonal LUHMES cells

Proliferating LUHMES cells were transduced by lentiviral delivery of aSyn-IRES-GFP or IRES-GFP constructs, a third-generation lentiviral system as described previously (Tiscornia *et al.*, 2006). Purified lentivirus encoding aSyn and GFP were kindly provided by Dr. B. Winner (Interdisciplinary Center for Clinical Research, Nikolaus-Fiebiger Center for Molecular Medicine, Erlangen). Cloning of stably-expressing (GFP-positive) cells was performed by single cell colony culture using limited dilution (LUHMES cells).

MGO treatment of LUHMES cells

For MGO treatment, pre-differentiated (day two) LUHMES cells were seeded into 96-well plates ($0.75x10^5$ cells) or into 24-well plates ($0.3x10^6$ cells) and incubated at 37 °C, 5 % CO_2 for three days. MGO stock was sterile filtered and pre-diluted 1:100 in sterile pure water. Pre-dilution was again diluted in LUHMES differentiation medium. Cell culture medium was removed. 120 µl of MGO dilution was added at the indicated concentrations. Cells were then incubated at 37 °C, 5 % CO_2 until the measurement of toxicity.

LUHMES viability assay (MTS) and immunocytochemistry

Cellular viability was determined by the conversion of (3-(4,5-dimethylthiazol-2-yl)-5-(3-carboxymethoxyphenyl)-2-(4-sulfophenyl)-2H-tetrazolium (MTS) to Formazan, measured by the absorbance (490nm) of intracellular formazan using a 96-well plate reader according to the manufactures protocol (MTS-assay, Promega).

For immunocytochemistry cells were cultured on 13mm glass coverslips in 24-well plates as described above. Cells were fixed for 15 to 20 min with 4% paraformaldehyde at RT, washed three times in TBS and incubated in Fish Skin Gelatin Buffer (FSGB) containing 0.1 % Triton X-100 for 20 min at RT. Primary antibodies (rat-anti aSyn, 15G7, 1:250; rabbit-anti Caspase 3a, 1:500, Cell Signaling Technology) were diluted in FSGB and applied ON at 4 °C. After washing, secondary antibodies (dk-anti-rt, rhodamine, 1:500, Dianova; dk-anti-rb, diluted in 300µl/well FSGB) were added and the plate was incubated at RT for 1h in the dark. After removing the secondary antibody and washing 1x with FSGB, DAPI (diluted in 500µL/well FSGB) was added and again incubated at RT for 15min. The coverslips were mounted with Prolong Antifade. Images were acquired using a Zeiss ApoTome microscope.

Differentiation of patient-derived iPSCs

The neuronal lineage control and patient human-induced pluripotent stem cells were isolated and characterized by The Parkinson's Institute (Byers *et al.*, 2011; Mak *et al.*, 2012) and made available through a joint BMBF-CIRM grant to TMJ (315050 AZ0101). An extensive comparative characterization between control and *SNCA* triplication is presented in (Oliveira *et al.*, 2015). aSyn KD in the triplication line was achieved with the transduction of a lentiviral shRNA using the pLKO.1 purovector containing the 5´ACCAAAGAGCAAGTGACAAAT-3´. Stage IV cells were cultivated and differentiated in two stages (Mak *et al.*, 2012): 10 days in DA1 medium (using 1 µM SAG) and 20 days in DA2 medium.

Cytotoxicity in iPS cells

Differentiated iPSCs were washed with "oxidative stress medium" (same formula as DA2 medium, but with a B-27 supplement lacking anti-oxidants (Life Technologies)) and MGO was directly added to medium. Cells were incubated at 37 °C for 18 h and cytotoxicity assessed by measuring the cell supernatant with the LDH cytotoxicity detection kit (Roche Applied Science). The samples were measured in triplicate on a PHERAstar FS plate reader (BMG Labtech).

Drosophila lines

Flies were raised at 25 °C in LD12:12 on standard maize food. The *elav-GAL4* (c155), *w; UASeGFP; +* (5431) and *w; +; UAS-aSyn* (8146) transgenic lines were obtained from the Bloomington Stock Center (Bloomington, Indiana). RNAi transgenic lines were obtained from the Vienna *Drosophila* RNAi Center (VDRC). For *Glo1* knockdown, the 101560 line from the KK Library (phiC31-based transgenes at a single, defined site) was used. For *Tpi* knockdown, two lines were employed from the GD Library (P-element based, random insertion site): 25643 (Fig. 2) and 25644 (Fig. S3).

Negative geotaxis and survival assays

Negative geotaxis assays were performed as described (Ali *et al.*, 2011). The same fly groups were tested at day 10, 20 and 30 post-eclosion. For the survival assay, female flies of the desired genotype were collected and kept in groups of 10 in separate

vials. Flies were passaged onto fresh food every two to three days and the number of dead individuals was scored.

Glycation studies in mice

Animal experiments were performed according to institutional and national regulations.

Brains from 4 (young) and 22 month-old (old) mice expressing human aSyn, were quickly removed and homogenized in RIPA buffer in the presence of protease and phosphatase inhibitors (Roche Complete and PhosStop). Brains from 2.5 (young), 11 and 17-month old (old) WT mice were also processed.

6-7 month old male mice expressing human aSyn under the control of Thy-1 promoter (aSyn Tg) (Rockenstein *et al.*, 2002) or B6D2F1 wild-type littermate controls (WT) received MGO, or vehicle (PBS, pH 7.4) injection under deep anaesthesia (80 mg/kg ketamine hydrochloride, 5 mg/kg xylasine hydrochloride). 2x1 µl of MGO (340 mM) or PBS were injected into the substantia nigra (stereotactic coordinates: AP: 3.1; L: -1,2; DV: -4,2 from Bregma) or the striatum (stereotactic coordinates: AP: 0.86; L: -1.5; DV: 5/5.5 from dura) using glass microcapillary with a flow rate of 250 nl/min.

For immunohistochemistry, mice were transcardially perfused with 4 % PFA 7 days post-injection. Brains were removed and post-fixed for 2h at 4 °C and then cryoprotected in Tris-phosphate-buffered solution (TBS, pH 7.6) containing 30 % sucrose (w/v) overnight at 4 °C. 30 µm coronal free floating sections were stained as reported previously (Szego *et al.*, 2012). Briefly, sections were incubated either with anti-tyrosine hydroxylase rabbit (Millipore, 1:1000), anti-CEL (Cosmobio, 1:1000), anti-aSyn (610786, 1:1000, BD Transduction laboratories), anti-phospho-synuclein (Ser129) (pSyn,

Wako, 1:1000), anti-vesicular monoamine transporter (VMAT, 1:2000, Abcam), anti-NeuN mouse (Millipore, 1:1000) or anti-aSyn aggregation clone 5G4 (MABN389, 1:1000, Millipore) for 48h at 4 °C. Sections were then treated either with AlexaFluor conjugated secondary antibody (1:1000, Invitrogen, CA, USA) or with biotinylated anti-mouse (NeuN) or anti-rabbit (tyrosine hydroxylase - TH) IgG (Vector Laboratories, 1:200) followed by avidin–biotin–horseradish peroxidase (HRP) complex (Vector Standard Elite Kit, 1:500). Peroxidase labelling was visualized by diaminobenzidine tetrahydrochloride. Omission of the primary antibody resulted in no staining.

Numbers of TH-, VMAT-, DAPI- or NeuN-positive neurons were counted and estimated by using the optical dissector (StereoInvestigator; MBF Bioscience) (Szego *et al.*, 2013); (100x objective, AxioImager M2; Zeiss; counting frame: 50 x 50 µm, grid size: 200 x 200 µm; every fourth section was analysed). Counts were performed manually and blinded for experimental grouping. Fluorescent images were taken using an Olympus IX-81 microscope (Olympus Germany, Hamburg, Germany). Exposure time was equal for the same staining across the experimental groups. Fiber density in the striatum was analyzed as previously described (Szego *et al.*, 2012).

For visualization of TH-positive fibers in the striatum, we used nickel intensification of the TH-staining (without Nissl counterstaining), as we described previously (Szego *et al.*, 2012). Briefly, sections were treated with anti-tyrosine-hydroxylase (rabbit polyclonal, 1:1000, Millipore, Billerica, MA, USA) antibody for 48 h at 4 °C, then treated with biotinylated anti-rabbit IgG (1:200; Vector Laboratories, Burlingame, CA, USA) followed by avidin–biotin–horseradish peroxidase (HRP)

complex (Vector Standard Elite Kit, 1:500). Peroxidase labeling was visualized by diaminobenzidine tetrahydrochloride.

For protein analysis, brains were quickly removed, striatum dissected and samples homogenized in RIPA buffer in the presence of protease and phosphatase inhibitors (Roche Complete and PhosStop). Samples were then rotated for 1h at 4 °C and centrifuged at 18.000 g for 30 min. For further analyses, we used the soluble fractions. aSyn was partially purified and enriched as described in (Vicente Miranda *et al.*, 2013). For immunobloting, we used anti aSyn (BD Transduction laboratories, S63320, 1:3000), anti CEL (Cosmobio, CAC-AGE-MG02, 1:500) or anti AGEs (Millipore, AB9890, 1:1000).

Animals used for electrophysiological studies

Wild type male Wistar rats with 8-12 weeks old were ordered from Harlan Interfauna Iberica, SL. All procedures used in the present study complied with the European Community guidelines (86/609/EEC) and Portuguese law on Animal Care (1005/92). Environmental conditions were kept constant: food and water ad libitum, 21±0.5°C, 60±10% relative humidity, 12h light/dark cycles.

Hippocampal slice preparation

Animals were anesthetized under halothane atmosphere and sacrificed by decapitation. Brains were rapidly removed and the hippocampi were dissected free in ice-cold artificial cerebrospinal fluid (aCSF) composed of (mM): 124 NaCl, 3 KCl, 1.25 NaH2PO4, 26 $NaHCO_3$, 1 $MgSO_4$, 2 $CaCl_2$, and 10 D-glucose, previously gassed with

95% O_2 and 5% CO_2, pH 7.4. Slices (400µm-thick) were cut transversally along the primary axis of the hippocampus with a McEwen tissue chopper and allowed to recover functionally and energetically for at least 60min in a resting chamber immersed in the same solution, at RT (22-25°C) (Fredholm *et al.*, 1984). Slices were then incubated for 90min either with vehicle, glycated aSyn (0.5mM MGO for 30h) or aSyn in gassed aCSF. The range of concentration chosen for aSyn incubation was based on previous data using 500nM of different aSyn species (Diogenes *et al.*, 2012). All incubations were performed at RT to avoid neuronal damage by hypoxic injury (Schiff and Somjen, 1985). After this pre-incubation period, one slice was carefully deposit in a recording chamber for submerged slices and continuously superfused with gassed aCSF at a constant flow (3ml/min) and temperature (32°C).

fEPSP recordings

Evoked field synaptic potentials (fEPSPs) were recorded through an extracellular microelectrode filled with 4M NaCl (2-4MΩ resistance) placed in the stratum radiatum of the CA1 area, as previously described (Diogenes *et al.*, 2011). The pathway of Schaffer collateral fibers was stimulated (rectangular pulses of 0.1ms duration) once every 10s by a bipolar wire electrode placed on the Schaffer fibers in the CA3 area. The initial intensity of the stimulus (200µA) was adjusted to obtain a submaximal fEPSP slope with a minimum population spike contamination, near one-third of the fEPSP slope obtained with supramaximal stimulation. The averages of eight consecutive fEPSPs from the Schaffer collateral CA1 pathway were obtained and quantified as the slope of the initial phase of the potential. Recordings were obtained with an Axoclamp 2B amplifier

(Molecular Devices), digitized and continuously stored on a personal computer with the WinLTP program (Anderson and Collingridge, 2001).

LTP induction

LTP was induced after obtaining a stable recording of fEPSP (each fEPSP is the average of eight individual fEPSPs) slope in the Schaffer collateral pathway for at least 30min. LTP was induced by a theta-burst protocol (10 trains separated by 200ms, four pulses each, 100Hz) in the Schaffer collaterals/CA1 synapse. The intensity of the stimulus was kept constant throughout these induction protocols. LTP was quantified as the percentage of change in the average slope of the fEPSP taken from 46 to 60min after LTP induction in relation to the average slope of the fEPSP measured during the 10min that have preceded the induction of LTP.

Glycation studies in human tissue

Human brain fragments from PD, Dementia with Lewy bodies, and control individuals were kindly provided by the Pathology Department, Hospital de Santa Maria and by Prof. Matthew Frosch from the Massachusetts Alzheimer's Disease Research Center. Protein samples were prepared as in (Vicente Miranda *et al.*, 2013). For immunobloting, we used anti aSyn (BD Transduction laboratories, S63320, 1:3000) and anti N^{ε}-(carboxyethyl) lysine (CEL) (Cosmobio, CAC-AGE-MG02, 1:500).

Mass spectrometry analysis

Total protein extracts from *glo1Δ* yeast expressing aSyn, H4 cells expressing aSyn treated with MGO (0.5 mM) and brain samples from B6D2F1 wild-type mice or Wistar wild-type rat were processed as in (Vicente Miranda *et al.*, 2013). Mass spectrometry was performed on an Applied Biosystems 4700 Proteomics Analyzer with TOF/TOF ion optics as previously described (Vicente Miranda *et al.*, 2013). All peptide mass values were considered monoisotopic, a MS mass tolerance was set at 100 ppm. Trypsin and endoproteinase Glu-C were assigned as digestion enzymes of aSyn. A triple miss cleavage was allowed and oxidation of methionyl residues, acetylation of the N-terminal, and carboxyethylation (CEL) of lysine residues were assumed as variable modifications. All peaks with S/N greater than 5 were included for matching against *in silico* digestion of corresponding aSyn sequence (*Homo sapiens*, *Mus muscullus* or *Rattus*) in mMass software (Strohalm *et al.*, 2010).

aSyn recombinant protein expression and purification

E. coli BL21 (DE3) pLysS competent cells (Novagen, San Diego, CA, USA) were transformed with human aSyn WT, A30P, A53T and E46K PT7-7 constructs. Expression and purification was performed as previously described (Vicente Miranda *et al.*, 2013) with the following changes: anion exchange was performed in Hitrap Q XL and size-exclusion in SuperdexTM 200 10/300 (GE Heathcare, Uppsala, Sweden). Protein concentration was determined by UV absorbance at 275nm ($\varepsilon_{aSyn275}$= 5600$M^{-1}cm^{-1}$). For ^{15}N-labelling of aSyn WT, cells were grown in M9 medium supplemented with ^{15}N-labeled ammonium chloride.

Kinetics of aSyn fibril formation

Solutions of human recombinant aSyn (100 µM) were agitated at 37 °C in the presence of MGO. Fibril formation was monitored with Thioflavin T (ThT) binding assay as previously described (Naiki *et al.*, 1989; Naiki *et al.*, 1990). Fluorescence measurements were performed using a Perkin Elmer LS50B spectrofluorimeter, in quartz cuvettes with 1 cm excitation light path. ThT fluorescence was recorded immediately after ThT binding from 470 to 600 nm with excitation at 450 nm, an increment of 0.5 nm, an integration time of 1 s and 5 nm slits for both excitation and emission. For each sample, the signal was obtained as the ThT intensity at 482nm from which was subtracted a blank measurement recorded prior to the addition of aSyn to the ThT solution.

Secondary structure kinetic analysis by circular dichroism

Secondary structure analysis of MGO-incubated aSyn was performed by far-UV (185-260nm) circular dichroism (CD) in a Jasco J810 spectropolarimeter equipped with a temperature control unit Julabo F25. Far-UV CD spectra were recorded in solutions of a 100 µM of aSyn in a 0.01 cm (linear) path length quartz cuvette at 37 °C in 50 mM potassium phosphate buffer, pH 7.4, with 150 mM of NaF. For each spectrum, three scans were averaged.

aSyn oligomer formation analysis by size-exclusion chromatography (SEC)

Oligomerization of human aSyn upon methylglyoxal glycation was monitored by size-exclusion chromatography (SEC). Solutions of monomeric aSyn treated with vehicle (PBS) or MGO (5 mM) were incubated and agitated at 37 °C. Samples (50 µl at 100 µM)

were analysed by SEC at defined incubation times, after filtration with a 0.2 µm Whatman filter. SEC was performed with HPLC Jasco PU-2080 Plus isocratic pump with a UV detector Jasco 2075. The mobile phase was 50 mM PBS pH 7.4 with 150 mM NaF. Separation was achieved on a molecular exclusion analytical column (GE-Healthcare Superdex 75 10/300 GL) at a flow rate of 0.4 ml/min. Eluting peaks were monitored at 275 nm.

aSyn oligomer formation analysis by dynamic light scattering (DLS)

Oligomer formation was monitored by DLS as previously described (Martins *et al.*, 2008; Faustino *et al.*, 2014). DLS experiments performed on a Malvern Zetasizer Nano ZS (Malvern, UK) with backscattering detection at 173°, equipped with a He-Ne laser ($\lambda = 632.8$ nm), using glass cuvettes with round aperture at 25 °C. Agitated aSyn (30h at 900 rpm), treated with Tris-buffer or MGO (0.5 mM) was diluted to 7 µM in Tris-buffer. Samples were allowed to equilibrate for 15 min at 25 °C before each 10 measurements set (each set is the average of 10 runs, with 10 s per run). Each experiment was repeated at least 3 times. Data was evaluated in Zetasizer Nano ZS software (Malvern).

Nuclear magnetic resonance (NMR) spectroscopy

MGO-glycation of aSyn was obtained by incubating 50 µM of protein with 4.6 molar excess of MGO in 20 mM sodium phosphate buffer pH 7.5. After 2.5 days of reaction at 15 °C, buffer was exchanged to HEPES 25 mM pH 7.0 NaCl 50 mM. ^{1}H-^{15}N HSQC spectra of wild type and glycated ^{15}N-labelled aSyn samples were acquired at 15

°C on a 600 MHz Bruker spectrometer, in HEPES 25 mM pH 7.0 NaCl 50 mM, 10 % D_2O. aSyn backbone resonance assignment has been transferred from previous studies (Bertoncini *et al.*, 2005). In case of glycated aSyn, peak center has been adjusted only in regions of small signal overlap. Peaks affected by severe overlap were excluded from the analysis. NMR data were processed and analyzed by using NMRPipe (Delaglio *et al.*, 1995) and Sparky (T. D. Goddard and D. G. Kneller, University of California, San Francisco).

aSyn binding studies to small unilamellar vesicles (SUV)

Small Unilamellar Vesicles (SUVs) were prepared using 1-palmitoyl-2-oleoyl-sn-glycero-3-phosphocholine (POPC) and 1-palmitoyl-2-oleoyl-sn-glycero-3-phosphate (POPA) (Avanti Polar Lipids), at 1:1 molar ratio following the procedure described in (Karpinar *et al.*, 2009). SUVs were prepared in HEPES 25 mM pH 7.0 NaCl 50 mM. Starting from 12.5 mM total lipid concentration, the SUVs, isolated after sonication and ultracentrifugation, showed a hydrodynamic diameter of 25 ± 4 nm as determined by DLS. Again, MGO-glycation of aSyn was obtained by incubating 50 µM of protein with 4.6 molar excess of MGO in 20 mM sodium phosphate buffer pH 7.5. After 2.5 days of reaction at 15 °C, buffer was exchanged to HEPES 25 mM pH 7.0 NaCl 50 mM.

Far-UV CD spectra were recorded at 20 °C using 1 mm-length Hellma quartz cuvette in Chirascan (Applied Photophysics, UK) spectrometer, with 0.5 nm bandwidth. Samples were measured at 7 µM protein concentration in 5 mM sodium phosphate buffer pH 7.0. To obtain the spectra of free and SUV-bound aSyn, measurements were done in triplicate

and the contribution of buffer and vesicles to the CD signal was subtracted as appropriate.

Transmission electron microscopy

5 µl of aggregated aSyn (100 µM) treated with vehicle (PBS) or MGO (5 mM) was applied to carbon-coated Formvar 200 mesh grids (Electron Microscopy Sciences) and incubated at RT for 60 s. The grids were then washed sequentially by depositing 10 µl droplets of double distilled sterile water (2x) followed by a 10 µl droplet of fresh 2 % (w/v) uranyl acetate, which remained on the grid for 30 s. After each step, the excess solution was blotted with Whatman filter paper, and the grids were vacuum-dried from the edges. The samples were analysed using a Phillips CM-10 TEM microscope operated at 100kV acceleration voltage.

aSyn clearance

For CHX chase experiments, H4 cells were transfected as previously (Vicente Miranda *et al.*, 2013) with pSI-aSyn plasmid. After 24h, cells were treated with vehicle (H_2O) or MGO (0.5 mM) for 16 h. Media was renewed and cells re-challenged with vehicle or MGO for 24 h in the presence of cycloheximide (100 µM, added at given time points). Protein extracts were immunobloted.

Proteasome impairment was assessed as the amount of GFPu accumulation. H4 cells were cotransfected with E.V. with GFPu; aSyn with GFPu or SynT with GFPu. 24h post transfection, media was renewed and cells treated with vehicle (H_2O) or MGO

(0.5 mM) for 16 h and processed for immunobloting with anti-GFP antibody (NeuroMab, P42212).

For autophagy impairment studies, H4 cells were transfected with E.V., with aSyn or co-transfected with SynT together with Synph 1. 24h post transfection, media was renewed and cells treated for 16 h with vehicle (H_2O) or MGO (0.5 mM). Media was again renewed and cells were re-challenged with vehicle or MGO during autophagy blockage with ammonium chloride (20 mM) together with leupeptin (200 µM) for 2 h. Autophagy activity was measured as the amount of accumulated LC3 after treatment with autophagy blockers as previously (Macedo *et al.*, 2015). P62 basal levels were also assessed in cells treated with vehicle or MGO (0,5 mM),for 16h. Then, the media was renewed and cells were treated again with vehicle or MGO for 4h (SQSTM1 D-3, sc-28359, 1:3000).

For aSyn release studies, H4 cells, co-transfected with SynT and Synph 1 for 24 h were treated with MGO (0.5 mM) for 16 h. Media was renewed, and cells were again treated with MGO (0.5 mM) for 6 h, media collected, applied in Dot-blot system and immunobloted with anti-aSyn by standard procedures.

In vitro ubiquitination assays

Recombinant aSyn was glycated in vitro as described above. Both glycated or non-glycated aSyn were incubated in a reaction mixture containing 40 mM Tris-HCl (pH 7.6), 5 mM $MgCl_2$, 2 mM DTT, 1 mM ATP-γ-S, 7.5 µg ubiquitin, 1 µM ubiquitin aldehyde, 100 ng E1 and 200 ng UbcH5b, in the presence or absence of 500 ng SIAH-2. Samples were incubated at 37 °C for 1 h, and the reaction was stopped by the addition of

SDS sample buffer. Samples were immunobloted and mono-ubiquitinated aSyn determined using an anti-aSyn antibody.

MGO scavengers treatment in H4 cells

24h after SynT and Synph 1 co-transfection, cells seeded at 20 000 cells cm^2 in 35 mm imaging dishes (Ibidi) or seeded at 30 000 cells cm^2 in 6-well plates (TPP) were treated with vehicle (H_2O), MGO (0.5mM), AG (100 or 250μM), TS (100 or 250μM) or co-treated with vehicle or MGO (0.5mM) with AG (250 μM) for 16h. aSyn clearance assays were also performed in the presence of AG (250 μM) or TS (250 μM).

Treatment of Drosophila with Aminoguanidine hydrochloride or tenilsetam

Aminoguanidine hydrochloride (SIGMA: 396494), dissolved in PBS, Tenilsetam (Axon Medchem, Axon 1470) dissolved in DMSO, PBS or DMSO were added to standard maize media at the required doses (100 or 300 μM). Newly emerged flies were placed on the drug food and kept for 10 days changing them daily with freshly prepared food containing the compound. Climbing activity was assessed at day 10.

Compliance with Ethical Standards

The human samples used in our study were obtained from the ADRC at MGH, Boston, so all ethical considerations were taken into account. Animal work was performed with the approval from the animal care committee of IMM, Lisbon, Portugal.

Results

MGO induces aSyn aggregation and toxicity in cell models of PD

First, we investigated the effect of MGO on aSyn aggregation and toxicity in yeast cells constitutively expressing aSyn (Outeiro and Lindquist, 2003). We modulated MGO levels, using either increased amounts of D-glucose in the media, or genetically, using *Glo1* (*Δglo1*) or triose phosphate isomerase (*Tpi*) deletion (*Δtpi*) strains, conditions known to increase the levels of MGO and promote the formation of AGEs (Gomes *et al.*, 2005; Guix *et al.*, 2009; Orosz *et al.*, 2009). We found that these glycation-promoting conditions increase MGO levels ~3-fold (Fig S1 A). Glycating conditions increased both the percentage of cells with aSyn inclusions (Fig. 1 A), and aSyn toxicity in *Δglo1* and *Δtpi* mutant cells expressing WT aSyn (Fig. 1 B). Similar results were obtained with the PD-associated aSyn familial mutants A53T or E46K (Fig. S1 B, C). The increased toxicity upon glucose treatment was further confirmed by assessing yeast viability, and we observed a reduction in the number of CFUs (Fig. S1 D).

To further assess the effect of glycation on aSyn aggregation and toxicity, human H4 cells were co-transfected with an aggregation-prone variant of aSyn, known as SynT (full-length aSyn fused with the first 83 amino acids of GFP), together with synphilin-1 (Synph 1), an aSyn-interacting protein that potentiates aSyn aggregation (McLean *et al.*, 2001). As we previously reported, this model facilitates the visualization of aSyn inclusions, in contrast with the expression of unmodified aSyn, that does not form inclusions (Klucken *et al.*, 2012; Basso *et al.*, 2013; Guerreiro *et al.*, 2013; Lazaro *et al.*, 2014). We selected 0.5 mM MGO as the working concentration since it increased protein glycation without increasing overall cytotoxicity in naïve cells (Fig. S2 A-C). We found that this concentration, widely used in various studies (Nass *et al.*, 2014; Chang *et al.*,

2016; Hansen *et al.*, 2016), increased the levels of MGO ~1.4-fold (Fig. S2 D). Treatment with MGO resulted in a striking increase in the percentage of cells with inclusions (from ~51 % to ~85 %). We also observed an increase in the number of inclusions per cell (~17 % to ~35 % increase of cells displaying at least 10 inclusions, or ~34 to ~62 % within cells with inclusions) (Fig. 1 C). Although MGO induced cytotoxicity in E.V. transfected cells, MGO increased aSyn toxicity (2.5-fold vs vehicle treated SynT + Synph 1) (Fig. 1 D), and induced both aSyn Triton X-100 insolubility (3-fold vs Ctrl) (Fig. 1 E), and the formation of high molecular weight species, as assessed in 5-30 % sucrose gradients (Fig. 1 F). The combination of MGO treatment in aSyn-expressing cells elicited a significant increase in cytotoxicity, but each insult alone was also cytotoxic. Therefore, it remains to be further investigated whether the combination of both insults represents a synergistic effect. We also assessed whether MGO induced aSyn glycation. For this, we immunoprecipitated aSyn from cells expressing aSyn or from cells co-expressing SynT and Synph 1 after treatment with MGO (0.5 mM). Remarkably, we observed an increase in the levels of glycated aSyn or SynT (Fig. 1 G). This was also observed in whole cell lysates, where the glycation levels of several proteins are increased upon treatment with MGO (Fig. S2 E): However, the levels of Synph 1 were not altered in glycating conditions (Fig. S2 F).

MGO induces aSyn toxicity in DA-neural iPSCs and DA-LUHMES cells

We next asked whether the correlation between aSyn expression and MGO-induced toxicity was conserved in human neurons. For this, we evaluated the effects of MGO in two different dopaminergic (DA) cell models: differentiated human DA-neural

induced pluripotent stem cells (iPSCs) and Lund human mesencephalic cells (LUHMES). iPSCs, derived from dermal fibroblasts from a patient carrying a triplication of the *SNCA locus* and from an age-matched healthy relative (Byers *et al.*, 2011), were cultured and differentiated into DA neurons according to established protocols (Mak *et al.*, 2012; Oliveira *et al.*, 2015). LUHMES cells transduced with lentiviruses encoding aSyn-IRES-GFP or IRES-GFP, were differentiated into TH-positive neurons (DA-LUHMES) (Scholz *et al.*, 2011). Both types of human cells were treated with increasing concentrations of MGO. We observed a dose-dependent increase in MGO toxicity in terminally differentiated iPSCs carrying the *SNCA* gene triplication (SNCA 3X) (Fig. 1 H) (Byers *et al.*, 2011). To determine whether toxicity was indeed associated with the expression of aSyn, we knocked down aSyn using shRNA (SNCA 3X KD) as in (Oliveira *et al.*, 2015) (Fig. 1 I). This reduced MGO-induced toxicity (Fig. 1 H), confirming the interplay between MGO and aSyn. Likewise, DA-LUHMES cells expressing aSyn were more sensitive to MGO compared both to GFP-expressing and to non-transduced cells (Fig. 1 J), as observed through the appearance of dystrophic processes (Fig. 1 K). Together, these results revealed a strong connection between increased levels of aSyn and glycating conditions.

Glycation decreases motor performance, lifespan and survival in Drosophila

We next asked whether MGO-induced aSyn toxicity affected motor performance. To address this, we used an established *Drosophila* model of PD based on the pan-neuronal expression of human aSyn via the GAL4/UAS system (Feany and Bender, 2000) and interrogated whether genetic modulation of glycation, via knockdown of *Glo1*

or *Tpi*, altered aSyn-induced defects. We previously observed that knockdown of *Glo1* or *Tpi* increases the overall levels of glycation (Vicente Miranda *et al.*, 2016b), a phenotype that was also confirmed in this study (Fig. 2 A). Importantly, we observed that knockdown of *Glo1* or *Tpi* alone did not elicit neurodegeneration, as assessed by counting the number of rabdomeres (photoreceptors) (Vicente Miranda *et al.*, 2016b). Here, we observed that aSyn expression significantly impaired motor performance (measured as climbing ability, due to negative geotaxis) of the flies and, importantly, when aSyn was expressed in the RNAi lines, the climbing impairment was aggravated (Fig. 2 B, C and Fig. S3 A). Nevertheless, *Tpi* or *Glo1* knockdown also elicited a climbing impairment per si.

In addition, the maximal lifespan in *Glo1* knockdown reduced 2 days (comparing to non-silenced aSyn expressing flies) (Fig. 2 D). Although silencing of *Tpi* shortened the lifespan by 4 days in both WT flies and aSyn expressing flies (Fig. 2 E), we observed a striking decrease in survival starting 6 days post-eclosion (by day 13, 77 ± 4 % vs. 93 ± 3 %) survival for aSyn expressing flies (Fig. 2 E and Fig. S3 B).

Glycation induces neuronal loss in a mouse model of PD and impairs synaptic transmission in brain slices

Next, to determine whether glycation modulates aSyn toxicity in the brain *in vivo*, we evaluated the effects of MGO in Tg mice expressing human aSyn under the control of the Thy1 promoter. We injected MGO and PBS in the two hemispheres (in the substantia nigra (SN) or striatum) of aSyn Tg or WT control mice. Immunohistochemical analyses revealed a marked decrease in the number of TH-positive neurons in the MGO-injected

side of the aSyn Tg mice, when compared to the PBS-injected side (Fig. 3 A). Neuritic degeneration was also evident in the striatum, where the terminals of the nigral TH-positive neurons are located (Fig. 3 A). Remarkably, we detected high levels of CEL immunoreactivity only in the MGO-injected SN of aSyn Tg mice, but not in the MGO-injected WT control SN (Fig. 3 B). Stereology analyses showed that injection of MGO induced a 32.9 ± 3.5 % loss of TH-positive neurons, a 46 ± 5.1 % loss of VMAT, and a 43.0 ± 3.0 % loss of DAPI positive neurons (as a percentage of the PBS-injected side, comparing to 9.6 ± 5.7; 9.7 ± 3.4; and 5.8 ± 7.4 % loss of TH, VMAT or DAPI positive neurons in WT mice) (Fig. 3 C). We should highlight that the results shown do not simply correspond to the total number of labeled neurons (TH, VMAT or DAPI), but to the percentage of neurons normalized to the corresponding control (MGO/PBS in WT mice – black bars, or MGO/PBS in aSyn Tg mice – green bars). Immunostaining for TH in coronal sections (revealed with DAB) confirmed that TH-positive neuronal loss was specifically observed in aSyn Tg mice injected with MGO (Fig. S4 A). When MGO was injected in the striatum, we also found a significant loss of NeuN-positive neurons in aSyn Tg animals (13.5 ± 3.9 %), while WT animals were almost unaffected (3.7 ± 1.7 %) (Fig. S4 B). In addition, striatal TH fiber density was reduced in both the aSyn Tg and WT control animals, but was much more pronounced in aSyn Tg mice (18.6 ± 4.1 vs. 7.1 ± 2.2 %) (Fig. S4 B).

To establish whether MGO also promoted aSyn glycation, we enriched aSyn from striatal-injected extracts (Vicente Miranda *et al.*, 2013) and measured the levels of N-ε-(carboxyethyl)lysine (CEL), the AGE derived from the reaction of MGO with lysine residues of proteins (Ahmed *et al.*, 1997), on aSyn. Since we showed by IP that aSyn was

glycated and that glycated aSyn migrated with an identical molecular weight to that of aSyn (Fig. 1 G), we assumed that the CEL protein band overlapping with aSyn, corresponded to glycated aSyn. Upon quantification, we found that aSyn glycation increased ~2-fold in MGO-injected aSyn Tg animals (Fig. 3 D).

Interestingly, we found high reactivity against aggregated aSyn in the SN of the MGO-injected aSyn Tg mice (Fig. 3 E). By analyzing higher magnifications of SN sections, we observed aggregated aSyn both in cell bodies and neuronal processes (Fig. S5 A). In addition, we found stronger staining against phosphorylated aSyn (serine 129 phosphorylation, pS129) in the SN of MGO-injected aSyn Tg mice (Fig. S5 B) indicating increased aSyn pathology. pS129 signal was specifically present in surviving TH-positive neurons in MGO-injected aSyn Tg mice as well (Fig. S5 C).

Immunohistochemistry for aSyn in mice injected in the striatum revealed presynaptic staining for both WT and aSyn Tg mice. However, in aSyn Tg mice treated with MGO, aSyn was also found in cell bodies. Importantly, staining with methoxy-XO4 (MX), an amyloid-binding dye (Klunk *et al.*, 2002), revealed amyloid-like inclusions adjacent to the MGO injection site in the aSyn Tg mice (Fig. S5 D).

To assess whether glycation induced functional alterations on synaptic transmission, we used a paradigm based on the treatment of hippocampal brain slices with aSyn oligomeric species (Diogenes *et al.*, 2012). We found that aSyn that was previously glycated with MGO strongly impaired synaptic plasticity in the rat hippocampus (LTP_{aSyn} 47 ± 3%; $LTP_{aSyn\text{-}MGO}$ 22 ± 4%) (Fig. 3 F-I). Importantly, PBS or MGO (35 μM) treatment did not affect LTP (Fig. S6).

aSyn is glycated in human brains and increases with ageing in mice

To further assess the relevance of aSyn glycation in PD and other synucleinopathies, we analyzed the glycation pattern of aSyn in extracts from the cortex from human brain tissue enriched for aSyn (Vicente Miranda *et al.*, 2013). Using the previous assumption, we observed that samples derived from both control individual, without overt symptoms of neurological disorders, and from individuals diagnosed with PD or Lewy body dementia (LBD), showed reactivity for CEL. Strikingly, aSyn was also reactive for this modification (Fig. 3 J).

To establish whether this modification varied with ageing, as we predicted, we analyzed brain samples from WT mice or human aSyn BAC transgenic (Tg) mice at different ages. In Tg mice, the expression of human aSyn is controlled by the human promoter, thereby avoiding possible confounding issues associated with aSyn overexpression. Importantly, we observed that aSyn was reactive for CEL (overlaping signal), and that this reactivity increased with age in both WT (~1.3-fold increase in old vs young animals) and aSyn BAC Tg mice (2.3-fold increase in old vs young animals) (Fig. 3 K, L).

Glycation occurs mainly in the N-terminal region of aSyn

Given that aSyn was found to be glycated in human brain and in mouse models, we sought to identify where glycation occurred in aSyn. For this, we employed a proteomic approach (Vicente Miranda *et al.*, 2013). Briefly, we used mass spectrometry to analyze aSyn-enriched protein extracts from yeast Δ*glo1* cells expressing human aSyn, from human H4 cells expressing human aSyn treated with 0.5 mM MGO, and from

mouse and rat brain tissues. By matching the MS data with the m/z ratios calculated from in silico digested aSyn sequences (including CEL as variable PTM), we found that aSyn was mainly glycated in the N-terminal region (K6, K10, K12, K21, K23, K32, K34 and K43 and K45) in all samples analyzed (Fig. 3 M, Fig. S7 and Tables S1-16), hinting at possible effects on membrane binding and aggregation.

MGO promotes aSyn oligomerization and impairs lipid binding ability

MGO glycation was previously shown to interfere with amyloidogenesis by stabilizing intermediate species (Lee *et al.*, 2009; Oliveira *et al.*, 2011; Padmaraju *et al.*, 2011). Thus, we investigated whether MGO affected the aggregation of WT and of three mutant variants associated with familial PD (A30P, E46K, and A53T). In agreement with our previous findings (Oliveira *et al.*, 2011; Oliveira *et al.*, 2013), we found that, although glycation decreased aSyn fibril formation in vitro (Fig. 4 A and Fig. S8 A-C), it potentiated the formation of aSyn oligomeric species, as observed by size exclusion chromatography (SEC) analyses of MGO-treated vs. non-treated aSyn (30 h of fibrillization). We found that oligomeric aSyn species were only present in samples with MGO (elution at 28 and 18 min) (Fig. 4 B-D and Fig. S8 D). Consistently, analysis of the particle size distribution by dynamic light scattering (DLS), revealed a more heterogeneous size distribution of glycated aSyn, with a significant increase in particles with a hydrodynamic diameter above 2300nm (Fig. 4 C, D). Moreover, using transmission electron microscopy (TEM), we observed that vehicle-treated aSyn formed typical amyloid fibrils, whereas glycated aSyn formed amorphous aggregates and ring-

shaped particles (Fig. 4 E), consistent with aSyn oligomers (Lashuel *et al.*, 2002a; Lashuel *et al.*, 2002b).

To assess the effects of glycation on the structure of aSyn, we performed NMR analyses. We found that glycation induced a 76 % reduction of the NMR backbone $^{1}H^{15}N$ signals up to residue 64, demonstrating the N-terminal region of aSyn was the most affected (Fig. 4 F, G). The N-terminal domain of aSyn is involved in lipid-binding (Jo *et al.*, 2000). Interestingly, we observed that glycation impaired the typical transition between random-coil and α-helical structure, which occurs when aSyn binds to small unilamellar vesicles (SUV) (Fig. 4 H).

Glycation blocks aSyn ubiquitination and impairs its clearance and release

As described above, we found that aSyn was glycated in the N-terminal region (Fig. 3 M, Fig. S7 and Tables S1-16). Interestingly, several of those lysine residues are also known aSyn ubiquitination sites (Nonaka *et al.*, 2005; Anderson *et al.*, 2006). We hypothesized that if aSyn is glycated this might impair its normal ubiquitination and clearance. To investigate the mechanism through which MGO glycation potentiated aSyn-associated pathologies, we used a human cell model of aSyn aggregation (H4 cells, SynT-synphylin model). Strikingly, while we observed several ubiquitin and aSyn-positive inclusions in vehicle treated cells (as in LBs), no co-staining was observed in MGO-treated cells (Fig. 5 A). To further confirm that glycation competed ubiquitination, we performed an in vitro assay using SIAH-2, an E3 ubiquitin ligase known to ubiquitinate aSyn. We observed that mono-ubiquitination of aSyn was reduced from 43 to 13 % (Fig. 5 B).

Next, we followed the clearance of aSyn in cells upon blocking *de novo* protein synthesis with cycloheximide (CHX). Importantly, we found that MGO treatment reduced aSyn clearance (Fig. 5 C). To further dissect the effects of glycation on aSyn clearance, we investigated the activity of known aSyn clearance pathways (Ebrahimi-Fakhari *et al.*, 2012). First, to assess the effects on the ubiquitin proteasome system (UPS), we used an unstable version of GFP (GFPu) that reports on the overall activity of the UPS (Bence *et al.*, 2001). In control cells, no accumulation of GFP was observed. Upon aSyn expression, GFP accumulated in both vehicle and MGO-treated cells but the levels were ~2.5-fold higher in MGO vs PBS-treated cells (Fig. 5 D). Together, our data indicate that UPS impairment is potentiated when aSyn is glycated.

Second, to study the effect of glycation on the autophagy-lysosome pathway (ALP), we treated cells with a combination of ammonium chloride (NH_4Cl) and leupeptin (leup), known blockers of autophagy, according to established guidelines (Klionsky *et al.*, 2016). We observed that MGO severely decreased LC3-II levels in either aSyn or SynT expressing cells (~90 % decrease) (Fig. 5 E). Consistently, we found that the basal levels of P62 were increased (Fig. S9 A). These data indicate that glycation impairs the ALP.

Finally, as aSyn can be released from cells (Marques and Outeiro, 2012), we assessed whether this could also be affected by glycation. Interestingly, we found a significant reduction in aSyn release in cells treated with MGO (~50 % decrease), therefore contributing to the intracellular accumulation of aSyn (Fig. 5 F).

MGO scavengers correct the clearance of aSyn, reduce aggregation and toxicity, and alleviate motor phenotypes in *Drosophila*

Anti-MGO drugs such as aminoguanidine (AG) and tenilsetam (TS) are known scavengers of MGO (Webster *et al.*, 2005). Thus, we asked whether MGO scavenging could interfere with aSyn aggregation and toxicity. Importantly, both MGO scavengers reduced the intracellular levels of MGO by ~20 % (Fig. 6A), resulting in a decrease of aSyn aggregation and toxicity by 20 and 50 %, respectively (Fig. 6 B, C). In addition, treatment with either AG or TS reverted the impairment of aSyn clearance upon glycation (Fig. 6 D and Fig. S9 B).

To further assess the therapeutic potential of AG and TS, we tested their effect in vivo, using *Drosophila*. Strikingly, treatment with AG or TS for 10 days improved the motor performance of aSyn expressing flies in a dose-dependent manner. Treatment with AG resulted in an improvement from 15 ± 1 %, to 30 ± 2 % with 100 µM, and to 37 ± 2 % with 300 µM (Fig. 6 E). With TS, we observed an improvement from 34 ± 1 %, to 48 ± 2 % with 100 µM, and to 54 ± 2 % with 300 µM (Fig. 6 F).

Discussion

At present, the understanding of the molecular mechanisms underlying neurodegeneration in PD and other synucleinopathies is still limited. In particular, the age-dependency of most neurodegenerative disorders is intriguing, suggesting common factors may play important roles in both processes. While aSyn misfolding and

accumulation is a major pathological hallmark in synucleinopathies, aSyn mutations occur only in a small fraction of all PD cases. Thus, it is logical to think that non-genetic factors, such as PTMs, might modulate the aggregation and toxicity of aSyn, since this is common among idiopathic and familial forms of synucleinopathies. Indeed, phosphorylation on S129 and in other sites has been extensively studied and found to modulate aSyn aggregation and toxicity in various model systems (Wang *et al.*, 2012; Tenreiro *et al.*, 2014a). However, during the normal lifetime of aSyn, several other PTMs are likely to occur, thereby modulating its normal behavior (Oueslati *et al.*, 2010; Gonçalves *et al.*, 2012; Beyer and Ariza, 2013). In this context, we propose that particular PTMs may act as 'second-hits' that induce structural and stability alterations, thereby potentiating aSyn aggregation and toxicity.

Although diabetes has been extensively linked to neurodegenerative diseases (Hu *et al.*, 2007; Sun *et al.*, 2012; Crane *et al.*, 2013; Vagelatos and Eslick, 2013; Vicente Miranda *et al.*, 2016a), the molecular basis for this connection remains unclear. A known consequence of increased glucose levels is the, unavoidable, age-associated modification of specific amino acid residues in proteins in a process known as glycation, altering protein structure and function (Vicente Miranda and Outeiro, 2010). Importantly, we recently found that glycation potentiates neurodegeneration in models of Huntington's disease (Vicente Miranda *et al.*, 2016b), further suggesting an association between hyperglycemia and neurodegeneration. Strikingly, a recent clinical trial revealed that a drug used to treat diabetes resulted in improvements in both motor and cognitive metrics in PD subjects (Aviles-Olmos *et al.*, 2013). Here, we demonstrated that glycation, a direct

consequence of diabetes, might play an important and underappreciated role in PD and other synucleinopathies by modulating aSyn biology (Fig. 7).

Exploiting a yeast model of aSyn-mediated cellular pathologies, we found that glycation exacerbates aSyn toxicity and aggregation, and we then showed this effect was conserved in human cell lines and, importantly, in differentiated patient-derived iPSCs. Interestingly, upon knock down of aSyn in iPS cells, the cytotoxicity of MGO is abolished, confirming that cytotoxicity is associated with the levels of aSyn.

Next, we evaluated the effects of glycation in animal models of PD. Remarkably, by promoting aSyn glycation through genetic or pharmacological manipulation of MGO levels, we recapitulated several pathological alterations in both aSyn transgenic *Drosophila* and mice. Glycation not only reduces the motor performance of aSyn expressing flies, but also decreases survival. In aSyn expressing mice, MGO injection in the SN causes an impressive loss of neuronal cells, including TH-positive neurons. Neuritic degeneration extended to the striatum, a region innervated by dopaminergic neurons from the SN. We also found extensive labeling for aggregated aSyn in SNpc and of pS129 aSyn, confirming that glycation induces the aggregation of aSyn and leads to the accumulation of pathological aSyn.

To further establish that aSyn glycation can indeed affect neuronal function, we used a functional paradigm that enables us to assess the effects of aSyn on synaptic transmission. As an experimental paradigm, we used rat hippocampal brain slices (Diogenes *et al.*, 2012). Indeed, we found that glycated aSyn impairs hippocampal long-term potentiation.

The concentrations of MGO used in our study are within, or below, the range used in other studies, and resulted in an increase in the levels of intracellular MGO (~36%). Importantly, our findings are strongly backed up by genetic manipulations in yeast and flies and, therefore, constitute proof of concept that glycation of aSyn exacerbates its aggregation and toxicity. Strikingly, we demonstrate that glycated aSyn is present in aged human brains. Given the low number of available human brain samples, and the fact that all samples were derived from elderly individuals (>73 years old), we could not establish whether the levels of CEL-glycated aSyn were higher in disease vs. control brains. Thus, future studies with larger numbers of human brain samples should enable additional confirmation. Nevertheless, using brain tissue from WT or human aSyn BAC transgenic mice (expressed under the regulation of the human aSyn promoter), we observed that the levels of glycated aSyn increase with age. These findings strongly support our hypothesis that glycation might be associated with synucleinopathies in an age-dependent manner.

Our in vitro studies provide valuable mechanistic insight into the effects glycation has on aSyn. We found it increases aSyn oligomerization and interferes with the N-terminal structure of the protein, reducing the ability of aSyn to bind to lipid membranes. Together, these findings confirm that glycation may perturb the physiological role of aSyn on vesicular trafficking (Nemani *et al.*, 2010; Scott *et al.*, 2010).

Given that CEL-glycation occurs specifically in lysine residues, we asked whether it affected aSyn ubiquitination and clearance. Our findings confirm our hypothesis, and demonstrate that MGO-treatment, reduced aSyn ubiquitination, reduced UPS- (in the aSyn aggregation model) and ALP-mediated degradation of aSyn, and also the release of

aSyn from cells. It is possible that the proteasome dysregulation induced by aSyn in the conditions tested saturates the system, limiting the ability to detect an additional accumulation of GFPu under glycation conditions. Overall, the failure in these proteostasis components contributes for the accumulation, aggregation and cytotoxicity of aSyn.

Finally, we sought to demonstrate the potential value of pharmacological modulation of glycation in models of synucleinopathy. Using anti-glycation agents, we could attenuate or revert the phenotypes observed. Remarkably, we demonstrate that anti-MGO treatment improves motor performance *in vivo* in aSyn-expressing flies, and reduces both aSyn aggregation and toxicity in cultured cells by restoring aSyn clearance.

Generally, glycation is responsible for increasing oxidative stress and inflammation via activation of the receptor for AGE (RAGE) (Bierhaus *et al.*, 2001; Vicente Miranda and Outeiro, 2010). Thus, our findings are in line with previous studies reporting elevated RAGE levels in PD tissue (Dalfo *et al.*, 2005). Since RAGE ablation was shown to protect against MPTP/MPP^+-induced dopaminergic cell loss (Teismann *et al.*, 2012), we hypothesize that strategies aimed at blocking RAGE might prove valuable in PD.

Our findings further support the hypothesis that hyperglycemia, which directly correlates with increased levels of MGO, might play an unanticipated role in the molecular basis of PD and other synucleinopathies through the modulation of aSyn aggregation, accumulation, and toxicity. This is strongly supported by the fact that diabetes is considered to be a risk factor for PD (Vicente Miranda *et al.*, 2016a). Importantly, a direct genetic association between glycation and PD is already known,

although it has not been explored. This link comes from the fact that mutations in DJ-1 (*PARK7*), a protein recently shown to be an anti-MGO enzyme with glyoxalase and deglycase activities (Lee *et al.*, 2012; Mihoub *et al.*, 2015; Richarme *et al.*, 2015), are associated with recessive forms of PD. Importantly, DJ-1 restores the activity of several glycated proteins, including glyceraldehyde-3-phosphate dehydrogenase, aldolase and aspartate aminotransferase. Thus, PD cases associated with DJ-1 mutations might result from excessive protein glycation. Consistently, we already established a physical interaction between DJ-1 and aSyn, and showed that human WT DJ-1 as well as yeast DJ-1 orthologues, protect against aSyn toxicity (Zondler *et al.*, 2014). In our view, this constitutes an important link that is only now beginning to be appreciated, and suggests that the modulation of anti-glycation enzymes, such as DJ-1 or *Glo1* (as we demonstrate in the present study), or the direct manipulation of MGO levels using scavengers, constitute novel and attractive strategies for therapeutic intervention in synucleinopathies.

Altogether, our study suggests that glycation may constitute a missing link in our understanding of the molecular pathogenesis of PD and other synucleinopathies, acting as a 'second hit' that increases the risk for disease onset, at least in a significant subset of synucleinopathy patients.

Acknowledgements

LUHMES cells were a kind gift of Dr. M. Leist, University of Konstanz, Germany. Methoxy-XO4 was a kind gift from Dr. William E. Klunk, University of Pittsburgh, USA. We thank Professor Rui Moreira and Dr. Susana Lucas for assistance with MGO purification and measurement, and Diana Macedo for assistance with flow

cytometry. We acknowledge the Pathology Department of Hospital de Santa Maria (Lisbon) and to Prof. Matthew Frosch from the Massachusetts Alzheimer's Disease Research Center for kindly providing the human brain samples used in our study. We acknowledge Ana Chegão and Bárbara Gomes for technical assistance during the revision process of the manuscript.

Funding

Authors were supported by: HVM (Fundação para a Ciência e Tecnologia (FCT), Portugal SFRH/BPD/64702/2009; EU FP7 project MEFOPA), LMAO (FCT - SFRH/BD/23604/2005; CIRM-BMFB joint grant, 315050 AZ0101-31P6855), RMO and TS (FCT SFRH/BPD/41416/2007; SFRH/BPD/31209/2006); WX (Deutsche Forschungsgemeinschaft, SFB539/A3); CB and FG (Parkinson's UK and the Medical Research Council, UK). SE is supported by Israel Academy of Sciences, Rappaport Family Institute for Research in the Medical Sciences, The Allen and Jewel Prince Center for Neurodegenerative Disorders of the Brain. TFO (EMBO Installation Grant; Marie Curie IRG, Neurofold; DFG Center for Nanoscale Microscopy and Molecular Physiology of the Brain; ICM (FCT SFRH/BPD/74287/2010; Investigador FCT IF/00772/2013). This work was supported by: FCT PTDC/SAU-NEU/105215/2008, PTDC/QUI/73430/2006, PTDC/SAU-ENB/117013/2010, PTDC/NEU-OSD/5644/2014; EU FP7 project MEFOPA; CIRM-BMFB joint grant (315050 AZ0101-31P6855); Max Planck Society; and European Union (NEURASYNC PITNGA-2009-238316).

Supplementary material

Supplementary Figures 1-9

Supplementary Movie 1

Supplementary Tables 1-16

References

Ahmed MU, Brinkmann Frye E, Degenhardt TP, Thorpe SR, Baynes JW. N-epsilon-(carboxyethyl)lysine, a product of the chemical modification of proteins by methylglyoxal, increases with age in human lens proteins. The Biochemical journal 1997; 324 (Pt 2): 565-70.

Ali YO, Escala W, Ruan K, Zhai RG. Assaying locomotor, learning, and memory deficits in Drosophila models of neurodegeneration. Journal of visualized experiments : JoVE 2011(49).

Anderson JP, Walker DE, Goldstein JM, de Laat R, Banducci K, Caccavello RJ*, et al.* Phosphorylation of Ser-129 is the dominant pathological modification of alpha-synuclein in familial and sporadic Lewy body disease. J Biol Chem 2006; 281(40): 29739-52.

Anderson WW, Collingridge GL. The LTP Program: a data acquisition program for on-line analysis of long-term potentiation and other synaptic events. Journal of neuroscience methods 2001; 108(1): 71-83.

Aviles-Olmos I, Dickson J, Kefalopoulou Z, Djamshidian A, Ell P, Soderlund T*, et al.* Exenatide and the treatment of patients with Parkinson's disease. The Journal of clinical investigation 2013; 123(6): 2730-6.

Basso E, Antas P, Marijanovic Z, Goncalves S, Tenreiro S, Outeiro TF. PLK2 modulates alpha-synuclein aggregation in yeast and mammalian cells. Molecular neurobiology 2013; 48(3): 854-62.

Baynes JW, Thorpe SR. Glycoxidation and lipoxidation in atherogenesis. Free Radic Biol Med 2000; 28(12): 1708-16.

Bence NF, Sampat RM, Kopito RR. Impairment of the ubiquitin-proteasome system by protein aggregation. Science 2001; 292(5521): 1552-5.

Bertoncini CW, Jung YS, Fernandez CO, Hoyer W, Griesinger C, Jovin TM, *et al.* Release of long-range tertiary interactions potentiates aggregation of natively unstructured alpha-synuclein. Proceedings of the National Academy of Sciences of the United States of America 2005; 102(5): 1430-5.

Beyer K, Ariza A. alpha-Synuclein posttranslational modification and alternative splicing as a trigger for neurodegeneration. Molecular neurobiology 2013; 47(2): 509-24.

Bierhaus A, Fleming T, Stoyanov S, Leffler A, Babes A, Neacsu C, *et al.* Methylglyoxal modification of Nav1.8 facilitates nociceptive neuron firing and causes hyperalgesia in diabetic neuropathy. Nature medicine 2012; 18(6): 926-33.

Bierhaus A, Schiekofer S, Schwaninger M, Andrassy M, Humpert PM, Chen J, *et al.* Diabetes-associated sustained activation of the transcription factor nuclear factor-kappaB. Diabetes 2001; 50(12): 2792-808.

Byers B, Cord B, Nguyen HN, Schule B, Fenno L, Lee PC, *et al.* SNCA triplication Parkinson's patient's iPSC-derived DA neurons accumulate alpha-synuclein and are susceptible to oxidative stress. PloS one 2011; 6(11): e26159.

Castellani R, Smith MA, Richey PL, Perry G. Glycoxidation and oxidative stress in Parkinson disease and diffuse Lewy body disease. Brain Res 1996; 737(1-2): 195-200.

Chang TJ, Tseng HC, Liu MW, Chang YC, Hsieh ML, Chuang LM. Glucagon-like peptide-1 prevents methylglyoxal-induced apoptosis of beta cells through improving mitochondrial function and suppressing prolonged AMPK activation. Sci Rep 2016; 6: 23403.

Chen TS, Richie JP, Jr., Lang CA. The effect of aging on glutathione and cysteine levels in different regions of the mouse brain. Proceedings of the Society for Experimental Biology and Medicine Society for Experimental Biology and Medicine 1989; 190(4): 399-402.

Crane PK, Walker R, Hubbard RA, Li G, Nathan DM, Zheng H, *et al.* Glucose levels and risk of dementia. The New England journal of medicine 2013; 369(6): 540-8.

Dalfo E, Portero-Otin M, Ayala V, Martinez A, Pamplona R, Ferrer I. Evidence of oxidative stress in the neocortex in incidental Lewy body disease. J Neuropathol Exp Neurol 2005; 64(9): 816-30.

Delaglio F, Grzesiek S, Vuister GW, Zhu G, Pfeifer J, Bax A. NMRPipe: a multidimensional spectral processing system based on UNIX pipes. Journal of biomolecular NMR 1995; 6(3): 277-93.

Diogenes MJ, Costenla AR, Lopes LV, Jeronimo-Santos A, Sousa VC, Fontinha BM*, et al.* Enhancement of LTP in aged rats is dependent on endogenous BDNF. Neuropsychopharmacology : official publication of the American College of Neuropsychopharmacology 2011; 36(9): 1823-36.

Diogenes MJ, Dias RB, Rombo DM, Vicente Miranda H, Maiolino F, Guerreiro P*, et al.* Extracellular alpha-synuclein oligomers modulate synaptic transmission and impair LTP via NMDA-receptor activation. The Journal of neuroscience : the official journal of the Society for Neuroscience 2012; 32(34): 11750-62.

Ebrahimi-Fakhari D, Wahlster L, McLean PJ. Protein degradation pathways in Parkinson's disease: curse or blessing. Acta neuropathologica 2012; 124(2): 153-72.

Faustino AF, Carvalho FA, Martins IC, Castanho MA, Mohana-Borges R, Almeida FC*, et al.* Dengue virus capsid protein interacts specifically with very low-density lipoproteins. Nanomedicine : nanotechnology, biology, and medicine 2014; 10(1): 247-55.

Feany MB, Bender WW. A Drosophila model of Parkinson's disease. Nature 2000; 404(6776): 394-8.

Fredholm BB, Dunwiddie TV, Bergman B, Lindstrom K. Levels of adenosine and adenine nucleotides in slices of rat hippocampus. Brain Res 1984; 295(1): 127-36.

Frye EB, Degenhardt TP, Thorpe SR, Baynes JW. Role of the Maillard reaction in aging of tissue proteins. Advanced glycation end product-dependent increase in imidazolium cross-links in human lens proteins. J Biol Chem 1998; 273(30): 18714-9.

Gomes RA, Sousa Silva M, Vicente Miranda H, Ferreira AE, Cordeiro CA, Freire AP. Protein glycation in Saccharomyces cerevisiae. Argpyrimidine formation and methylglyoxal catabolism. Febs J 2005; 272(17): 4521-31.

Gonçalves S, Vicente Miranda H, Outeiro TF. Novel Molecular Therapeutics in Parkinson's Disease. In: Whitehouse D, Rapley R, editors. Molecular and Cellular Therapeutics. Chichester, UK: John Wiley & Sons, Ltd; 2012. p. 245-65.

Guerreiro PS, Huang Y, Gysbers A, Cheng D, Gai WP, Outeiro TF, *et al.* LRRK2 interactions with alpha-synuclein in Parkinson's disease brains and in cell models. J Mol Med (Berl) 2013; 91(4): 513-22.

Guix FX, Ill-Raga G, Bravo R, Nakaya T, de Fabritiis G, Coma M, *et al.* Amyloid-dependent triosephosphate isomerase nitrotyrosination induces glycation and tau fibrillation. Brain 2009; 132(Pt 5): 1335-45.

Hansen F, Battu CE, Dutra MF, Galland F, Lirio F, Broetto N, *et al.* Methylglyoxal and carboxyethyllysine reduce glutamate uptake and S100B secretion in the hippocampus independently of RAGE activation. Amino Acids 2016; 48(2): 375-85.

Hu G, Jousilahti P, Bidel S, Antikainen R, Tuomilehto J. Type 2 diabetes and the risk of Parkinson's disease. Diabetes care 2007; 30(4): 842-7.

Jo E, McLaurin J, Yip CM, St George-Hyslop P, Fraser PE. alpha-Synuclein membrane interactions and lipid specificity. J Biol Chem 2000; 275(44): 34328-34.

Karpinar DP, Balija MB, Kugler S, Opazo F, Rezaei-Ghaleh N, Wender N, *et al.* Pre-fibrillar alpha-synuclein variants with impaired beta-structure increase neurotoxicity in Parkinson's disease models. The EMBO journal 2009; 28(20): 3256-68.

Klionsky DJ, Abdelmohsen K, Abe A, Abedin MJ, Abeliovich H, Acevedo Arozena A, *et al.* Guidelines for the use and interpretation of assays for monitoring autophagy (3rd edition). Autophagy 2016; 12(1): 1-222.

Klucken J, Poehler AM, Ebrahimi-Fakhari D, Schneider J, Nuber S, Rockenstein E, *et al.* Alpha-synuclein aggregation involves a bafilomycin A 1-sensitive autophagy pathway. Autophagy 2012; 8(5): 754-66.

Klunk WE, Bacskai BJ, Mathis CA, Kajdasz ST, McLellan ME, Frosch MP, *et al.* Imaging Abeta plaques in living transgenic mice with multiphoton microscopy and methoxy-X04, a systemically administered Congo red derivative. J Neuropathol Exp Neurol 2002; 61(9): 797-805.

Kuhla B, Boeck K, Luth HJ, Schmidt A, Weigle B, Schmitz M, *et al.* Age-dependent changes of glyoxalase I expression in human brain. Neurobiology of aging 2006; 27(6): 815-22.

Lashuel HA, Hartley D, Petre BM, Walz T, Lansbury PT, Jr. Neurodegenerative disease: amyloid pores from pathogenic mutations. Nature 2002a; 418(6895): 291.

Lashuel HA, Petre BM, Wall J, Simon M, Nowak RJ, Walz T*, et al.* Alpha-synuclein, especially the Parkinson's disease-associated mutants, forms pore-like annular and tubular protofibrils. Journal of molecular biology 2002b; 322(5): 1089-102.

Lazaro DF, Rodrigues EF, Langohr R, Shahpasandzadeh H, Ribeiro T, Guerreiro P*, et al.* Systematic comparison of the effects of alpha-synuclein mutations on its oligomerization and aggregation. PLoS Genet 2014; 10(11): e1004741.

Lee D, Park CW, Paik SR, Choi KY. The modification of alpha-synuclein by dicarbonyl compounds inhibits its fibril-forming process. Biochimica et biophysica acta 2009; 1794(3): 421-30.

Lee JY, Song J, Kwon K, Jang S, Kim C, Baek K*, et al.* Human DJ-1 and its homologs are novel glyoxalases. Human molecular genetics 2012; 21(14): 3215-25.

Lyles GA, Chalmers J. The metabolism of aminoacetone to methylglyoxal by semicarbazide-sensitive amine oxidase in human umbilical artery. Biochem Pharmacol 1992; 43(7): 1409-14.

Macedo D, Tavares L, McDougall GJ, Vicente Miranda H, Stewart D, Ferreira RB*, et al.* (Poly)phenols protect from alpha-synuclein toxicity by reducing oxidative stress and promoting autophagy. Human molecular genetics 2015; 24(6): 1717-32.

Mak SK, Huang YA, Iranmanesh S, Vangipuram M, Sundararajan R, Nguyen L*, et al.* Small molecules greatly improve conversion of human-induced pluripotent stem cells to the neuronal lineage. Stem cells international 2012; 2012: 140427.

Marques O, Outeiro TF. Alpha-synuclein: from secretion to dysfunction and death. Cell death & disease 2012; 3: e350.

Martins IC, Kuperstein I, Wilkinson H, Maes E, Vanbrabant M, Jonckheere W*, et al.* Lipids revert inert Abeta amyloid fibrils to neurotoxic protofibrils that affect learning in mice. The EMBO journal 2008; 27(1): 224-33.

McLean PJ, Kawamata H, Hyman BT. Alpha-synuclein-enhanced green fluorescent protein fusion proteins form proteasome sensitive inclusions in primary neurons. Neuroscience 2001; 104(3): 901-12.

Mihoub M, Abdallah J, Gontero B, Dairou J, Richarme G. The DJ-1 superfamily member Hsp31 repairs proteins from glycation by methylglyoxal and glyoxal. Biochem Biophys Res Commun 2015; 463(4): 1305-10.

Munch G, Luth HJ, Wong A, Arendt T, Hirsch E, Ravid R, *et al.* Crosslinking of alpha-synuclein by advanced glycation endproducts--an early pathophysiological step in Lewy body formation? J Chem Neuroanat 2000; 20(3-4): 253-7.

Naiki H, Higuchi K, Hosokawa M, Takeda T. Fluorometric determination of amyloid fibrils in vitro using the fluorescent dye, thioflavin T1. Analytical biochemistry 1989; 177(2): 244-9.

Naiki H, Higuchi K, Matsushima K, Shimada A, Chen WH, Hosokawa M, *et al.* Fluorometric examination of tissue amyloid fibrils in murine senile amyloidosis: use of the fluorescent indicator, thioflavine T. Laboratory investigation; a journal of technical methods and pathology 1990; 62(6): 768-73.

Nass N, Bromme HJ, Hartig R, Korkmaz S, Sel S, Hirche F, *et al.* Differential response to alpha-oxoaldehydes in tamoxifen resistant MCF-7 breast cancer cells. PloS one 2014; 9(7): e101473.

Nemani VM, Lu W, Berge V, Nakamura K, Onoa B, Lee MK, *et al.* Increased expression of alpha-synuclein reduces neurotransmitter release by inhibiting synaptic vesicle reclustering after endocytosis. Neuron 2010; 65(1): 66-79.

Nonaka T, Iwatsubo T, Hasegawa M. Ubiquitination of alpha-synuclein. Biochemistry 2005; 44(1): 361-8.

Oliveira LM, Falomir-Lockhart LJ, Botelho MG, Lin KH, Wales P, Koch JC, *et al.* Elevated alpha-synuclein caused by SNCA gene triplication impairs neuronal differentiation and maturation in Parkinson's patient-derived induced pluripotent stem cells. Cell death & disease 2015; 6: e1994.

Oliveira LM, Gomes RA, Yang D, Dennison SR, Familia C, Lages A, *et al.* Insights into the molecular mechanism of protein native-like aggregation upon glycation. Biochimica et biophysica acta 2013; 1834(6): 1010-22.

Oliveira LM, Lages A, Gomes RA, Neves H, Familia C, Coelho AV, *et al.* Insulin glycation by methylglyoxal results in native-like aggregation and inhibition of fibril formation. BMC biochemistry 2011; 12: 41.

Orosz F, Olah J, Ovadi J. Triosephosphate isomerase deficiency: new insights into an enigmatic disease. Biochimica et biophysica acta 2009; 1792(12): 1168-74.

Oueslati A, Fournier M, Lashuel HA. Role of post-translational modifications in modulating the structure, function and toxicity of alpha-synuclein: implications for Parkinson's disease pathogenesis and therapies. Progress in brain research 2010; 183: 115-45.

Outeiro TF, Lindquist S. Yeast cells provide insight into alpha-synuclein biology and pathobiology. Science 2003; 302(5651): 1772-5.

Padmaraju V, Bhaskar JJ, Prasada Rao UJ, Salimath PV, Rao KS. Role of advanced glycation on aggregation and DNA binding properties of alpha-synuclein. Journal of Alzheimer's disease : JAD 2011; 24 Suppl 2: 211-21.

Pearce RK, Owen A, Daniel S, Jenner P, Marsden CD. Alterations in the distribution of glutathione in the substantia nigra in Parkinson's disease. Journal of neural transmission 1997; 104(6-7): 661-77.

Reichard GA, Jr., Skutches CL, Hoeldtke RD, Owen OE. Acetone metabolism in humans during diabetic ketoacidosis. Diabetes 1986; 35(6): 668-74.

Richard JP. Mechanism for the formation of methylglyoxal from triosephosphates. Biochem Soc Trans 1993; 21(2): 549-53.

Richarme G, Mihoub M, Dairou J, Bui LC, Leger T, Lamouri A. Parkinsonism-associated Protein DJ-1/Park7 Is a Major Protein Deglycase That Repairs Methylglyoxal- and Glyoxal-glycated Cysteine, Arginine, and Lysine Residues. J Biol Chem 2015; 290(3): 1885-97.

Rockenstein E, Mallory M, Hashimoto M, Song D, Shults CW, Lang I*, et al.* Differential neuropathological alterations in transgenic mice expressing alpha-synuclein from the platelet-derived growth factor and Thy-1 promoters. Journal of neuroscience research 2002; 68(5): 568-78.

Schiff SJ, Somjen GG. The effects of temperature on synaptic transmission in hippocampal tissue slices. Brain Res 1985; 345(2): 279-84.

Scholz D, Poltl D, Genewsky A, Weng M, Waldmann T, Schildknecht S*, et al.* Rapid, complete and large-scale generation of post-mitotic neurons from the human LUHMES cell line. Journal of neurochemistry 2011; 119(5): 957-71.

Scott DA, Tabarean I, Tang Y, Cartier A, Masliah E, Roy S. A pathologic cascade leading to synaptic dysfunction in alpha-synuclein-induced neurodegeneration. The

Journal of neuroscience : the official journal of the Society for Neuroscience 2010; 30(24): 8083-95.

Spillantini MG, Crowther RA, Jakes R, Hasegawa M, Goedert M. alpha-Synuclein in filamentous inclusions of Lewy bodies from Parkinson's disease and dementia with lewy bodies. Proceedings of the National Academy of Sciences of the United States of America 1998; 95(11): 6469-73.

Strohalm M, Kavan D, Novak P, Volny M, Havlicek V. mMass 3: a cross-platform software environment for precise analysis of mass spectrometric data. Analytical chemistry 2010; 82(11): 4648-51.

Sun Y, Chang YH, Chen HF, Su YH, Su HF, Li CY. Risk of Parkinson disease onset in patients with diabetes: a 9-year population-based cohort study with age and sex stratifications. Diabetes care 2012; 35(5): 1047-9.

Szego EM, Gerhardt E, Kermer P, Schulz JB. A30P alpha-synuclein impairs dopaminergic fiber regeneration and interacts with L-DOPA replacement in MPTP-treated mice. Neurobiology of disease 2012; 45(1): 591-600.

Szego EM, Outeiro TF, Kermer P, Schulz JB. Impairment of the septal cholinergic neurons in MPTP-treated A30P alpha-synuclein mice. Neurobiology of aging 2013; 34(2): 589-601.

Teismann P, Sathe K, Bierhaus A, Leng L, Martin HL, Bucala R*, et al.* Receptor for advanced glycation endproducts (RAGE) deficiency protects against MPTP toxicity. Neurobiology of aging 2012; 33(10): 2478-90.

Tenreiro S, Eckermann K, Outeiro TF. Protein phosphorylation in neurodegeneration: friend or foe? Frontiers in molecular neuroscience 2014a; 7: 42.

Tenreiro S, Outeiro TF. Simple is good: yeast models of neurodegeneration. FEMS Yeast Res 2010; 10(8): 970-9.

Tenreiro S, Reimao-Pinto MM, Antas P, Rino J, Wawrzycka D, Macedo D*, et al.* Phosphorylation modulates clearance of alpha-synuclein inclusions in a yeast model of Parkinson's disease. PLoS Genet 2014b; 10(5): e1004302.

Thornalley PJ, Langborg A, Minhas HS. Formation of glyoxal, methylglyoxal and 3-deoxyglucosone in the glycation of proteins by glucose. The Biochemical journal 1999; 344 Pt 1: 109-16.

Tiscornia G, Singer O, Verma IM. Production and purification of lentiviral vectors. Nature protocols 2006; 1(1): 241-5.

Vagelatos NT, Eslick GD. Type 2 Diabetes as a Risk Factor for Alzheimer's Disease: The Confounders, Interactions, and Neuropathology Associated With This Relationship. Epidemiologic reviews 2013.

Vander Jagt DL, Robinson B, Taylor KK, Hunsaker LA. Reduction of trioses by NADPH-dependent aldo-keto reductases. Aldose reductase, methylglyoxal, and diabetic complications. J Biol Chem 1992; 267(7): 4364-9.

Vicente Miranda H, El-Agnaf OM, Outeiro TF. Glycation in Parkinson's disease and Alzheimer's disease. Mov Disord 2016a.

Vicente Miranda H, Gomes MA, Branco-Santos J, Breda C, Lazaro DF, Lopes LV*, et al.* Glycation potentiates neurodegeneration in models of Huntington's disease. Sci Rep 2016b; 6: 36798.

Vicente Miranda H, Outeiro TF. The sour side of neurodegenerative disorders: the effects of protein glycation. The Journal of pathology 2010; 221(1): 13-25.

Vicente Miranda H, Xiang W, de Oliveira RM, Simoes T, Pimentel J, Klucken J*, et al.* Heat-mediated enrichment of alpha-synuclein from cells and tissue for assessing post-translational modifications. Journal of neurochemistry 2013; 126(5): 673-84.

Wales P, Pinho R, Lazaro DF, Outeiro TF. Limelight on alpha-synuclein: pathological and mechanistic implications in neurodegeneration. Journal of Parkinson's disease 2013; 3(4): 415-59.

Wang Y, Shi M, Chung KA, Zabetian CP, Leverenz JB, Berg D*, et al.* Phosphorylated alpha-synuclein in Parkinson's disease. Science translational medicine 2012; 4(121): 121ra20.

Webster J, Urban C, Berbaum K, Loske C, Alpar A, Gartner U*, et al.* The carbonyl scavengers aminoguanidine and tenilsetam protect against the neurotoxic effects of methylglyoxal. Neurotox Res 2005; 7(1-2): 95-101.

Willingham S, Outeiro TF, DeVit MJ, Lindquist SL, Muchowski PJ. Yeast genes that enhance the toxicity of a mutant huntingtin fragment or alpha-synuclein. Science 2003; 302(5651): 1769-72.

Yao D, Brownlee M. Hyperglycemia-induced reactive oxygen species increase expression of the receptor for advanced glycation end products (RAGE) and RAGE ligands. Diabetes 2010; 59(1): 249-55.

Zondler L, Miller-Fleming L, Repici M, Goncalves S, Tenreiro S, Rosado-Ramos R, *et al.* DJ-1 interactions with alpha-synuclein attenuate aggregation and cellular toxicity in models of Parkinson's disease. Cell death & disease 2014; 5: e1350.

Competing Financial Interests

The authors declare no competing financial interests.

Figure Legends

Fig. 1. MGO induces aSyn aggregation and toxicity in yeast and mammalian cell models of PD. BY4741 WT reference strain and *Δglo1* or *Δtpi* yeast cells transformed with empty p426GPD vector (Ctrl) or with p426GPD-aSyn WT (WT) were grown in YNB-U. Cells were also grown in higher glucose concentrations (4%). **(A)** % of yeast cells displaying aSyn inclusions. **(B)** Toxicity of aSyn under glycating conditions. **(C)** H4 cells co-expressing SynT and Synph 1 were treated with vehicle (Ctrl) or MGO (0.5 mM) for 16h and processed for ICC (aSyn, green). % of cells with aggregates (n=3). **(D)** H4 cells co-transfected with empty vector (E.V.) or SynT and Synph 1 were treated with vehicle (Ctrl) or MGO (0.5 mM) for 16h. MGO toxicity was measured by caspase-3 release (n=3). **(E)** H4 cells, as in (C) were treated with vehicle (Ctrl) or MGO (0.5mM) for 16h. Triton X-100 soluble and insoluble (TS and TI) fractions were probed for aSyn. The ratio between TI and TS is presented as SynT insolubility (n=4). **(F)** H4 cells, as in

(C), were treated with vehicle (Ctrl) or MGO (0.5 mM) for 16h. Native protein extracts were separated in a sucrose gradient. Fractions were immunoblotted and probed for aSyn. **(G)** H4 cells were treated as in (C). Cells were lysed and immunoprecipitated (IP) with an antibody against aSyn. Whole cell lysates (WCL) were probed for aSyn and for the corresponding loading control (β-actin). IP samples were probed for aSyn and AGEs. Blue and green arrows indicate aSyn and SynT, respectively (n=3 times). **(H)** Patient-derived neuronal differentiated iPSCs from a family with a *SNCA* locus triplication (SNCA 3X), an age-matched healthy control (Ctrl) and an aSyn shRNA silenced cell line derived from the SNCA 3X (SNCA 3X KD) were treated with increasing concentrations of MGO (0-2mM). MGO toxicity was measured by the activity of released LDH, normalized to total cell death (n=3), and is displayed as % of cytotoxicity. **(I)** Protein extracts collected from iPSCs from Ctrl, SNCA 3X and SNCA 3X KD lines were immunoblotted with anti-aSyn and anti-tubulin antibodies. **(J)** Differentiated LUHMES cells, naive (Ctrl), stably expressing only GFP, or aSyn and GFP were treated with increasing concentrations of MGO (0-5 mM). MGO toxicity was assessed by the MTS assay (n=3). **(K)** Cells stably expressing GFP or aSyn treated with vehicle (PBS) or 1.5mM MGO were processed for immunocytochemistry (ICC) and stained for aSyn (white), Caspase 3 (red) and DNA (blue). Scale bar 40µm. Data in all panels are average ± SD, * $p < 0.05$, ** $p < 0.01$, *** $p < 0.001$, **** $p < 0.0001$. For (A), unpaired two-tailed t-test with equal SD; for (C) and (D) 2-way ANOVA, followed by Tukey's multiple comparisons test; for (E), unpaired two-tailed t-test with equal SD. For (H) SNCA 3X vs. Ctrl **** $p < 0.0001$; SNCA 3X vs. SNCA 3X KD † $p < 0.05$, †††† $p < 0.0001$; and SNCA

3X vs. Ctrl ‡ $p < 0.05$, 2-way ANOVA, followed by Tukey's multiple comparisons test. For (J) 2-way ANOVA, followed by Tukey's multiple comparisons test.

Fig. 2. Down-regulation of *Glo1* and *Tpi* increases glycation and impairs negative geotaxis and lifespan in flies. (A) Protein extracts from *Drosophila* heads were immunoblotted and probed for CEL. Silencing of *Glo1* and *TPI* increases protein glycation. *Drosophila* motor performance assessed as % of flies climbing more than 8 cm within 10 s. RNAi silencing of *Glo1* **(B)** and *Tpi* **(C)** caused a reduction in climbing behavior in both WT and aSyn flies when compared to the respective controls (n=50 per condition). Survival rate was evaluated in flies with pan-neuronal knockdown of *Glo1* **(D)** and *Tpi* **(E)** in WT and aSyn backgrounds (n=100 per genotype). GAL4 Ctrl and UAS Ctrl data is common between panels. Data in all panels are mean ± SEM, * $p < 0.05$, ** $p < 0.01$, **** $p < 0.0001$; for (B) and (C) 2-way ANOVA, followed by Tukey's multiple comparisons test; for (D) and (E) Kaplan–Meier survival curve analysis with log-rank test.

Fig. 3. MGO is neurotoxic in mice, induces aSyn glycation and aggregation, and impairs synaptic transmission. WT and aSyn-Tg mice were injected in the SN (schematic view) either with MGO or vehicle (PBS) and analyzed 7 days post-injection. **(A)** Representative micrographs of brain sections immunostained for TH (red) (scale bar 500 μm and 1000 μm for striatum and SN, respectively). Dashed line delineates the area corresponding to the SN. **(B)** Representative micrographs of brain sections immunostained for TH (red), CEL (green) or stained with Hoechst (blue) (scale bar

300 µm). The merged signal is also shown (scale bar 200 µm). The dashed line delineates the SN. **(C)** The % of TH, VMAT or DAPI positive cells (ratio MGO/PBS) is presented (at least n=3 per condition). **(D)** Striatal thermoenriched protein extracts were probed with anti-CEL (red) and anti-aSyn (green, samples from 2 animals are shown). Representative blots are shown. The ratio between CEL and aSyn is shown as CEL/aSyn fold of WT contralateral (Ctrl) (at least n=3 per condition). **(E)** Representative image of brain sections immunostained for aggregated-aSyn (5G4, green) and TH (red) (scale bar 2000 µm for isolated channels and 1000 µm for merge). **(F)** Experimental setup for Long-term potentiation. Rat hippocampal slices were pre-incubated for 90 min with aSyn (500 nM) treated with PBS (Ctrl) or MGO. The slices were allowed to stabilize for 30 min before θ–burst. **(G)** Traces from representative experiments shown in (H) obtained before and 46–60 min after LTP induction, composed of the stimulus artifact followed by the presynaptic volley and the field excitatory postsynaptic potential (fEPSP). **(H)** Changes in fEPSP slope induced by θ–burst stimulation were recorded from the CA1 region of hippocampal slices pre-treated with aSyn or with glycated aSyn (aSyn-MGO) (aSyn 47 ± 3 %, n=4; aSyn-MGO 22 ± 4 %, n=4) **(I)** Bar graph of the LTP magnitude (change in fEPSP slope at 50-60min) in relation to pre-θ-burst values (100 %) from experiments shown in (H) as indicated below each column (n=4). Thermo-enriched brain samples from PD, LBD, or from control individuals **(J)**, or from young or old WT (**K**) or aSyn-Tg mice (**L**) were probed with anti-CEL (red) and anti-aSyn (green). Arrows indicate aSyn MW. The ratio between CEL and aSyn is shown as the CEL/aSyn ratio in young vs. old mice. **(M)** Detection of lysine glycation sites in aSyn by peptide mass fingerprinting analysis of aSyn protein in total lysates from Thy1-aSyn Tg mouse brain.

The spectrum shows glycated aSyn peptides in red and other aSyn peptides in blue. Corresponding peptide sequences are illustrated (residues in red are glycated). For (C) and (D), data are presented as average ± SD. For (C), (D), (I), (K) and (L) * $p < 0.05$, ** $p < 0.01$, *** $p < 0.001$. For (C), 2-way ANOVA, followed by Tukey's multiple comparisons test. For (D), 1-way ANOVA, followed by Tukey's multiple comparisons test. Data in panels (H) and (I) are mean ± SEM. For (H) and (I), one-way ANOVA test, followed by a Bonferroni's multiple comparison post-hoc test. For (K) and (L) unpaired t-test with equal SD.

Fig. 4. *In vitro* MGO-glycation promotes aSyn oligomerization and impairs aSyn SUV binding. (A) Fibrillization of recombinant WT aSyn at 100 µM treated with vehicle (Ctrl, black) or MGO (1 mM, green; and 5 mM, red) was followed by ThT fluorescence. **(B)** Recombinant WT aSyn species at 100 µM before (0 h, black) and after 30 h of fibrillization treated with vehicle (30 h, green) or MGO at 1 mM (30 h MGO, purple) were analysed by SEC. **(C)** Recombinant WT aSyn at 70µM treated with vehicle (30 h) or MGO at 0.5mM (30 h MGO) was fibrillized for 30 h and analyzed by DLS. Size (hydrodynamic diameter) distributions plotted as a function of scattered light intensity percentage (n=3 for 30 h and n=4 for 30 h MGO). **(D)** DLS size distributions by classes presented as scattered light intensity percentage. **(E)** Recombinant WT aSyn at 100 µM after 72 h of fibrillization treated with vehicle (Ctrl) or MGO (5 mM) was analyzed by TEM (left panels, scale bar 400 nm). A higher magnification of glycated aSyn is presented in the right panel (scale bar 200 nm). Red square outlines digitally magnified region (scale bar 50 nm). **(F)** Superposition of 2D ^{1}H-^{15}N HSQC NMR spectra of

recombinant ^{15}N-labelled aSyn before (green) and after (purple) treatment with MGO. Inset shows a selected region showing the glycation-induced NMR signal perturbation. **(G)** Residue-specific changes of ^{1}H-^{15}N HSQC signal intensity of aSyn upon MGO-glycation. Schematic of aSyn highlighting the N-terminal (green), NAC (purple) and C-terminal (red) domains, and location of lysine residues (K). **(H)** Far-UV CD spectra of unmodifed (Ctrl) and glycated-aSyn (MGO) in the absence and presence of POPC/POPA (1:1) SUVs at different protein-to-lipid (L) molar ratios.

Fig. 5. Glycation impairs aSyn clearance through the proteasome and autophagy and reduces aSyn release. (A) H4 cells expressing SynT and Synph 1 for 24 h were treated with vehicle (Ctrl) or MGO (0.5 mM) and stained for aSyn and ubiquitin. Micrographs of XY, YZ and XZ MIPs are shown (scale bar 20 μm). **(B)** *In vitro* aSyn ubiquitination reactions (of glycated or non-glycated aSyn) were conducted in the absence or presence of SIAH-2. Monoubiquitination of aSyn was detected by immunobloting against aSyn and represented as % of monoubiquitinated aSyn vs total aSyn. **(C)** Cells co-expressing SynT and Synph 1 were pre-treated with vehicle (Ctrl) or MGO (0.5 mM) for 16h. Cells were treated with vehicle or MGO for 24 h together with CHX for the last 4, 8 or 12 h. Protein extracts were probed for aSyn and β-actin, for normalization. **(D)** E.V. and GFPu (Ctrl), aSyn and GFPu (aSyn) or SynT and GFPu (SynT) cells were treated with vehicle (-) or MGO (0.5 mM) (+) for 16h. Protein extracts were probed for GFP and β-actin. GFP signal was normalized to β-actin signal and to aSyn. The ratio between the levels of GFPu in cells treated with MGO or vehicle is presented. **(E)** E.V. (Ctrl), aSyn or SynT + Synph 1 expressing cells were pre-treated with

vehicle (Ctrl) or MGO (0.5 mM) for 16h. Cells were treated with vehicle or MGO for 2h together with vehicle (-) or NH_4Cl and leupeptin (+). Protein extracts were probed for LC3 and β-actin. LC3-II levels were normalized to β-actin and the difference between NH_4Cl and vehicle treatments was calculated. The ratio between MGO and Ctrl is presented as autophagy induction ratio. **(F)** aSyn or SynT + Synph 1 expressing cells were treated with vehicle (Ctrl) or MGO (0.5 mM) for 16h. Media was collected and probed for aSyn. Data is presented as MGO fold to Ctrl. See also Movie S1. Data in all panels are average ± SD, * $p < 0.05$, ** $p < 0.01$, **** $p < 0.0001$. For (B) and (E), 1-way ANOVA, followed by Tukey's multiple comparison test; for (C), 2-way ANOVA, followed by Sidak's multiple comparison test; for (D) and (F), unpaired two-tailed t-test with equal SD.

Fig. 6. MGO scavengers reduce aSyn aggregation and toxicity, increase aSyn clearance in mammalian cells, and rescue motor performance in aSyn transgenic flies. (A) H4 cells co-expressing SynT and Synph 1 were treated with vehicle (Ctrl), AG or TS for 16h. MGO levels were measured by HPLC and normalized to Ctrl. **(B)** H4 cells, as in (A), were treated with vehicle (Ctrl), AG or TS for 16h and processed for ICC. Fold-reduction in aggregation is presented (n=3). **(C)** Toxicity of vehicle (Ctrl), AG or TS 22h-treated cells, as in (A), measured by LDH release (n=3) and normalized to Ctrl. **(D)** Cells, as in (A) were pre-treated with vehicle (Ctrl) or MGO (0.5 mM) for 16h. Cells were treated with vehicle, MGO, MGO and AG, or MGO and TS for 16h. Media was replaced and cells were treated again for 12h, together with CHX for 4, 8 or 12 h. Protein extracts were probed for aSyn and β-actin, for normalization. Data for Ctrl and MGO is

the same as in Fig. 5 B. **(E)** AG and TS treatment partially rescued the motor performance of aSyn flies in dose-dependent manner. Data in panels (A), (B) and (C) are average ± SD. Data in panel (E) and (F) is mean ± SEM. * $p < 0.05$, ** $p < 0.01$, *** $p < 0.001$, **** $p < 0.0001$. For (A), unpaired two-tailed t-test with equal SD; for (B) and (C) ordinary 1-way ANOVA, followed by Dunnett's multiple comparisons test; for (D) 2-way ANOVA, followed by Tukey's multiple comparison test; for (E) and (F) ordinary 1-way ANOVA, followed by Newman-Keuls multiple comparisons test.

Fig. 7. Effects of MGO in models of PD. (A) Glycation promotes aSyn-mediated toxicity and aggregation in cell models of PD, promotes neuronal loss in mice, and decreases motor performance in *Drosophila*. **(B)** MGO scavengers protect against aSyn toxicity and aggregation and improve motor performance in *Drosophila*. **(C)** Mechanistically, glycation induces aSyn oligomerization and promotes aSyn inclusion formation in cell models of PD. Glycation also decreases aSyn clearance by impairing the ubiquitin proteasome system **(D)**, the autophagy lysosome pathway **(E)**, and the release of aSyn **(F)**.

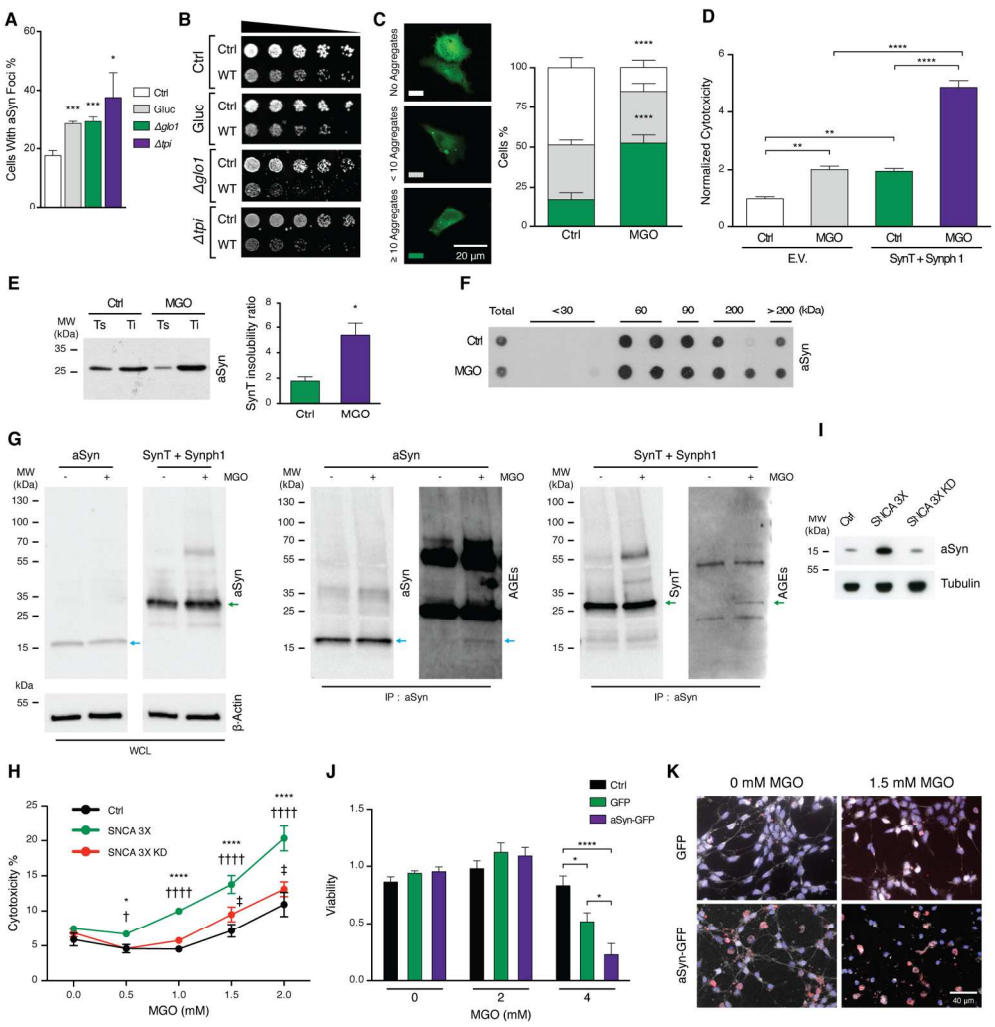

Fig. 1. MGO induces aSyn aggregation and toxicity in yeast and mammalian cell models of PD. BY4741 WT reference strain and glo1 or tpi yeast cells transformed with empty p426GPD vector (Ctrl) or with p426GPD-aSyn WT (WT) were grown in YNB-U. Cells were also grown in higher glucose concentrations (4%). (A) % of yeast cells displaying aSyn inclusions. (B) Toxicity of aSyn under glycating conditions. (C) H4 cells co-expressing SynT and Synph 1 were treated with vehicle (Ctrl) or MGO (0.5 mM) for 16h and processed for ICC (aSyn, green). % of cells with aggregates (n=3). (D) H4 cells co-transfected with empty vector (E.V.) or SynT and Synph 1 were treated with vehicle (Ctrl) or MGO (0.5 mM) for 16h. MGO toxicity was measured by caspase-3 release (n=3). (E) H4 cells, as in (C) were treated with vehicle (Ctrl) or MGO (0.5mM) for 16h. Triton X-100 soluble and insoluble (TS and TI) fractions were probed for aSyn. The ratio between TI and TS is presented as SynT insolubility (n=4). (F) H4 cells, as in (C), were treated with vehicle (Ctrl) or MGO (0.5 mM) for 16h. Native protein extracts were separated in a sucrose gradient. Fractions were immunoblotted and probed for aSyn. (G) H4 cells were treated as in (C). Cells were lysed and immunoprecipitated (IP) with an antibody against aSyn. Whole cell lysates (WCL) were probed for aSyn and for the corresponding loading control (β-actin). IP samples were probed for aSyn and AGEs. Blue and green arrows indicate aSyn and SynT, respectively (n=3 times). (H) Patient-derived neuronal differentiated iPSCs from a family with a SNCA locus triplication (SNCA 3X), an age-matched healthy control (Ctrl) and an aSyn shRNA silenced cell line derived from the SNCA 3X (SNCA 3X KD) were treated with increasing concentrations of MGO (0-2mM). MGO toxicity was measured by the activity of released LDH, normalized to total cell death (n=3), and is displayed as % of cytotoxicity. (I) Protein extracts collected from iPSCs from Ctrl, SNCA 3X and SNCA 3X KD lines were immunoblotted with anti-aSyn and anti-tubulin antibodies. (J)

Differentiated LUHMES cells, naive (Ctrl), stably expressing only GFP, or aSyn and GFP were treated with increasing concentrations of MGO (0-5 mM). MGO toxicity was assessed by the MTS assay (n=3). (K) Cells stably expressing GFP or aSyn treated with vehicle (PBS) or 1.5mM MGO were processed for immunocytochemistry (ICC) and stained for aSyn (white), Caspase 3 (red) and DNA (blue). Scale bar 40µm. Data in all panels are average ± SD, * $p < 0.05$, ** $p < 0.01$, *** $p < 0.001$, **** $p < 0.0001$. For (A), unpaired two-tailed t-test with equal SD; for (C) and (D) 2-way ANOVA, followed by Tukey's multiple comparisons test; for (E), unpaired two-tailed t-test with equal SD. For (H) SNCA 3X vs. Ctrl **** $p < 0.0001$; SNCA 3X vs. SNCA 3X KD † $p < 0.05$, †††† $p < 0.0001$; and SNCA 3X vs. Ctrl ‡ $p < 0.05$, 2-way ANOVA, followed by Tukey's multiple comparisons test. For (J) 2-way ANOVA, followed by Tukey's multiple comparisons test.

Fig. 1

174x178mm (300 x 300 DPI)

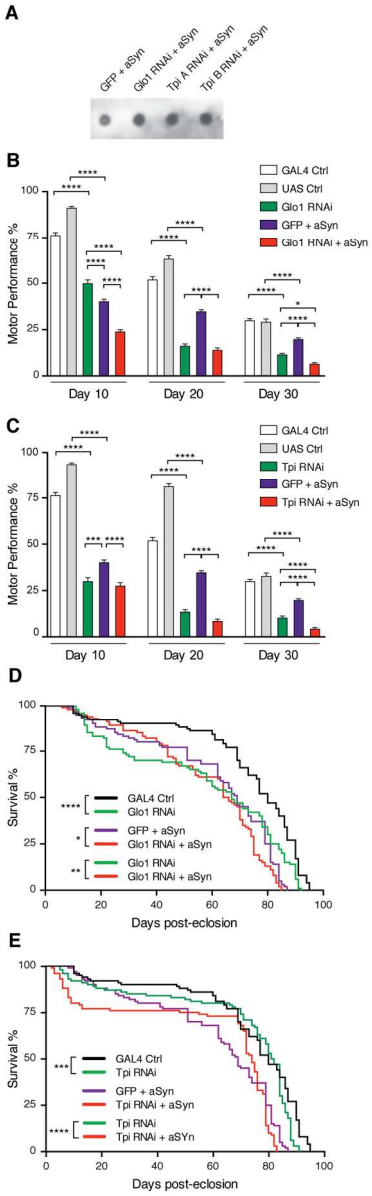

Fig. 2. Down-regulation of Glo1 and Tpi increases glycation and impairs negative geotaxis and lifespan in flies. (A) Protein extracts from Drosophila heads were immunoblotted and probed for CEL. Silencing of Glo1 and TPI increases protein glycation. Drosophila motor performance assessed as % of flies climbing more than 8 cm within 10 s. RNAi silencing of Glo1 (B) and Tpi (C) caused a reduction in climbing behavior in both WT and aSyn flies when compared to the respective controls (n=50 per condition). Survival rate was evaluated in flies with pan-neuronal knockdown of Glo1 (D) and Tpi (E) in WT and aSyn backgrounds (n=100 per genotype). GAL4 Ctrl and UAS Ctrl data is common between panels. Data in all panels are mean ± SEM, * $p < 0.05$, ** $p < 0.01$, **** $p < 0.0001$; for (B) and (C) 2-way ANOVA, followed by Tukey's multiple comparisons test; for (D) and (E) Kaplan–Meier survival curve analysis with log-rank test.

Fig. 2

61x197mm (300 x 300 DPI)

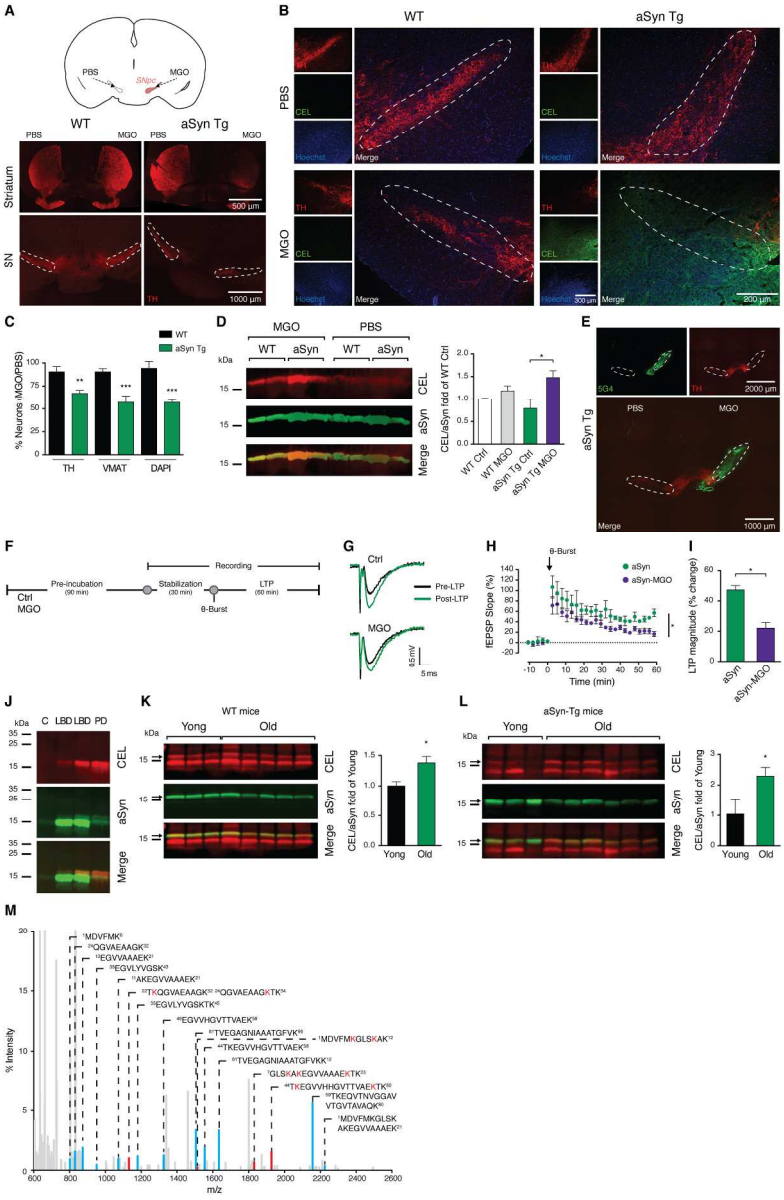

Fig. 3. MGO is neurotoxic in mice, induces aSyn glycation and aggregation, and impairs synaptic transmission. WT and aSyn-Tg mice were injected in the SN (schematic view) either with MGO or vehicle (PBS) and analyzed 7 days post-injection. (A) Representative micrographs of brain sections immunostained for TH (red). Dashed line delineates SN. (B) Representative micrographs of brain sections immunostained for TH (red), CEL (green) or stained with Hoechst (blue). The merged signal is also shown (scale bar 200 µm). The dashed line delineates the SN. (C) The % of TH, VMAT or DAPI positive cells (ratio MGO/PBS) is presented (at least n=3 per condition). (D) Striatal thermoenriched protein extracts were probed with anti-CEL (red) and anti-aSyn (green, samples from 2 animals are shown). Representative blots are shown. The ratio between CEL and aSyn is shown as CEL/aSyn fold of WT contralateral (Ctrl) (at least n=3 per condition). (E) Representative image of brain sections immunostained for aggregated-aSyn (5G4, green) and TH (red). (F) Experimental setup for Long-term potentiation. Rat hippocampal slices were pre-incubated for 90 min with aSyn (500 nM) treated with PBS (Ctrl) or MGO. The slices were allowed to stabilize for 30 min before θ–burst. (G) Traces from representative experiments shown in (H) obtained before and 46–

60 min after LTP induction, composed of the stimulus artifact followed by the presynaptic volley and the field excitatory postsynaptic potential (fEPSP). (H) Changes in fEPSP slope induced by θ–burst stimulation were recorded from the CA1 region of hippocampal slices pre-treated with aSyn or with glycated aSyn (aSyn-MGO) (aSyn 47 ± 3 %, n=4; aSyn-MGO 22 ± 4 %, n=4) (I) Bar graph of the LTP magnitude (change in fEPSP slope at 50-60min) in relation to pre--burst values (100 %) from experiments shown in (H) as indicated below each column (n=4). Thermo-enriched brain samples from PD, LBD, or from control individuals (J), or from young or old WT (K) or aSyn-Tg mice (L) were probed with anti-CEL (red) and anti-aSyn (green). Arrows indicate aSyn MW. The ratio between CEL and aSyn is shown as the CEL/aSyn ratio in young vs. old mice. (M) Detection of lysine glycation sites in aSyn by peptide mass fingerprinting analysis of aSyn protein in total lysates from Thy1-aSyn Tg mouse brain. The spectrum shows glycated aSyn peptides in red and other aSyn peptides in blue. Corresponding peptide sequences are illustrated (residues in red are glycated). For (C) and (D), data are presented as average ± SD. For (C), (D), (I), (K) and (L) * $p < 0.05$, ** $p < 0.01$, *** $p < 0.001$. For (C), 2-way ANOVA, followed by Tukey's multiple comparisons test. For (D), 1-way ANOVA, followed by Tukey's multiple comparisons test. Data in panels (H) and (I) are mean ± SEM. For (H) and (I), one-way ANOVA test, followed by a Bonferroni's multiple comparison post-hoc test. For (K) and (L) unpaired t-test with equal SD.

Fig. 3

174x264mm (300 x 300 DPI)

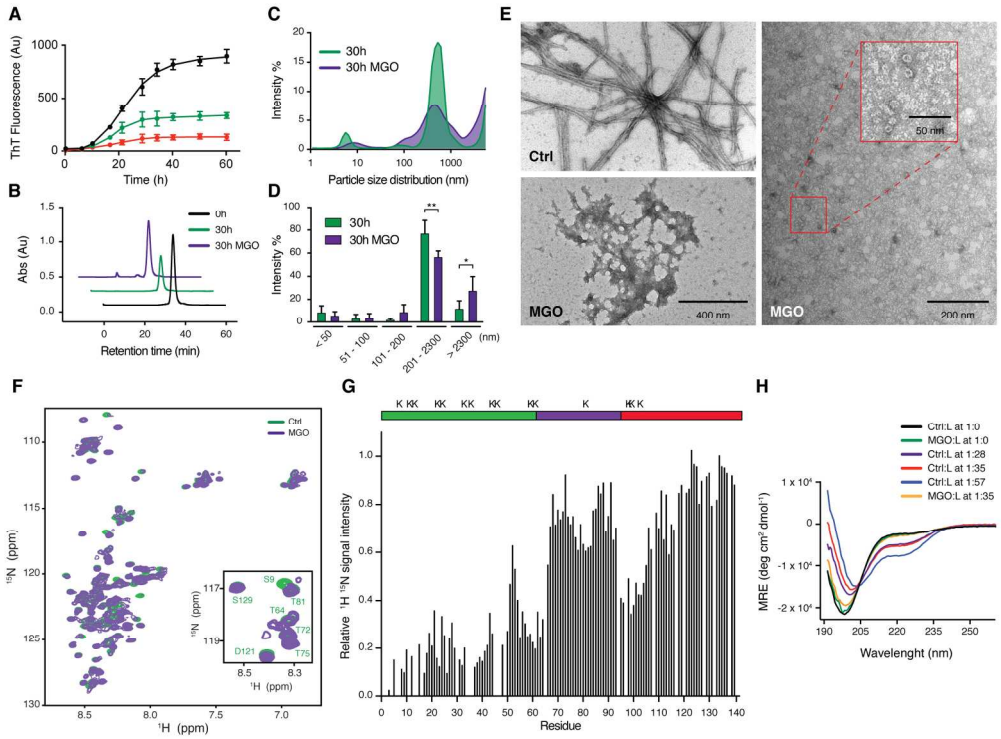

Fig. 4. In vitro MGO-glycation promotes aSyn oligomerization and impairs aSyn SUV binding. (A) Fibrillization of recombinant WT aSyn at 100 μM treated with vehicle (Ctrl, black) or MGO (1 mM, green; and 5 mM, red) was followed by ThT fluorescence. (B) Recombinant WT aSyn species at 100 μM before (0 h, black) and after 30 h of fibrillization treated with vehicle (30 h, green) or MGO at 1 mM (30 h MGO, purple) were analysed by SEC. (C) Recombinant WT aSyn at 70μM treated with vehicle (30 h) or MGO at 0.5mM (30 h MGO) was fibrillized for 30 h and analyzed by DLS. Size (hydrodynamic diameter) distributions plotted as a function of scattered light intensity percentage (n=3 for 30 h and n=4 for 30 h MGO). (D) DLS size distributions by classes presented as scattered light intensity percentage. (E) Recombinant WT aSyn at 100 μM after 72 h of fibrillization treated with vehicle (Ctrl) or MGO (5 mM) was analyzed by TEM (left panels, scale bar 400 nm). A higher magnification of glycated aSyn is presented in the right panel (scale bar 200 nm). Red square outlines digitally magnified region (scale bar 50 nm). (F) Superposition of 2D 1H-15N HSQC NMR spectra of recombinant 15N-labelled aSyn before (green) and after (purple) treatment with MGO. Inset shows a selected region showing the glycation-induced NMR signal perturbation. (G) Residue-specific changes of 1H-15N HSQC signal intensity of aSyn upon MGO-glycation. Schematic of aSyn highlighting the N-terminal (green), NAC (purple) and C-terminal (red) domains, and location of lysine residues (K). (H) Far-UV CD spectra of unmodifed (Ctrl) and glycated-aSyn (MGO) in the absence and presence of POPC/POPA (1:1) SUVs at different protein-to-lipid (L) molar ratios.

Fig. 4

174x129mm (300 x 300 DPI)

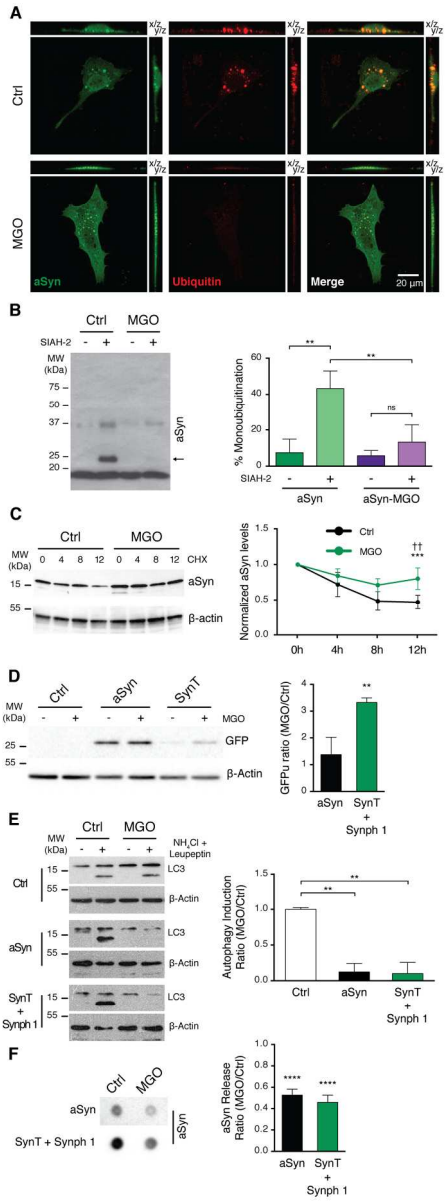

Fig. 5. Glycation impairs aSyn clearance through the proteasome and autophagy and reduces aSyn release. (A) H4 cells expressing SynT and Synph 1 for 24 h were treated with vehicle (Ctrl) or MGO (0.5 mM) and stained for aSyn and ubiquitin. Micrographs of XY, YZ and XZ MIPs are shown (scale bar 20 µm). (B) In vitro aSyn ubiquitination reactions (of glycated or non-glycated aSyn) were conducted in the absence or presence of SIAH-2. Monoubiquitination of aSyn was detected by immunobloting against aSyn and represented as % of monoubiquitinated aSyn vs total aSyn. (C) Cells co-expressing SynT and Synph 1 were pre-treated with vehicle (Ctrl) or MGO (0.5 mM) for 16h. Cells were treated with vehicle or MGO for 24 h together with CHX for the last 4, 8 or 12 h. Protein extracts were probed for aSyn and β-actin, for normalization. (D) E.V. and GFPu (Ctrl), aSyn and GFPu (aSyn) or SynT and GFPu (SynT) cells were treated with vehicle (-) or MGO (0.5 mM) (+) for 16h. Protein extracts were probed for GFP and β-actin. GFP signal was normalized to β-actin signal and to aSyn. The ratio between the levels of GFPu in cells treated with MGO or vehicle is presented. (E) E.V. (Ctrl), aSyn or SynT + Synph 1 expressing cells were pre-treated with vehicle (Ctrl) or MGO (0.5 mM) for 16h. Cells were treated with vehicle or MGO for 2h together with vehicle (-) or NH4Cl and

leupeptin (+). Protein extracts were probed for LC3 and β-actin. LC3-II levels were normalized to β-actin and the difference between NH4Cl and vehicle treatments was calculated. The ratio between MGO and Ctrl is presented as autophagy induction ratio. (F) aSyn or SynT + Synph 1 expressing cells were treated with vehicle (Ctrl) or MGO (0.5 mM) for 16h. Media was collected and probed for aSyn. Data is presented as MGO fold to Ctrl. See also Movie S1. Data in all panels are average ± SD, * $p < 0.05$, ** $p < 0.01$, **** $p < 0.0001$. For (B) and (E), 1-way ANOVA, followed by Tukey's multiple comparison test; for (C), 2-way ANOVA, followed by Sidak's multiple comparison test; for (D) and (F), unpaired two-tailed t-test with equal SD.

Fig. 5

85x224mm (300 x 300 DPI)

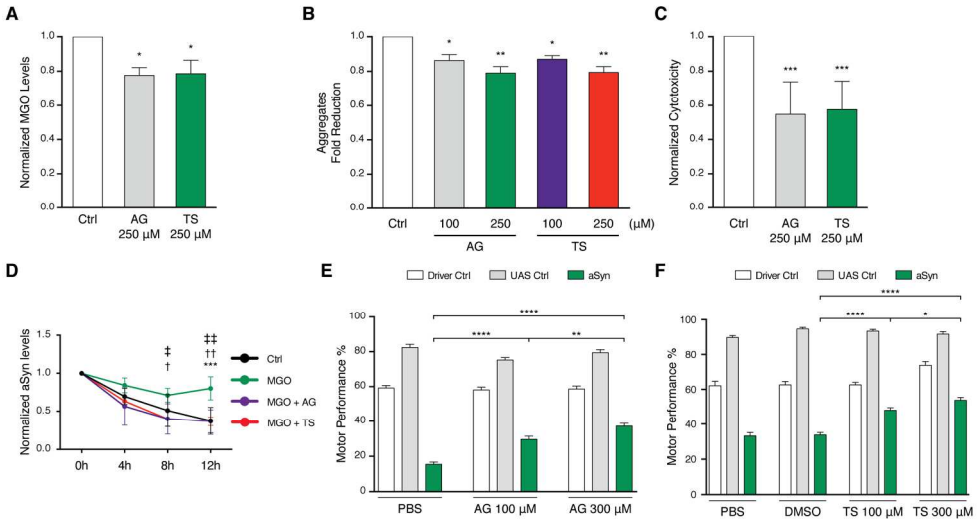

Fig. 6. MGO scavengers reduce aSyn aggregation and toxicity, increase aSyn clearance in mammalian cells, and rescue motor performance in aSyn transgenic flies. (A) H4 cells co-expressing SynT and Synph 1 were treated with vehicle (Ctrl), AG or TS for 16h. MGO levels were measured by HPLC and normalized to Ctrl. (B) H4 cells, as in (A), were treated with vehicle (Ctrl), AG or TS for 16h and processed for ICC. Fold-reduction in aggregation is presented (n=3). (C) Toxicity of vehicle (Ctrl), AG or TS 22h-treated cells, as in (A), measured by LDH release (n=3) and normalized to Ctrl. (D) Cells, as in (A) were pre-treated with vehicle (Ctrl) or MGO (0.5 mM) for 16h. Cells were treated with vehicle, MGO, MGO and AG, or MGO and TS for 16h. Media was replaced and cells were treated again for 12h, together with CHX for 4, 8 or 12 h. Protein extracts were probed for aSyn and β-actin, for normalization. Data for Ctrl and MGO is the same as in Fig. 5 B. (E) AG and TS treatment partially rescued the motor performance of aSyn flies in dose-dependent manner. Data in panels (A), (B) and (C) are average ± SD. Data in panel (E) and (F) is mean ± SEM. * $p < 0.05$, ** $p < 0.01$, *** $p < 0.001$, **** $p < 0.0001$. For (A), unpaired two-tailed t-test with equal SD; for (B) and (C) ordinary 1-way ANOVA, followed by Dunnett's multiple comparisons test; for (D) 2-way ANOVA, followed by Tukey's multiple comparison test; for (E) and (F) ordinary 1-way ANOVA, followed by Newman-Keuls multiple comparisons test.

Fig. 6
174x93mm (300 x 300 DPI)

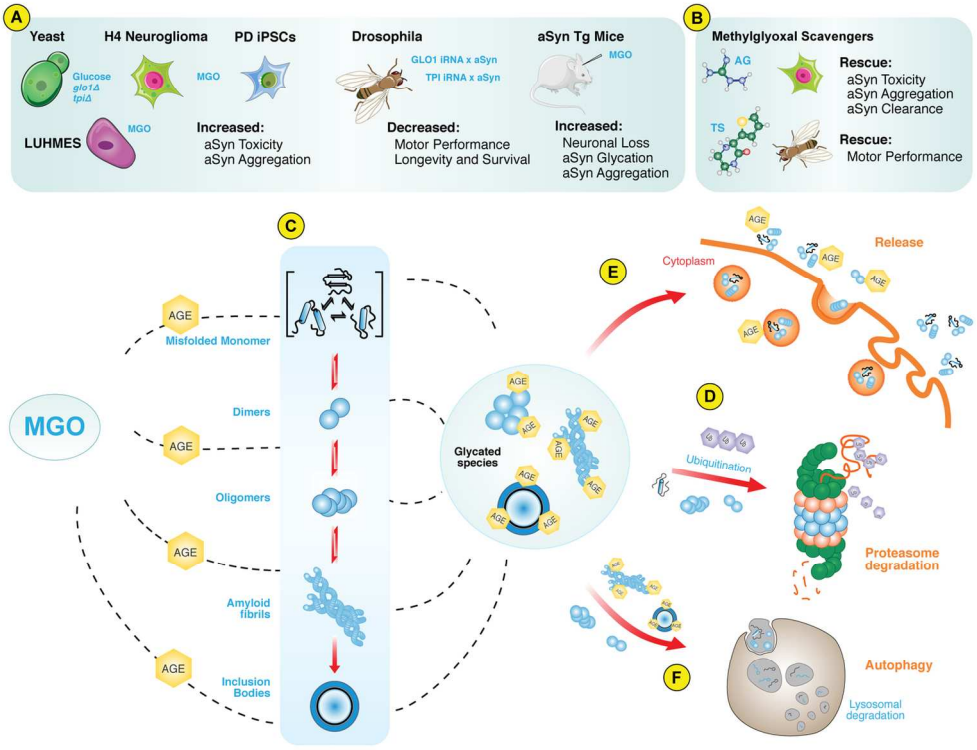

Fig. 7. Effects of MGO in models of PD. (A) Glycation promotes aSyn-mediated toxicity and aggregation in cell models of PD, promotes neuronal loss in mice, and decreases motor performance in Drosophila. (B) MGO scavengers protect against aSyn toxicity and aggregation and improve motor performance in Drosophila. (C) Mechanistically, glycation induces aSyn oligomerization and promotes aSyn inclusion formation in cell models of PD. Glycation also decreases aSyn clearance by impairing the ubiquitin proteasome system (D), the autophagy lysosome pathway (E), and the release of aSyn (F).

Fig. 7

139x106mm (300 x 300 DPI)

Glycation potentiates α-synuclein-associated neurodegeneration in synucleinopathies

Hugo Vicente Miranda, Éva Mónika Szegő, Luís Miguel Araujo Oliveira, Carlo Breda, Ekrem Darendelioglu, Rita Machado de Oliveira, Diana Gabriela Ferreira, Marcos António Gomes, Ruth Rott, Márcia Oliveira, Francesca Munari, Francisco Javier Enguita, Tânia Simões, Eva Ferreira Rodrigues, Michael Heinrich, Ivo Cristiano Martins, Irina Zamolo, Olaf Riess, Carlos Cordeiro, Ana Ponces-Freire, Hilal Ahmed Lashuel, Nuno Correia Santos, Luisa Vaqueiro Lopes, Wei Xiang, Thomas Michael Jovin, Deborah Penque, Simone Engelender, Markus Zweckstetter, Jochen Klucken, Flaviano Giorgini, Alexandre Quintas, and Tiago Fleming Outeiro

Supplementary Figure Legends

Fig. S1. MGO induces mutant aSyn aggregation and toxicity in yeast models of PD. (A) Yeast BY4741 reference strain and *Δglo1* or *Δtpi* cells transformed with empty p426GPD vector were grown in YNB-U. Yeast cells were also grown in higher glucose concentrations (4%). Equal numbers of cells were harvested and the intracellular levels of MGO were determined by HPLC and normalized to Ctrl. **(B)** Yeast cells were transformed with aSyn mutants associated with familial forms of PD (A53T and E46K). The % of yeast cells displaying aSyn inclusions is presented. **(C)** Toxicity of aSyn under glycating conditions, as in (B) (spotting assays of Ctrl and WT are repeated as in Fig. 1 B). **(D)** Cell viability assessed by the number of colony forming units (CFUs) as in (C) in control vs glucose challenge. Data in all panels are average ± SD, * $p < 0.05$,

** $p < 0.01$, *** $p < 0.001$, **** $p < 0.0001$. For (A) and (B), unpaired two-tailed t-test with equal SD. For (D), 2-way ANOVA followed by Sidak's multiple comparisons test.

Fig. S2. MGO toxicity and glycation in human H4 cells. (A) H4 cells treated with vehicle (Ctrl) or increasing concentrations of MGO (0.25, 0.5, 0.75 and 1mM) for 16h. **(B)** MGO toxicity measured by propidium iodide staining, presented as fold of Ctrl. Data are presented as average ± SD, * $p < 0.05$, unpaired two-tailed t-test with equal SD. **(C)** Protein extracts from H4 cells treated with vehicle (Ctrl) or MGO for 16h were immunoblotted with anti-AGE and anti-β-actin antibodies. **(D)** H4 cells were treated as in (A) with 0.5mM of MGO. The intracellular levels of MGO were measured by HPLC and normalized to Ctrl. **(E)** H4 cells co-transfected with SynT and Synph 1 (tagged with V5) for 24h were treated with vehicle (Ctrl) or MGO (0.5mM) for 16h. The medium was replaced and cells were retreated with MGO (0.5mM) for 6h. Protein extracts were immunoblotted with an antibody against AGEs and with the corresponding loading control (anti- β-Actin) or with an antibody against aSyn, against the V5-tag (synph 1), and the corresponding loading control (β-Actin) **(F)**. For (B), 1-way ANOVA, followed by Tukey's multiple comparisons test. For (D) unpaired t-test with equal SD.

Fig. S3. Down-regulation of *Tpi* impairs negative geotaxis and lifespan in flies. Measurement of *Drosophila* motor performance in a second *Tpi* RNAi line, assessed as percentage of flies more than 8cm within 10sec. **(A)** RNAi silencing of *Tpi* caused a reduction in climbing behavior in both WT and aSyn flies when compared to their relative controls (n=50 per condition). **(B)** Survival rate was evaluated in flies with pan-neuronal knockdown of *Tpi* in WT and aSyn backgrounds (n=100 per genotype). Data in all panels are mean ± SEM, **** $p < 0.001$, **** $p < 0.0001$. For (A) 2-way ANOVA,

followed by Tukey's multiple comparisons test. For (B) Kaplan–Meier survival curve analysis with log-rank test.

Fig. S4. MGO injection in the substantia nigra or in the striatum induces aSyn neurotoxicity in mice. (A) WT and aSyn-Tg mice were injected with MGO or vehicle (PBS) in the SN as in Fig. 3 A-E. Representative image of a coronal section immunostained with an antibody against TH to label TH-positive neurons, and developed with DAB. Extensive damage in MGO-treated aSyn Tg mice is observed (scale bar 1000 µm). **(B)** WT and aSyn-Tg mice were injected in the striatum (schematic view) with MGO or vehicle (PBS) and analyzed 7 days post-injection. Representative micrographs of brain sections immunostained for NeuN or TH (scale bar 300 µm). The % of Neu-N cells or TH fiber density (ratio MGO/PBS) is presented (at least n=3 per condition). Data are presented as average ± SD, ** $p < 0.01$, unpaired t-test with equal SD.

Fig. S5. MGO induces aSyn aggregation and phosphorylation on S129. WT and aSyn-Tg mice were injected in the SN or in the striatum with MGO or vehicle (PBS) and analyzed 7 days post-injection. **(A)** Representative images of brain sections immunostained for aggregated aSyn (5G4, red), aSyn (green), TH (blue) or nuclei (Hoechst, grey) (scale bar 300 µm). Merged signal is presented (scale bar 200 µm). **(B)** Representative images of SN immunostained for TH (red), pS129 aSyn (green) or nuclei (Hoechst, blue) (scale bar 300 µm). Merged signal is presented (scale bar 200 µm). Dashed line delineates the SN. **(C)** Representative images of SN immunostained for TH (red), pS129 aSyn (green) or stained with Hoechst (blue) at higher magnification (scale bar 30 µm). Merged signal is presented (scale bar 20 µm).

(D) Section of the striatum of striatum-MGO-injected aSyn-Tg mice immunostained for aSyn (green), and stained with MX-O4 (labeling amyloid-like structures, red) (scale bar 20 μm).

Fig. S6. MGO does not affect LTP in rat hippocampal slices. (A) Changes in fEPSP slope induced by θ–burst stimulation were recorded from the CA1 region of hippocampal slices pre-treated with PBS (Ctrl - black), 35 μM MGO (white), aSyn (aSyn - green) or glycated aSyn (aSyn-MGO - purple) (data from aSyn and aSyn-MGO are the same presented in Fig. 3 H-I. **(B)** Bar graph of the LTP magnitude (change in fEPSP slope at 50-60min) in relation to pre-θ-burst values (100 %) from experiments shown in (A) as indicated below each column (at least n=3). * $p < 0.05$ aSyn-MGO vs aSyn, †† $p < 0.01$ aSyn-MGO vs MGO, ‡‡ $p < 0.01$ aSyn-MGO vs Ctrl. For (A) and (B), one-way ANOVA test, followed by a Bonferroni's multiple comparison post-hoc test.

Fig. S7. Glycation occurs primarily in the N-terminal region of aSyn. Schematic representation of the glycation sites (red), together with unmodified lysine residues (yellow). Mass spectrometry analysis of tryptic or Glu-C digestion of **(A)** H4 cells transfected with aSyn treated with 0.5mM MGO; **(B)** yeast *Δglo1* transformed with aSyn; **(C)** Mouse brain (3 month-old animals); and **(D)** rat brain protein extracts (3 month-old animals). The identity between the N-terminal domain sequences of the species analyzed was 98% (Expasy, SIM-Alignment Tool for protein sequences).

Fig. S8. *In vitro* MGO-glycation promotes aSyn oligomerization (A) Fibrillization of recombinant A30P, A53T and E46K aSyn at 100 μM treated with vehicle (Ctrl) or

MGO (1 mM; and 5 mM) was followed by ThT fluorescence. Data are presented as average ± SD. **(B)** Fibrillization of recombinant WT, A30P, A53T and E46K aSyn at 100μM treated with vehicle (Ctrl) or MGO (1 and 5mM) analyzed by CD (MRE, mean residue ellipticity). **(C)** Structure transition followed at 222nm. **(D)** Recombinant A30P, A53T and E46K aSyn species at 100 μM before (0 h) and after 30 h of fibrillization treated with vehicle (30 h) or MGO at 1 mM (30 h MGO) were analysed by SEC.

Fig. S9. Effect of glycation on aSyn clearance. (A) H4 cells co-expressing SynT and Synph 1 were treated with vehicle (-) or MGO (+, 0.5 mM) for 16h. Media was replaced and cells were retreated with MGO for 4h. Protein extracts were probed for P62 (SQSTM1) and for the corresponding loading control (β-Actin). The ratio between the levels of P62 in cells treated with MGO or vehicle (Ctrl) is presented. **(B)** Cells as in (A) were treated with vehicle, MGO or MGO together with AG or TS for 24 h together with CHX for the last 4, 8 and 12 h. Protein extracts were probed for aSyn and β-actin, for normalization. Results shown for Ctrl and MGO are repeated as in Fig. 5C. Data in (A) are average ± SD, * $p < 0.05$, unpaired two-tailed t-test with equal SD.

Supplementary Movie Legend

Movie S1. aSyn co-localization with ubiquitin in H4 cells. H4 cells co-transfected with SynT and Synph 1. 48h post-transfection, cells were processed for immunofluorescence with anti aSyn (green) and ubiquitin (red) and imaged using confocal microscopy. This movie shows a composite green/red image of a reconstruction from a Z-series of 24B planes with 0.42μm between planes. Scale bar 20μm.

Supplementary Tables

Suppl. Table 1. aSyn glycation in yeast cells, identified by Peptide mass fingerprint (PMF) (trypsin digestion). Theoretical peptide mass (Da); error (ppm); Start-end Identified peptides; peptide sequences; putative glycated residues. Oxid (M), N-terminal acetylation and carboxyethyl (K) as variable modifications.

Theoretical peptide mass (Da)	Deviation (ppm)	Peptide Sequence	Peptide sequence and modifications	Putative Glycated Residues
1259.601	8.6	[1-10]	MDVFMKGLSK [1xCarboxyethyl; 2xOxidation]	K6
1243.6061	-4.3	[1-10]	MDVFMKGLSK [1xCarboxyethyl; 1xOxidation]	K6
1227.6112	-50.5	[1-10]	MDVFMKGLSK [1xCarboxyethyl]	K6
1530.7542	43.8	[1-12]	MDVFMKGLSKAK [2xCarboxyethyl; 2xOxidation]	K6 + K10
1514.7593	15	[1-12]	MDVFMKGLSKAK [2xCarboxyethyl; 1xOxidation]	K6 + K10
1426.7433	7.8	[1-12]	MDVFMKGLSKAK [1xCarboxyethyl]	K6, K10
1500.7437	5	[1-12]	MDVFMKGLSKAK [1xAcetyl; 1xCarboxyethyl; 2xOxidation]	K6, K10
1458.7331	-4.7	[1-12]	MDVFMKGLSKAK [1xCarboxyethyl; 2xOxidation]	K6, K10
1572.7648	-38.5	[1-12]	MDVFMKGLSKAK [1xAcetyl; 2xCarboxyethyl; 2xOxidation]	K6 + K10
2313.1829	16.7	[1-21]	MDVFMKGLSKAKEGVVAAAEK [1xCarboxyethyl; 2xOxidation]	K6, K10, K12
2281.1931	-9.9	[1-21]	MDVFMKGLSKAKEGVVAAAEK [1xCarboxyethyl]	K6, K10, K12
675.4036	-58.4	[7-12]	GLSKAK [1xCarboxyethyl]	K10
1529.8533	-8.1	[7-21]	GLSKAKEGVVAAAEK [1xCarboxyethyl]	K10, K12
1831.0171	-44.3	[7-23]	GLSKAKEGVVAAAEKTK [2xCarboxyethyl]	K10, K12, K21
1758.996	-73.8	[7-23]	GLSKAKEGVVAAAEKTK [1xCarboxyethyl]	K10, K12, K21
1445.7846	-21.7	[11-23]	AKEGVVAAAEKTK [2xCarboxyethyl]	K12 + K21
2215.1929	-9.9	[13-34]	EGVVAAAEKTKQGVAEAAGKTK [1xCarboxyethyl]	K21, K23, K32
2287.214	-11.1	[13-34]	EGVVAAAEKTKQGVAEAAGKTK [2xCarboxyethyl]	K21, K23, K32
1131.6004	9.9	[22-32]	TKQGVAEAAGK [1xCarboxyethyl]	K23
1360.7431	-28.2	[22-34]	TKQGVAEAAGKTK [1xCarboxyethyl]	K23, K32
1553.8421	-7.4	[33-45]	TKEGVLYVGSKTK [2xCarboxyethyl]	K34 + K43
1481.821	-28	[33-45]	TKEGVLYVGSKTK [1xCarboxyethyl]	K34, K43
2601.377	-53.9	[35-58]	EGVLYVGSKTKEGVVHGVATVAEK [2xCarboxyethyl]	K43 + K45
2830.5197	32.5	[35-60]	EGVLYVGSKTKEGVVHGVATVAEKTK [2xCarboxyethyl]	K43, K45, K58
1826.0018	-41.8	[44-60]	TKEGVVHGVATVAEKTK [1xCarboxyethyl]	K45, K58
2229.2085	-20.2	[59-80]	TKEQVTNVGGAVVTGVTAVAQK [1xCarboxyethyl]	K60

Suppl. Table 2. aSyn in yeast cells, identified by PMF (trypsin digestion). Theoretical peptide mass (Da); error (ppm); Start-end identified peptides; peptide sequences; putative glycated residues. Oxid (M) and N-terminal acetylation as variable modifications.

Theoretical peptide mass (Da)	Deviation (ppm)	Peptide Sequence	Peptide sequence and modifications
770.3575	-3.9	[1-6]	MDVFMK
786.3525	1.9	[1-6]	MDVFMK [1xOxidation]
802.3474	4.4	[1-6]	MDVFMK [2xOxidation]
812.3681	-2.2	[1-6]	MDVFMK [1xAcetyl]
828.363	-2.9	[1-6]	MDVFMK [1xAcetyl; 1xOxidation]
844.3579	-0.8	[1-6]	MDVFMK [1xAcetyl; 2xOxidation]
1155.5901	11.3	[1-10]	MDVFMKGLSK
1171.585	-13.6	[1-10]	MDVFMKGLSK [1xOxidation]
1197.6006	-2.2	[1-10]	MDVFMKGLSK [1xAcetyl]
1229.5905	1.1	[1-10]	MDVFMKGLSK [1xAcetyl; 2xOxidation]
1354.7221	3	[1-12]	MDVFMKGLSKAK
1412.7276	5	[1-12]	MDVFMKGLSKAK [1xAcetyl; 1xOxidation]
2209.1719	-14.4	[1-21]	MDVFMKGLSKAKEGVVAAAEK
2225.1668	0.5	[1-21]	MDVFMKGLSKAKEGVVAAAEK [1xOxidation]
2283.1723	-1.5	[1-21]	MDVFMKGLSKAKEGVVAAAEK [1xAcetyl; 2xOxidation]
603.3824	57.8	[7-12]	GLSKAK
1072.5997	-4	[11-21]	AKEGVVAAAEK
873.4676	-1.3	[13-21]	EGVVAAAEK
1288.7219	-4.8	[22-34]	TKQGVAEAAGKTK
2221.2187	-48.4	[22-43]	TKQGVAEAAGKTKEGVLYVGSK
830.4367	-26.6	[24-32]	QGVAEAAGK
2221.2187	-48.4	[24-45]	QGVAEAAGKTKEGVLYVGSKTK
1180.6572	1.1	[33-43]	TKEGVLYVGSK
1409.7999	1.6	[33-45]	TKEGVLYVGSKTK
2686.4774	-2	[33-58]	TKEGVLYVGSKTKEGVVHGVATVAEK
951.5146	2.3	[35-43]	EGVLYVGSK
1180.6572	1.1	[35-45]	EGVLYVGSKTK
2686.4774	-2	[35-60]	EGVLYVGSKTKEGVVHGVATVAEKTK
1524.838	-1.3	[44-58]	TKEGVVHGVATVAEK
1753.9807	-6	[44-60]	TKEGVVHGVATVAEKTK
1295.6954	0.2	[46-58]	EGVVHGVATVAEK
1524.838	-1.3	[46-60]	EGVVHGVATVAEKTK
2157.1874	1.1	[59-80]	TKEQVTNVGGAVVTGVTAVAQK
1928.0447	1	[61-80]	EQVTNVGGAVVTGVTAVAQK
2148.1659	-2.3	[81-102]	TVEGAGSIAAATGFVKKDQLGK
1478.7849	0.4	[81-96]	TVEGAGSIAAATGFVK

1606.8799	2	[81-97]	TVEGAGSIAAATGFVKK
688.3988	-93.1	[97-102]	KDQLGK
560.3039	-1.2	[98-102]	DQLGK

Suppl. Table 3. aSyn glycation in yeast cells, identified by PMF (Glu-C digestion). Theoretical peptide mass (Da); error (ppm); Start-end Identified peptides; peptide sequences; putative glycated residues. Oxid (M), N-terminal acetylation and carboxyethyl (K) as variable modifications.

Theoretical peptide mass (Da)	Deviation (ppm)	Peptide Sequence	Peptide sequence and modifications	Putative Glycated Residues
1597.7964	-27.2	[1-13]	MDVFMKGLSKAKE [1xAcetyl; 1xCarboxyethyl]	K6, K10, K12
1659.7968	25.5	[1-13]	MDVFMKGLSKAKE [2xCarboxyethyl; 2xOxidation]	K6, K10, K12
1715.823	-7	[1-13]	MDVFMKGLSKAKE [3xCarboxyethyl; 1xOxidation]	K6 + K10 + K12
2195.1087	1.3	[1-20]	MDVFMKGLSKAKEGVVAAAE [1xAcetyl; 1xCarboxyethyl]	K6, K10, K12
2211.1036	24	[1-20]	MDVFMKGLSKAKEGVVAAAE [1xAcetyl; 1xCarboxyethyl; 1xOxidation]	K6, K10, K12
3068.5642	-4.3	[1-28]	MDVFMKGLSKAKEGVVAAAEKTKQGVAE [1xAcetyl; 1xCarboxyethyl; 2xOxidation]	K6, K10, K12, K21, K23
1529.817	-3.6	[14-28]	GVVAAAEKTKQGVAE [1xCarboxyethyl]	K21, K23
1601.8381	-3.7	[14-28]	GVVAAAEKTKQGVAE [2xCarboxyethyl]	K21 + K23
1617.8806	-3.6	[21-35]	KTKQGVAEAAGKTKE [1xCarboxyethyl]	K23, K32, K34
1689.9018	27.8	[21-35]	KTKQGVAEAAGKTKE [2xCarboxyethyl]	K23, K32, K34
1761.9229	-1.8	[21-35]	KTKQGVAEAAGKTKE [3xCarboxyethyl]	K23 + K32 + K34
2272.2183	-0.9	[36-57]	GVLYVGSKTKEGVVHGVATVAE [1xCarboxyethyl]	K43, K45
577.3192	0	[58-61]	KTKE [1xCarboxyethyl]	K60

Suppl. Table 4. aSyn in yeast cells, identified by PMF (Glu-C digestion). Theoretical peptide mass (Da); error (ppm); Start-end identified peptides; peptide sequences; putative glycated residues. Oxid (M) and N-terminal acetylation as variable modifications.

Theoretical peptide mass (Da)	Deviation (ppm)	Peptide Sequence	Peptide sequence and modifications
802.3474	-67.7	[1-6]	MDVFMK [2xOxidation]
1396.7327	-16.2	[1-12]	MDVFMKGLSKAK [1xAcetyl]
1499.7596	-23.2	[1-13]	MDVFMKGLSKAKE [1xOxidation]
1515.7546	15	[1-13]	MDVFMKGLSKAKE [2xOxidation]
1541.7702	-33.4	[1-13]	MDVFMKGLSKAKE [1xAcetyl; 1xOxidation]
1557.7651	-1.1	[1-13]	MDVFMKGLSKAKE [1xAcetyl; 2xOxidation]
2155.0774	-7.2	[1-20]	MDVFMKGLSKAKEGVVAAAE [1xAcetyl; 2xOxidation]
2954.5326	-15.5	[1-28]	MDVFMKGLSKAKEGVVAAAEKTKQGVAE [2xOxidation]
616.3301	9.2	[14-20]	GVVAAAE
2143.1717	-43.6	[14-35]	GVVAAAEKTKQGVAEAAGKTKE
860.4836	-0.8	[21-28]	KTKQGVAE
2191.1353	3.7	[84-105]	GAGSIAAATGFVKKDQLGKNEE
630.2729	-17.7	[105-110]	EGAPQE
1822.7688	8.6	[111-126]	GILEDMPVDPDNEAYE [1xOxidation]
1838.7095	48.8	[115-130]	DMPVDPDNEAYEMPSE
971.3663	-53.7	[124-131]	AYEMPSEE [1xOxidation]
592.2283	18.5	[127-131]	MPSEE
608.2232	5	[127-131]	MPSEE [1xOxidation]
1363.4995	92.8	[127-137]	MPSEEGYQDYE [1xOxidation]
774.2941	69.8	[132-137]	GYQDYE

Suppl. Table 5. aSyn glycation in H4 cells, identified by PMF (trypsin digestion). Theoretical peptide mass (Da); error (ppm); Start-end Identified peptides; peptide sequences; putative glycated residues. Oxid (M), N-terminal acetylation and carboxyethyl (K) as variable modifications.

Theoretical peptide mass (Da)	Deviation (ppm)	Peptide Sequence	Peptide sequence and modifications	Putative Glycated Residues
1243.6061	-13.2	[1-10]	MDVFMKGLSK [1xCarboxyethyl; 1xOxidation]	K6
1259.601	11	[1-10]	MDVFMKGLSK [1xCarboxyethyl; 2xOxidation]	K6
1500.7437	7.5	[1-12]	MDVFMKGLSKAK [1xAcetyl; 1xCarboxyethyl; 2xOxidation]	K6, K10
1529.8533	5.6	[7-21]	GLSKAKEGVVAAAEK [1xCarboxyethyl]	K10, K12
2215.1929	-59.3	[13-34]	EGVVAAAEKTKQGVAEAAGKTK [1xCarboxyethyl]	K21, K23, K32

Suppl. Table 6. aSyn in H4 cells, identified by PMF (trypsin digestion). Theoretical peptide mass (Da); error (ppm); Start-end identified peptides; peptide sequences; putative glycated residues. Oxid (M) and N-terminal acetylation as variable modifications.

Theoretical peptide mass (Da)	Deviation (ppm)	Peptide Sequence	Peptide sequence and modifications
828.363	9.6	[1-6]	MDVFMK [1xAcetyl; 1xOxidation]
844.3579	-22.1	[1-6]	MDVFMK [1xAcetyl; 2xOxidation]
1155.5901	-14	[1-10]	MDVFMKGLSK
1171.585	-18.8	[1-10]	MDVFMKGLSK [1xOxidation]
1229.5905	11.5	[1-10]	MDVFMKGLSK [1xAcetyl; 2xOxidation]
1412.7276	-11.1	[1-12]	MDVFMKGLSKAK [1xAcetyl; 1xOxidation]
2225.1668	-12.8	[1-21]	MDVFMKGLSKAKEGVVAAAEK [1xOxidation]
2283.1723	-5.5	[1-21]	MDVFMKGLSKAKEGVVAAAEK [1xAcetyl; 2xOxidation]
603.3824	0	[7-12]	GLSKAK
1457.8322	-85.9	[7-21]	GLSKAKEGVVAAAEK
1072.5997	-7.4	[11-21]	AKEGVVAAAEK
873.4676	-5.5	[13-21]	EGVVAAAEK
1180.6572	-3.5	[33-43]	TKEGVLYVGSK
951.5146	7.8	[35-43]	EGVLYVGSK
1524.838	3.3	[44-58]	TKEGVVHGVATVAEK
1295.6954	1.1	[46-58]	EGVVHGVATVAEK
1524.838	3.3	[46-60]	EGVVHGVATVAEKTK
2157.1874	-5.8	[59-80]	TKEQVTNVGGAVVTGVTAVAQK
1928.0447	-2.4	[61-80]	EQVTNVGGAVVTGVTAVAQK
1478.7849	3.4	[81-96]	TVEGAGSIAAATGFVK
1606.8799	7.2	[81-97]	TVEGAGSIAAATGFVKK
560.3039	0	[98-102]	DQLGK

Suppl. Table 7. aSyn glycation in H4 cells, identified by PMF (Glu-C digestion). Theoretical peptide mass (Da); error (ppm); Start-end Identified peptides; peptide sequences; putative glycated residues. Oxid (M), N-terminal acetylation and carboxyethyl (K) as variable modifications.

Theoretical peptide mass (Da)	Deviation (ppm)	Peptide Sequence	Peptide sequence and modifications	Putative Glycated Residues
1643.8019	-9	[1-13]	MDVFMKGLSKAKE [2xCarboxyethyl; 1xOxidation]	K6, K10, K12
1529.817	-5.2	[14-28]	GVVAAAEKTKQGVAE [1xCarboxyethyl]	K21, K23
1601.8381	15.6	[14-28]	GVVAAAEKTKQGVAE [2xCarboxyethyl]	K21 + K23
1617.8806	-40	[21-35]	KTKQGVAEAAGKTKE [1xCarboxyethyl]	K32, K34

848.436	15.4	[29-35]	AAGKTKE [2xCarboxyethyl]	K32 + K34
2272.2183	-8.1	[36-57]	GVLYVGSKTKEGVVHGVATVAE [1xCarboxyethyl]	K43, K45

Suppl. Table 8. aSyn in H4 cells, identified by PMF (Glu-C digestion). Theoretical peptide mass (Da); error (ppm); Start-end identified peptides; peptide sequences; putative glycated residues. Oxid (M) and N-terminal acetylation as variable modifications.

Theoretical peptide mass (Da)	Deviation (ppm)	Peptide Sequence	Peptide sequence and modifications
1557.7651	40.7	[1-13]	MDVFMKGLSKAKE [1xAcetyl; 2xOxidation]
2097.0719	0.1	[1-20]	MDVFMKGLSKAKEGVVAAAE [1xOxidation]
1870.6994	37.5	[115-130]	DMPVDPDNEAYEMPSE [2xOxidation]
971.3663	8.6	[124-131]	AYEMPSEE [1xOxidation]

Suppl. Table 9. aSyn glycation in rat brain, identified by PMF (trypsin digestion). Theoretical peptide mass (Da); error (ppm); Start-end Identified peptides; peptide sequences; putative glycated residues. Oxid (M), N-terminal acetylation and carboxyethyl (K) as variable modifications.

Theoretical peptide mass (Da)	Deviation (ppm)	Peptide Sequence	Peptide sequence and modifications	Putative Glycated Residues
1227.6112	16.1	[1-10]	MDVFMKGLSK [1xCarboxyethyl]	K6
1243.6061	-0.4	[1-10]	MDVFMKGLSK [1xCarboxyethyl; 1xOxidation]	K6
1259.601	-2.5	[1-10]	MDVFMKGLSK [1xCarboxyethyl; 2xOxidation]	K6
1269.6218	5.2	[1-10]	MDVFMKGLSK [1xAcetyl; 1xCarboxyethyl]	K6
1285.6167	11.3	[1-10]	MDVFMKGLSK [1xAcetyl; 1xCarboxyethyl; 1xOxidation]	K6
1301.6116	13.7	[1-10]	MDVFMKGLSK [1xAcetyl; 1xCarboxyethyl; 2xOxidation]	K6
1468.7538	2.7	[1-12]	MDVFMKGLSKAK [1xAcetyl; 1xCarboxyethyl]	K6, K10
1500.7437	-1.5	[1-12]	MDVFMKGLSKAK [1xAcetyl; 1xCarboxyethyl; 2xOxidation]	K6, K10
1514.7593	0.6	[1-12]	MDVFMKGLSKAK [2xCarboxyethyl; 1xOxidation]	K6 + K10
1540.775	17.1	[1-12]	MDVFMKGLSKAK [1xAcetyl; 2xCarboxyethyl]	K6 + K10
2281.1931	-13.2	[1-21]	MDVFMKGLSKAKEGVVAAAEK [1xCarboxyethyl]	K6, K10, K12
2297.188	3.7	[1-21]	MDVFMKGLSKAKEGVVAAAEK [1xCarboxyethyl; 1xOxidation]	K6, K10, K12

2313.1829	-3.5	[1-21]	MDVFMKGLSKAKEGVVAAAEK [1xCarboxyethyl; 2xOxidation]	K6, K10, K12
2353.2142	-41.2	[1-21]	MDVFMKGLSKAKEGVVAAAEK [2xCarboxyethyl]	K6, K10, K12
2355.1934	-20.9	[1-21]	MDVFMKGLSKAKEGVVAAAEK [1xAcetyl; 1xCarboxyethyl; 2xOxidation]	K6, K10, K12
2369.2091	-11.1	[1-21]	MDVFMKGLSKAKEGVVAAAEK [2xCarboxyethyl; 1xOxidation]	K6, K10, K12
2411.2197	-26.6	[1-21]	MDVFMKGLSKAKEGVVAAAEK [1xAcetyl; 2xCarboxyethyl; 1xOxidation]	K6, K10, K12
1529.8533	3.4	[7-21]	GLSKAKEGVVAAAEK [1xCarboxyethyl]	K10, K12
1601.8745	-0.3	[7-21]	GLSKAKEGVVAAAEK [2xCarboxyethyl]	K10 + K12
1758.996	-63.2	[7-23]	GLSKAKEGVVAAAEKTK [1xCarboxyethyl]	K10, K12, K21
1831.0171	-57.2	[7-23]	GLSKAKEGVVAAAEKTK [2xCarboxyethyl]	K10, K12, K21
2185.1823	-40.6	[11-32]	AKEGVVAAAEKTKQGVAEAAGK [1xCarboxyethyl]	K12, K21, K23
2215.1929	-13.2	[13-34]	EGVVAAAEKTKQGVAEAAGKTK [1xCarboxyethyl]	K21, K23, K32
2287.214	-21.2	[13-34]	EGVVAAAEKTKQGVAEAAGKTK [2xCarboxyethyl]	K21, K23, K32
1131.6004	-3.6	[22-32]	TKQGVAEAAGK [1xCarboxyethyl]	K23
1131.6004	-3.6	[24-34]	QGVAEAAGKTK [1xCarboxyethyl]	K32
2064.0972	-10.6	[24-43]	QGVAEAAGKTKEGVLYVGSK [1xCarboxyethyl]	K32, K34
1252.6783	-37.7	[33-43]	TKEGVLYVGSK [1xCarboxyethyl]	K34
1481.821	-13.6	[33-45]	TKEGVLYVGSKTK [1xCarboxyethyl]	K34, K43
2788.5091	-59.8	[33-58]	TKEGVLYVGSKTKEGVVHGVTTVAEK [1xCarboxyethyl]	K34, K43, K45
1252.6783	-37.7	[35-45]	EGVLYVGSKTK [1xCarboxyethyl]	K43
1626.8697	-8.2	[44-58]	TKEGVVHGVTTVAEK [1xCarboxyethyl]	K45
1856.0124	-38.5	[44-60]	TKEGVVHGVTTVAEKTK [1xCarboxyethyl]	K45, K58
1928.0335	1.3	[44-60]	TKEGVVHGVTTVAEKTK [2xCarboxyethyl]	K45 + K58
1626.8697	-8.2	[46-60]	EGVVHGVTTVAEKTK [1xCarboxyethyl]	K58
2229.2085	-14.9	[59-80]	TKEQVTNVGGAVVTGVTAVAQK [1xCarboxyethyl]	K60
1705.9119	8.3	[81-97]	TVEGAGNIAAATGFVKK [1xCarboxyethyl]	K96
2281.1493	6	[81-102]	TVEGAGNIAAATGFVKKDQMGK [1xCarboxyethyl; 1xOxidation]	K96, K97
2353.1704	-22.6	[81-102]	TVEGAGNIAAATGFVKKDQMGK [2xCarboxyethyl; 1xOxidation]	K96 + K97

Suppl. Table 10. aSyn in rat brain, identified by PMF (trypsin digestion). Theoretical peptide mass (Da); error (ppm); Start-end identified peptides; peptide sequences; putative glycated residues. Oxid (M) and N-terminal acetylation as variable modifications.

Theoretical peptide mass (Da)	Deviation (ppm)	Peptide Sequence	Peptide sequence and modifications
770.3575	-2	[1-6]	MDVFMK
802.3474	-13.4	[1-6]	MDVFMK [2xOxidation]
812.3681	2.1	[1-6]	MDVFMK [1xAcetyl]

828.363	4.1	[1-6]	MDVFMK [1xAcetyl; 1xOxidation]
844.3579	-1.7	[1-6]	MDVFMK [1xAcetyl; 2xOxidation]
1155.5901	4.4	[1-10]	MDVFMKGLSK
1171.585	-10.8	[1-10]	MDVFMKGLSK [1xOxidation]
1213.5955	-17.1	[1-10]	MDVFMKGLSK [1xAcetyl; 1xOxidation]
1229.5905	-4.6	[1-10]	MDVFMKGLSK [1xAcetyl; 2xOxidation]
1354.7221	-32.6	[1-12]	MDVFMKGLSKAK
1428.7225	-5.3	[1-12]	MDVFMKGLSKAK [1xAcetyl; 2xOxidation]
2225.1668	-9	[1-21]	MDVFMKGLSKAKEGVVAAAEK [1xOxidation]
2283.1723	-0.7	[1-21]	MDVFMKGLSKAKEGVVAAAEK [1xAcetyl; 2xOxidation]
1457.8322	-46.5	[7-21]	GLSKAKEGVVAAAEK
1072.5997	-7.5	[11-21]	AKEGVVAAAEK
1301.7423	-7.4	[11-23]	AKEGVVAAAEKTK
873.4676	6.2	[13-21]	EGVVAAAEK
1059.5793	-9.5	[22-32]	TKQGVAEAAGK
1288.7219	0.6	[22-34]	TKQGVAEAAGKTK
830.4367	-28.8	[24-32]	QGVAEAAGK
1059.5793	-9.5	[24-34]	QGVAEAAGKTK
1180.6572	-0.3	[33-43]	TKEGVLYVGSK
1409.7999	-3.2	[33-45]	TKEGVLYVGSKTK
951.5146	-4.6	[35-43]	EGVLYVGSK
1180.6572	-0.3	[35-45]	EGVLYVGSKTK
1554.8486	-0.1	[44-58]	TKEGVVHGVTTVAEK
1783.9912	-9.5	[44-60]	TKEGVVHGVTTVAEKTK
1325.706	-7.4	[46-58]	EGVVHGVTTVAEK
1554.8486	-0.1	[46-60]	EGVVHGVTTVAEKTK
2157.1874	1.2	[59-80]	TKEQVTNVGGAVVTGVTAVAQK
1928.0447	-0.6	[61-80]	EQVTNVGGAVVTGVTAVAQK
1505.7958	-1.2	[81-96]	TVEGAGNIAAATGFVK
1633.8908	-0.1	[81-97]	TVEGAGNIAAATGFVKK
722.3502	-29	[97-102]	KDQMGK [1xOxidation]
578.2603	9.5	[98-102]	DQMGK
594.2552	-0.6	[98-102]	DQMGK [1xOxidation]

Suppl. Table 11. aSyn glycation in rat brain, identified by PMF (Glu-C digestion). Theoretical peptide mass (Da); error (ppm); Start-end Identified peptides; peptide sequences; putative glycated residues. Oxid (M), N-terminal acetylation and carboxyethyl (K) as variable modifications.

Theoretical peptide mass (Da)	Deviation (ppm)	Peptide Sequence	Peptide sequence and modifications	Putative Glycated Residues
1627.807	-7.1	[1-13]	MDVFMKGLSKAKE [2xCarboxyethyl]	K6, K10, K12
1643.8019	37.2	[1-13]	MDVFMKGLSKAKE [2xCarboxyethyl; 1xOxidation]	K6, K10, K12

2195.1087	-1.9	[1-20]	MDVFMKGLSKAKEGVVAAAE [1xAcetyl; 1xCarboxyethyl]	K6, K10, K12
2287.214	-34.2	[14-35]	GVVAAAEKTKQGVAEAAGKTKE [2xCarboxyethyl]	K21, K23, K32
848.436	-21.1	[29-35]	AAGKTKE [2xCarboxyethyl]	K32 + K34

Suppl. Table 12. aSyn in rat brain, identified by PMF (Glu-C digestion). Theoretical peptide mass (Da); error (ppm); Start-end identified peptides; peptide sequences; putative glycated residues. Oxid (M) and N-terminal acetylation as variable modifications.

Theoretical peptide mass (Da)	Deviation (ppm)	Peptide Sequence	Peptide sequence and modifications
1541.7702	-22.7	[1-13]	MDVFMKGLSKAKE [1xAcetyl; 1xOxidation]
1557.7651	-0.9	[1-13]	MDVFMKGLSKAKE [1xAcetyl; 2xOxidation]
2155.0774	-1.5	[1-20]	MDVFMKGLSKAKEGVVAAAE [1xAcetyl; 2xOxidation]
2097.0719	-1.9	[1-20]	MDVFMKGLSKAKEGVVAAAE [1xOxidation]
2996.5431	-17.3	[1-28]	MDVFMKGLSKAKEGVVAAAEKTKQGVAE [1xAcetyl; 2xOxidation]
1180.6572	-57.4	[36-46]	GVLYVGSKTKE
2230.2078	-4.3	[36-57]	GVLYVGSKTKEGVVHGVTTVAE
2614.441	4.8	[58-83]	KTKEQVTNVGGAVVTGVTAVAQKTVE
2128.1608	-2.2	[62-83]	QVTNVGGAVVTGVTAVAQKTVE
2066.0335	9.8	[84-104]	GAGNIAAATGFVKKDQMGKGE [1xOxidation]
2195.0761	12.9	[84-105]	GAGNIAAATGFVKKDQMGKGEE [1xOxidation]
3181.547	6	[84-114]	GAGNIAAATGFVKKDQMGKGEEGYPQEGILE [1xOxidation]
2195.9359	75.9	[111-130]	GILEDMPVDPSSEAYEMPSE
971.3663	5.1	[124-131]	AYEMPSEE [1xOxidation]

Suppl. Table 13. aSyn glycation in mouse brain, identified by PMF (trypsin digestion). Theoretical peptide mass (Da); error (ppm); Start-end Identified peptides; peptide sequences; putative glycated residues. Oxid (M), N-terminal acetylation and carboxyethyl (K) as variable modifications.

Theoretical peptide mass (Da)	Deviation (ppm)	Peptide Sequence	Peptide sequence and modifications	Putative Glycated Residues
1269.6218	41.5	[1-10]	MDVFMKGLSK [1xAcetyl; 1xCarboxyethyl]	K6
1442.7382	17.5	[1-12]	MDVFMKGLSKAK [1xCarboxyethyl; 1xOxidation]	K6, K10
1514.7593	-1	[1-12]	MDVFMKGLSKAK [2xCarboxyethyl; 1xOxidation]	K6 + K10

1572.7648	-5.2	[1-12]	MDVFMKGLSKAK [1xAcetyl; 2xCarboxyethyl; 2xOxidation]	K6 + K10
2323.2036	-3.2	[1-21]	MDVFMKGLSKAKEGVVAAAEK [1xAcetyl; 1xCarboxyethyl]	K6, K10, K12
1529.8533	-43.4	[7-21]	GLSKAKEGVVAAAEK [1xCarboxyethyl]	K10, K12
1758.996	81.2	[7-23]	GLSKAKEGVVAAAEKTK [1xCarboxyethyl]	K10, K12, K21
1831.0171	-22.4	[7-23]	GLSKAKEGVVAAAEKTK [2xCarboxyethyl]	K10, K12, K21
2215.1929	-11.1	[13-34]	EGVVAAAEKTKQGVAEAAGKTK [1xCarboxyethyl]	K21, K23, K32
1131.6004	-11.8	[22-32]	TKQGVAEAAGK [1xCarboxyethyl]	K23
1360.7431	69.3	[22-34]	TKQGVAEAAGKTK [1xCarboxyethyl]	K23, K32
1131.6004	-11.8	[24-34]	QGVAEAAGKTK [1xCarboxyethyl]	K32
2229.2085	-24.7	[59-80]	TKEQVTNVGGAVVTGVTAVAQK [1xCarboxyethyl]	K60

Suppl. Table 14. aSyn in mouse brain, identified by PMF (trypsin digestion). Theoretical peptide mass (Da); error (ppm); Start-end identified peptides; peptide sequences; putative glycated residues. Oxid (M) and N-terminal acetylation as variable modifications.

Theoretical peptide mass (Da)	Deviation (ppm)	Peptide Sequence	Peptide sequence and modifications
1171.585	8.6	[1-10]	MDVFMKGLSK [1xOxidation]
1213.5955	43.7	[1-10]	MDVFMKGLSK [1xAcetyl; 1xOxidation]
1428.7225	9.7	[1-12]	MDVFMKGLSKAK [1xAcetyl; 2xOxidation]
2225.1668	0.6	[1-21]	MDVFMKGLSKAKEGVVAAAEK [1xOxidation]
2283.1723	2.2	[1-21]	MDVFMKGLSKAKEGVVAAAEK [1xAcetyl; 2xOxidation]
873.4676	-2.9	[13-21]	EGVVAAAEK
1554.8486	4	[44-58]	TKEGVVHGVTTVAEK
1325.706	-7	[46-58]	EGVVHGVTTVAEK
1554.8486	4	[46-60]	EGVVHGVTTVAEKTK
2157.1874	-0.7	[59-80]	TKEQVTNVGGAVVTGVTAVAQK
1928.0447	-0.5	[61-80]	EQVTNVGGAVVTGVTAVAQK
1505.7958	3.4	[81-96]	TVEGAGNIAAATGFVK
1633.8908	3.5	[81-97]	TVEGAGNIAAATGFVKK
722.3502	-44.2	[97-102]	KDQMGK [1xOxidation]
578.2603	2	[98-102]	DQMGK
594.2552	-6.4	[98-102]	DQMGK [1xOxidation]

Suppl. Table 15. aSyn glycation in mouse brain, identified by PMF (Glu-C digestion). Theoretical peptide mass (Da); error (ppm); Start-end Identified peptides; peptide sequences; putative glycated residues. Oxid (M), N-terminal acetylation and carboxyethyl (K) as variable modifications

Theoretical peptide mass (Da)	Deviation (ppm)	Peptide Sequence	Peptide sequence and modifications	Putative Glycated Residues
1741.8387	-11.3	[1-13]	MDVFMKGLSKAKE [1xAcetyl; 3xCarboxyethyl]	K6 + K10 + K12
2211.1036	-2.5	[1-20]	MDVFMKGLSKAKEGVVAAAE [1xAcetyl; 1xCarboxyethyl; 1xOxidation]	K6, K10, K12
2225.1192	0.1	[1-20]	MDVFMKGLSKAKEGVVAAAE [2xCarboxyethyl]	K6, K10, K12
2283.1247	5.3	[1-20]	MDVFMKGLSKAKEGVVAAAE [1xAcetyl; 2xCarboxyethyl; 1xOxidation]	K6, K10, K12
2299.1196	-5	[1-20]	MDVFMKGLSKAKEGVVAAAE [1xAcetyl; 2xCarboxyethyl; 2xOxidation]	K6, K10, K12
1529.817	-14.4	[14-28]	GVVAAAEKTKQGVAE [1xCarboxyethyl]	K21, K23
2215.1929	-28.6	[14-35]	GVVAAAEKTKQGVAEAAGKTKE [1xCarboxyethyl]	K21, K23, K32
848.436	-33.9	[29-35]	AAGKTKE [2xCarboxyethyl]	K32 + K34
1324.6995	-2.1	[36-46]	GVLYVGSKTKE [2xCarboxyethyl]	K43 + K45

Suppl. Table 16. aSyn in mouse brain, identified by PMF (Glu-C digestion). Theoretical peptide mass (Da); error (ppm); Start-end identified peptides; peptide sequences; putative glycated residues. Oxid (M) and N-terminal acetylation as variable modifications.

Theoretical peptide mass (Da)	Deviation (ppm)	Peptide Sequence	Peptide sequence and modifications
616.3301	-53.3	[14-20]	GVVAAAE
1866.0331	-40.3	[29-46]	AAGKTKEGVLYVGSKTKE
2230.2078	-12.9	[36-57]	GVLYVGSKTKEGVVHGVTTVAE
1068.5684	13.8	[47-57]	GVVHGVTTVAE
1554.8486	22.3	[47-61]	GVVHGVTTVAEKTKE
2179.0812	-30.9	[84-105]	GAGNIAAATGFVKKDQMGKGEE
722.2992	1.2	[105-110]	EGYPQE
2061.8957	-0.2	[105-123]	EGYPQEGILEDMPVDPGSE
593.2566	17.9	[106-110]	GYPQE
1005.4888	6.3	[106-114]	GYPQEGILE
842.3237	46.2	[124-130]	AYEMPSE [1xOxidation]
592.2283	0	[127-131]	MPSEE
608.2232	44.9	[127-131]	MPSEE [1xOxidation]

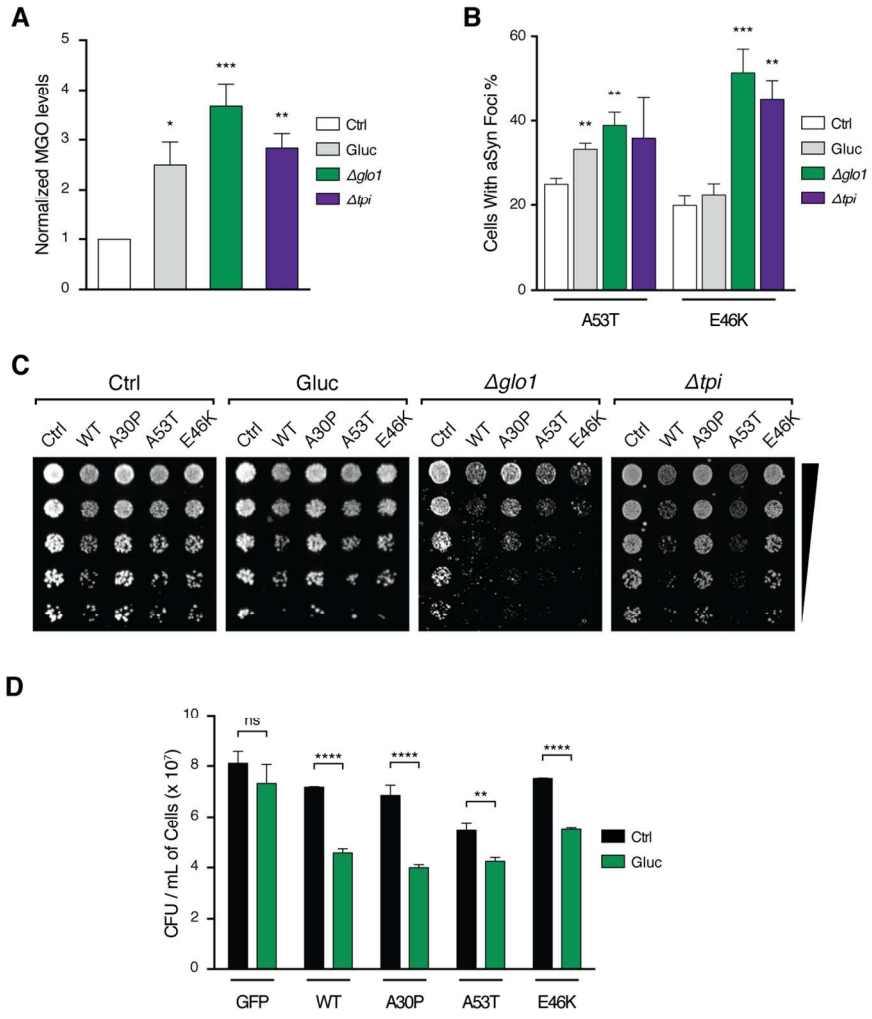

Fig. S1. MGO induces mutant aSyn aggregation and toxicity in yeast models of PD. (A) Yeast BY4741 reference strain and *Δglo1* or *Δtpi* cells transformed with empty p426GPD vector were grown in YNB-U. Yeast cells were also grown in higher glucose concentrations (4%). Equal numbers of cells were harvested and the intracellular levels of MGO were determined by HPLC and normalized to Ctrl. (B) Yeast cells were transformed with aSyn mutants associated with familial forms of PD (A53T and E46K). The % of yeast cells displaying aSyn inclusions is presented. (C) Toxicity of aSyn under glycating conditions, as in (B) (spotting assays of Ctrl and WT are repeated as in Fig. 1 B). Data in all panels are average ± SD, * $p < 0.05$, ** $p < 0.01$, *** $p < 0.001$. For (A), (B) and (D), unpaired two-tailed t-test with equal SD.

Fig. S1
120x124mm (300 x 300 DPI)

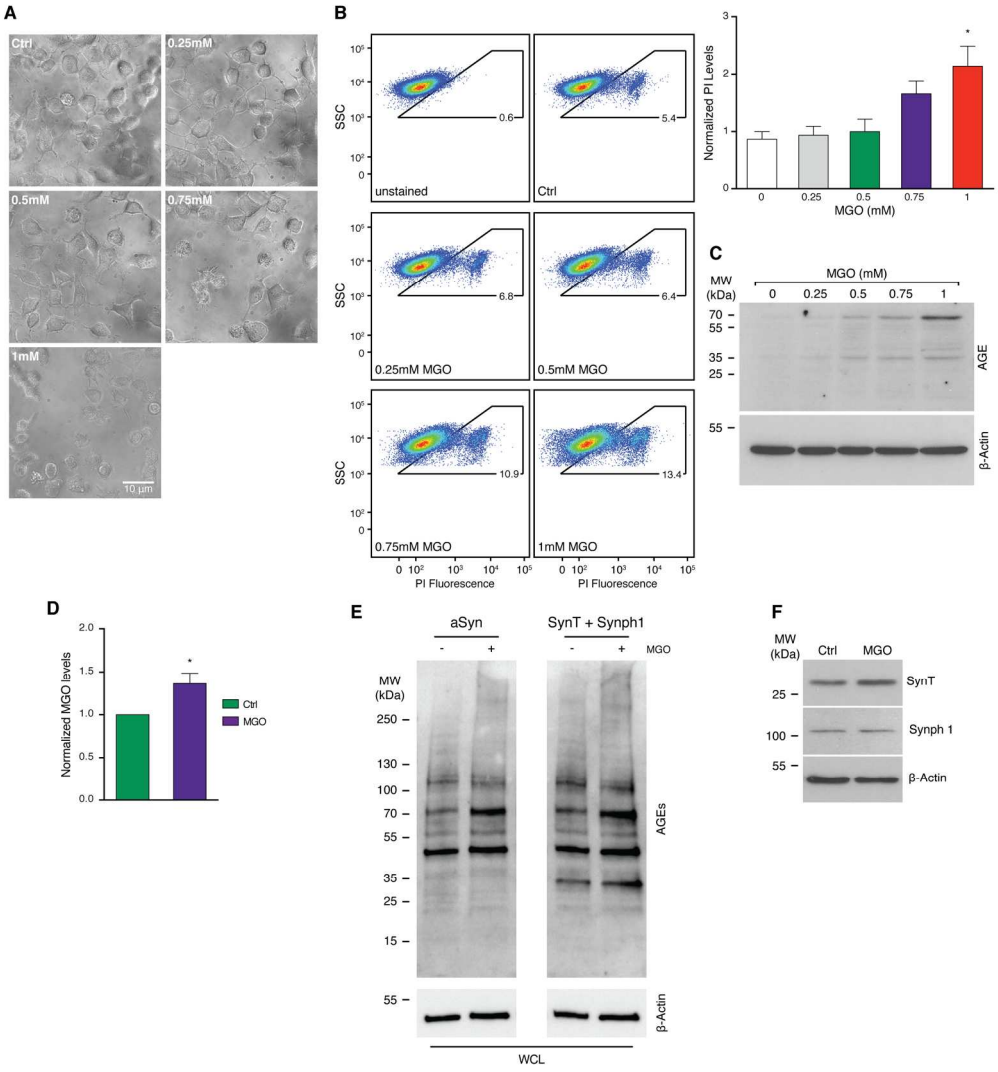

Fig. S2. MGO toxicity and glycation in human H4 cells. (A) H4 cells treated with vehicle (Ctrl) or increasing concentrations of MGO for 16h. (B) MGO toxicity measured by propidium iodide staining, presented as fold of Ctrl. Data are presented as average ± SD, * $p < 0.05$, unpaired two-tailed t-test with equal SD. (C) Protein extracts from H4 cells treated with vehicle (Ctrl) or MGO for 16h were immunoblotted with anti-AGE and anti-β-actin antibodies. (D) H4 cells were treated as in (A). The intracellular levels of MGO were measured by HPLC and normalized to Ctrl. (E) H4 cells co-transfected with SynT and Synph 1 (tagged with V5) for 24h were treated with vehicle (Ctrl) or MGO (0.5mM) for 16h. The medium was replaced and cells were retreated with MGO for 6h. Protein extracts were immunoblotted with an antibody against AGEs and with the corresponding loading control (anti- β-Actin) or with an antibody against aSyn, against the V5-tag (synph 1), and the corresponding loading control (β-Actin) (F). For (B), 1-way ANOVA, followed by Tukey's multiple comparisons test. For (D) unpaired t-test with equal SD.

Fig. S2
174x189mm (300 x 300 DPI)

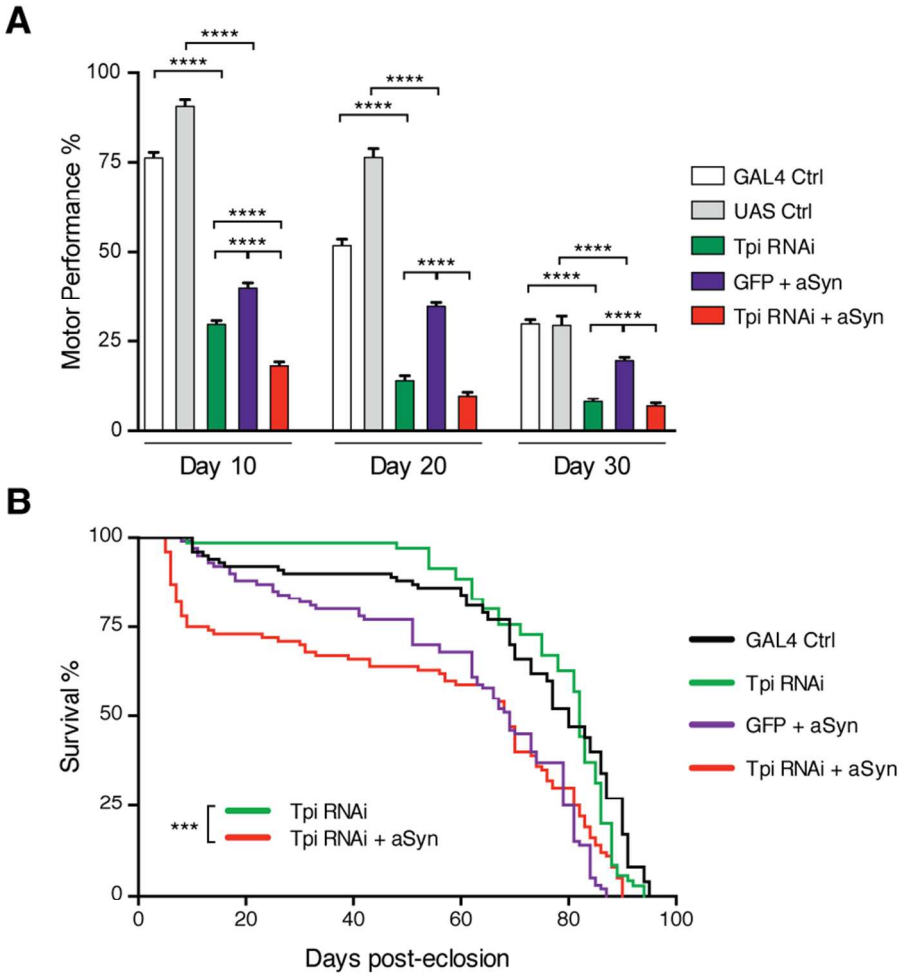

Fig. S3. Down-regulation of Tpi impairs negative geotaxis and lifespan in flies. Measurement of Drosophila motor performance in a second Tpi RNAi line, assessed as percentage of flies more than 8cm within 10sec. (A) RNAi silencing of Tpi caused a reduction in climbing behavior in both WT and aSyn flies when compared to their relative controls (n=50 per condition). (B) Survival rate was evaluated in flies with pan-neuronal knockdown of Tpi in WT and aSyn backgrounds (n=100 per genotype). Data in all panels are mean ± SEM, **** $p < 0.001$, **** $p < 0.0001$. For (A) 2-way ANOVA, followed by Tukey's multiple comparisons test. For (B) Kaplan–Meier survival curve analysis with log-rank test.
Fig. S3
85x85mm (300 x 300 DPI)

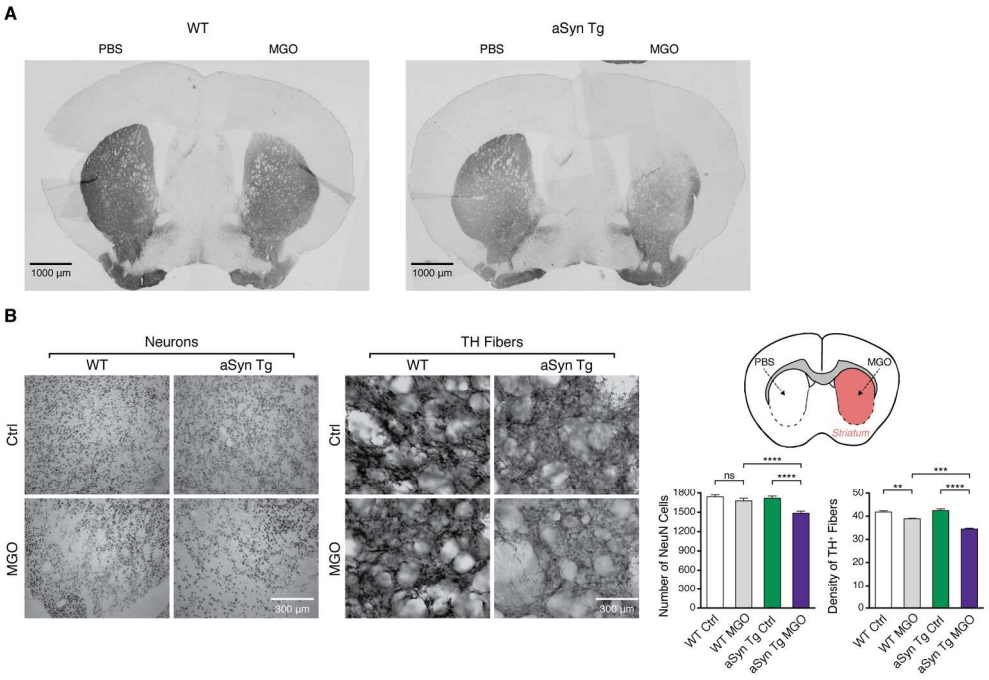

Fig. S4. MGO injection in the substantia nigra or in the striatum induces aSyn neurotoxicity in mice. (A) WT and aSyn-Tg mice were injected with MGO or vehicle (PBS) in the SN as in Fig. 3 A-E. Representative image of a coronal section immunostained with an antibody against TH to label TH-positive neurons, and developed with DAB. Extensive damage in MGO-treated aSyn Tg mice is observed (scale bar 1000 µm). (B) WT and aSyn-Tg mice were injected in the striatum (schematic view) with MGO or vehicle (PBS) and analyzed 7 days post-injection. Representative micrographs of brain sections immunostained for NeuN or TH (scale bar 300 µm). The % of Neu-N cells or TH fiber density (ratio MGO/PBS) is presented (at least n=3 per condition). Data are presented as average ± SD, ** $p < 0.01$, unpaired t-test with equal SD.

Fig. S4
174x119mm (300 x 300 DPI)

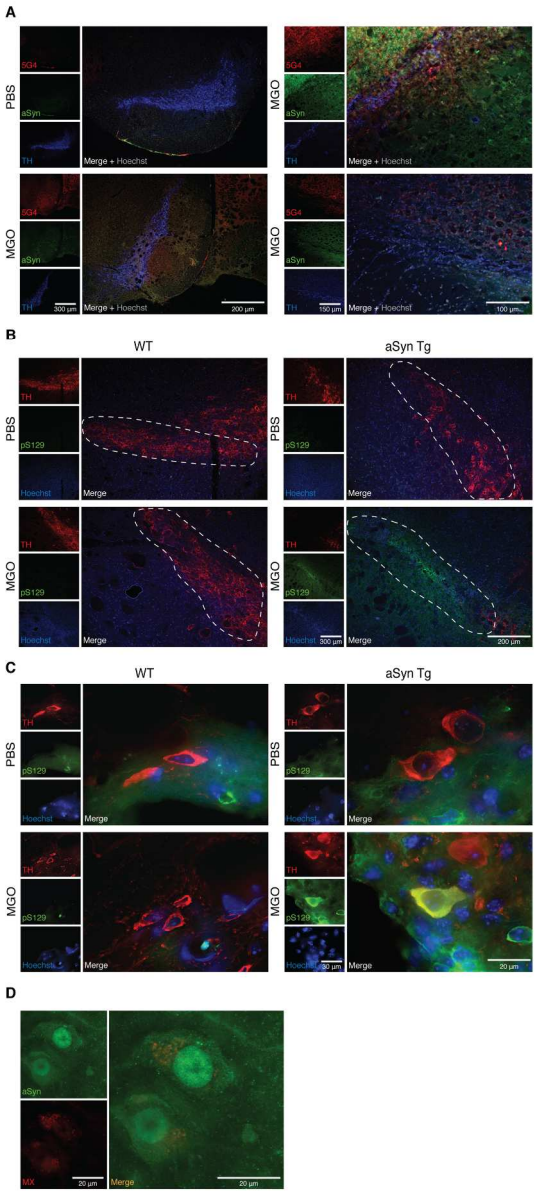

Fig. S5. MGO induces aSyn aggregation and phosphorylation on S129. WT and aSyn-Tg mice were injected in the SN or in the striatum with MGO or vehicle (PBS) and analyzed 7 days post-injection. (A) Representative images of brain sections immunostained for aggregated aSyn (5G4, red), aSyn (green), TH (blue) or nuclei (Hoechst, grey) (scale bar 300 µm). Merged signal is presented (scale bar 200 µm). (B) Representative images of SN immunostained for TH (red), pS129 aSyn (green) or nuclei (Hoechst, blue) (scale bar 300 µm). Merged signal is presented (scale bar 200 µm). Dashed line delineates the SN. (C) Representative images of SN immunostained for TH (red), pS129 aSyn (green) or stained with Hoechst (blue) at higher magnification (scale bar 30 µm). Merged signal is presented (scale bar 20 µm). (D) Section of the striatum of striatum-MGO-injected aSyn-Tg mice immunostained for aSyn (green), and stained with MX-O4 (labeling amyloid-like structures, red) (scale bar 20 µm).

Fig. S5
115x255mm (300 x 300 DPI)

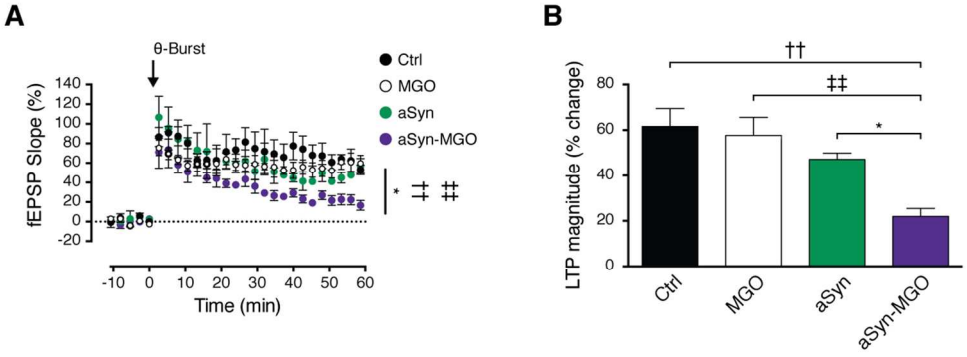

Fig. S6. MGO does not affect LTP in rat hippocampal slices. (A) Changes in fEPSP slope induced by –burst stimulation were recorded from the CA1 region of hippocampal slices pre-treated with PBS (Ctrl - black), 35 μM MGO (white), aSyn (aSyn - green) or glycated aSyn (aSyn-MGO - purple) (data from aSyn and aSyn-MGO are the same presented in Fig. 3 H-I. (B) Bar graph of the LTP magnitude (change in fEPSP slope at 50-60min) in relation to pre--burst values (100 %) from experiments shown in (A) as indicated below each column (at least n=3). * $p < 0.05$ aSyn-MGO vs aSyn, †† $p < 0.01$ aSyn-MGO vs MGO, ‡‡ $p < 0.01$ aSyn-MGO vs Ctrl. For (A) and (B), one-way ANOVA test, followed by a Bonferroni's multiple comparison post-hoc test.‼ ┼

Fig. S6

111x43mm (300 x 300 DPI)

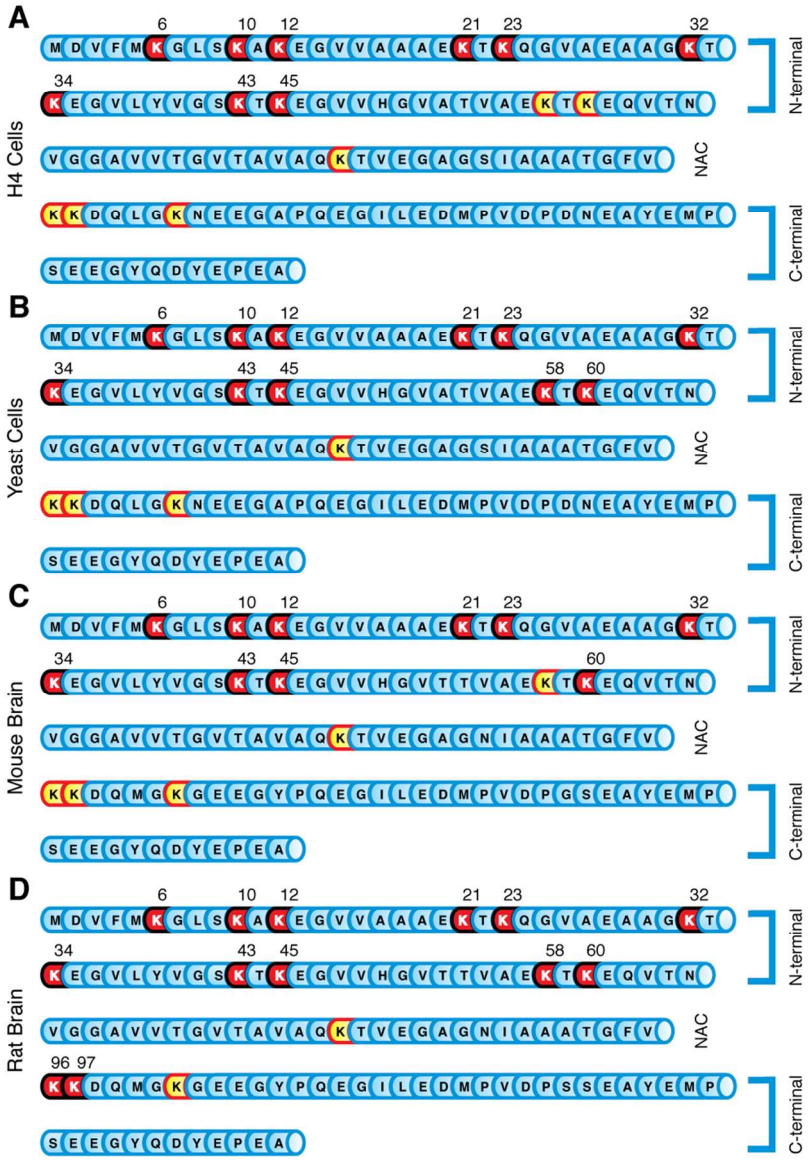

Fig. S7. Glycation occurs primarily in the N-terminal region of aSyn. Schematic representation of the glycation sites (red), together with unmodified lysine residues (yellow). Mass spectrometry analysis of tryptic or Glu-C digestion of (A) H4 cells transfected with aSyn treated with 0.5mM MGO; (B) yeast Δglo1 transformed with aSyn; (C) Mouse brain (3 month-old animals); and (D) rat brain protein extracts (3 month-old animals). The identity between the N-terminal domain sequences of the species analyzed was 98% (Expasy, SIM-Alignment Tool for protein sequences).

Fig. S7
85x124mm (300 x 300 DPI)

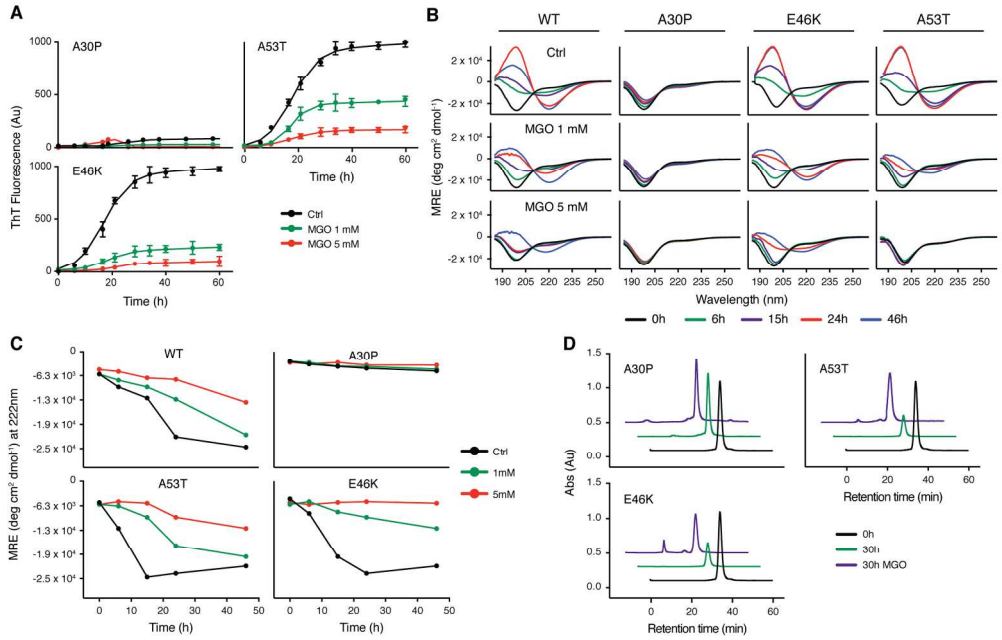

Fig. S8. In vitro MGO-glycation promotes aSyn oligomerization (A) Fibrillization of recombinant A30P, A53T and E46K aSyn at 100 μM treated with vehicle (Ctrl) or MGO (1 mM; and 5 mM) was followed by ThT fluorescence. Data are presented as average ± SD. (B) Fibrillization of recombinant WT, A30P, A53T and E46K aSyn at 100μM treated with vehicle (Ctrl) or MGO (1 and 5mM) analyzed by CD (MRE, mean residue ellipticity). (C) Structure transition followed at 222nm. (D) Recombinant A30P, A53T and E46K aSyn species at 100 μM before (0 h) and after 30 h of fibrillization treated with vehicle (30 h) or MGO at 1 mM (30 h MGO) were analysed by SEC.

Fig. S8

174x115mm (300 x 300 DPI)

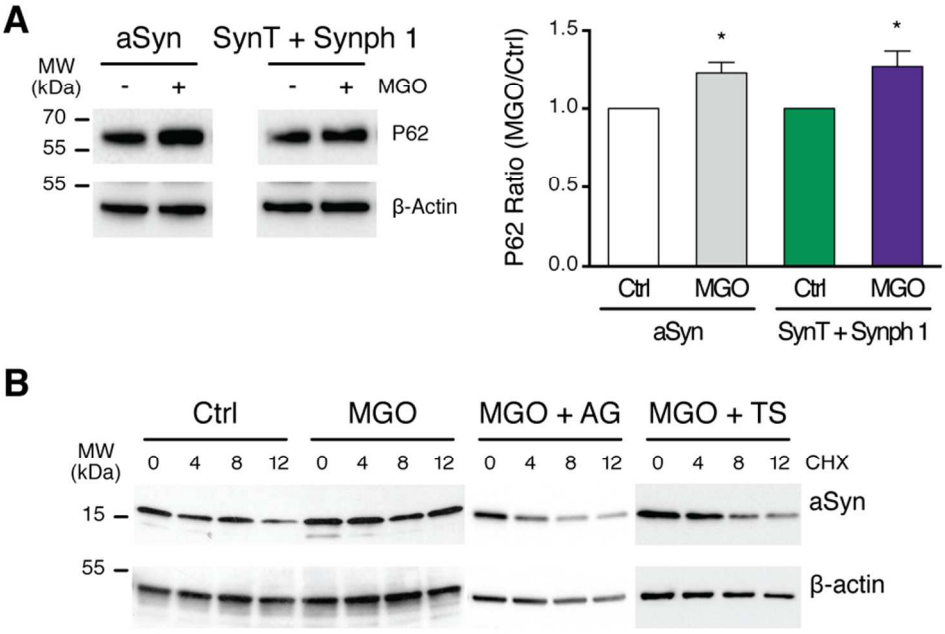

Fig. S9. Effect of glycation on aSyn clearance. (A) H4 cells co-expressing SynT and Synph 1 were treated with vehicle (-) or MGO (+, 0.5 mM) for 16h. Media was replaced and cells were retreated with MGO for 4h. Protein extracts were probed for P62 (SQSTM1) and for the corresponding loading control (β-Actin). The ratio between the levels of P62 in cells treated with MGO or vehicle (Ctrl) is presented. (B) Cells as in (A) were treated with vehicle, MGO or MGO together with AG or TS for 24 h together with CHX for the last 4, 8 and 12 h. Protein extracts were probed for aSyn and β-actin, for normalization. Results shown for Ctrl and MGO are repeated as in Fig. 5C. Data in (A) are average ± SD, * $p < 0.05$, unpaired two-tailed t-test with equal SD.

Fig. S9

85x55mm (300 x 300 DPI)